Structure and dynamics of highly turbulent premixed combustion

Adam M. Steinberg[a,*], Peter E. Hamlington[b], Xinyu Zhao[c]

[a]*Daniel Guggenheim School of Aerospace Engineering, Georgia Institute of Technology, Atlanta, GA, 30332, USA*
[b]*Paul M. Rady Department of Mechanical Engineering, University of Colorado, Boulder, CO, 80309, USA*
[c]*Department of Mechanical Engineering, University of Connecticut, Storrs, CT, 06269, USA*

Abstract

Turbulent premixed combustion involves simultaneous and mutually interacting fluid, chemical, and transport phenomena spanning a wide range of spatial and temporal scales. Many practical combustion devices – such as gas turbine combustors, afterburners, and ramjets – operate with turbulent flows that contain length and time scales smaller than those associated with premixed flame propagation. This paper reviews current knowledge and understanding of premixed flames at such "highly turbulent" conditions, including the effects of turbulence on the flame and of the flame on turbulence. At these conditions, turbulent fluid motions can have a leading-order effect on the flame thermochemical structure, scalar gradients, and the resultant scalar dynamics. At the same time, the turbulent flow itself is affected by heat release from the flame, resulting in differences compared to classical non-reacting turbulence and to turbulence in flames at lower intensities. We therefore aim to address the following overarching questions: (a) What are highly turbulent premixed flames, how do we characterize them, and what are some of their macroscale behaviors? (b) How are the flame thermochemical states, scalar gradients, diffusion, and other aspects of the flame structure affected by intense turbulence? (c) How are the structure and dynamics of the turbulence affected by the presence of the flame in terms of fluxes, spectra, kinetic energy, and other relevant quantities? We also provide a summary of critical knowledge gaps and an outlook for future research directions.

Keywords: Turbulent combustion, Premixed flames, Turbulence-flame interaction, Direct numerical simulations, Laser diagnostics

Nomenclature

Dimensionless Parameters

$\mathrm{Da}_{\ell,\delta}$	Damköhler number
$\mathrm{Ka}_{\delta,\mathrm{K}}$	Karlovitz number
Le	Lewis number
Re_{ℓ}	Integral scale Reynolds number

Greek

α	Thermal diffusivity
$\boldsymbol{\omega}$	Vorticity vector
χ_j	Scalar gradient
δ_{L}^0	Unstretched laminar flame thermal thickness
δ_{r}^0	Unstretched laminar flame reaction zone thickness
δ_{t}	Scalar field thickness
$\dot{\omega}_\beta$	Chemical source term
κ	Thermal conductivity
λ_{e}	Eigenvalue of eigenmode of chemical Jacobian
λ_{K}	Kolmogorov length scale
μ	Dynamic viscosity

*Corresponding author: adam.steinberg@gatech.edu

Email addresses: adam.steinberg@gatech.edu (Adam M. Steinberg), peh@colorado.edu (Peter E. Hamlington), xinyu.zhao@uconn.edu (Xinyu Zhao)

μ_{B} Bulk viscosity

ν Kinematic viscosity

Ω Enstrophy

ϕ Equivalence ratio

ψ Generic scalar

ρ Fluid density

τ_δ Characteristic laminar flame propagation time scale

τ_{i} Induction time

τ_{K} Kolmogorov time scale

τ_{r} Characteristic laminar flame reaction zone time scale

τ_{ij} Viscous stress tensor

ε Mean kinetic energy dissipation rate

φ_{s} Contribution of diffusion to evolution of CEM

φ_ω Contribution of reaction to evolution of CEM

Mathematical Operators

$(\cdot)'$ Fluctuation about ensemble average

ϵ_{ijk} Cyclic permutation tensor

$\bar{(\cdot)}$ Ensemble average

$\tilde{(\cdot)}$ Favre average

$(\cdot)''$ Fluctuation about Favre average

Roman

$\boldsymbol{a}_\mathrm{e}$	Right chemical eigenvector
$\boldsymbol{b}_\mathrm{e}$	Left chemical eigenvector
$\boldsymbol{e}$	Eigenvector of rate-of-strain tensor
$\boldsymbol{J}_\omega$	Chemical Jacobian
$\boldsymbol{k}$	Wavevector for spectral analysis
$\boldsymbol{n}$	Scalar isosurface normal vector
$\boldsymbol{r}$	Scale separation for structure function analysis
$\boldsymbol{u}$	Fluid velocity
$\dot{m}_\mathrm{r}$	Reactant mass flow rate
ℓ	Integral length scale
$\mathcal{D}$	Molecular transport coefficient
$\mathcal{D}_\mathrm{T}$	Turbulent diffusivity
$\mathcal{F}$	Body force
$\mathcal{T}$	Integral time scale
A_T	Turbulent flame surface area
$A_{\bar{c}=0.5}$	Mean flame brush area
a_{ij}	Anisotropy tensor
c	Reaction progress variable
c_K	Scaling factor relating λ_K, ℓ, and Re_ℓ

c_s	Scaling factor relating s_L^0, $\bar{\alpha}$ and δ_L^0
e_0	Total energy
I	Dependency of Karlovitz and Damköhler numbers on flow conditions and geometry
I_0	Flame speed stretch factor
II	Dependency of Karlovitz and Damköhler numbers on thermochemical parameters
k	Turbulence kinetic energy
L	Induction length
n_s	Number of chemical species
p	Pressure
P_{ij}	Plane parallel to scalar isosurface
s	Non-chemical source terms in CEM analysis
s_L^0	Unstretched laminar flame speed
s_D	Displacement speed
$s_\mathrm{T,GC}$	Global consumption speed of turbulent flame
S_{ij}	Rate-of-strain tensor
T	Temperature
u_ℓ	Integral velocity scale
u_K	Kolmogorov velocity scale
Y	Mass fraction

1. Introduction

Nearly all practical applications of combustion occur in turbulent flows, generally by design. Turbulent combustion involves non-linear multi-scale interactions between chemistry, transport, and fluid motions that have leading order effects on the flame and flow behavior. For premixed turbulent combustion, turbulent fluid motions lead to an increase in the surface area of reactive scalars that is associated with an increase in the turbulent burning rate. Turbulence also creates large gradients in thermodynamic and chemical quantities, resulting in substantially greater thermochemical complexity than in laminar flames (e.g., broader thermochemical phase spaces and highly varied thermochemical trajectories along Lagrangian fluid pathlines). Moreover, the fluid dynamic strain rate and vorticity directly affect the dynamics of reactive thermochemical scalar gradients, thus impacting, for example, the local flame orientation, thickness, and iso-surface propagation speed. Thermochemical gradients generated by combustion chemistry also influence the turbulence, both by altering transport properties and through thermal expansion (e.g., flow divergence, density gradients, etc.).

Although numerous studies, including several detailed reviews [1–10], have addressed turbulent premixed combustion occurring at relatively modest turbulence intensities, comparatively little research has addressed fundamental turbulence-flame interactions at the highly turbulent conditions relevant to many practical devices and situations, such as lean premixed gas turbine combustors, afterburners, ramjets, and other occurrences of fast subsonic flames [11]. Indeed, a surge of studies on highly turbulent premixed flames emerged around 2015. The purpose of this paper is to review the current state of knowledge regarding the structure and dynamics of highly-turbulent premixed flames, including both the effects of turbulence on the flame and the flame on turbulence.

The dynamical system describing turbulent combustion is outlined mathematically in Section 2. For now, it is sufficient to note that this system is nonlinear due to various physical effects represented in the governing equations, including advection, chemical sources, pressure-velocity coupling, and temperature-dependent molecular transport processes. Of

note is the advective nonlinearity in the Navier-Stokes equations describing conservation of momentum. In turbulent flows, this nonlinearity dominates over the (linear) effects of viscous diffusion of momentum. The integral-scale Reynolds number, Re_ℓ, which characterizes the relative magnitudes of the advective nonlinearity and viscous diffusion, is thus typically very large in turbulent flows.

As a result of the dominant nonlinearity in high Re_ℓ turbulent flows, large spatial and temporal variations in flow properties are created over a wide range of length and time scales. This multi-scale spatio-temporal complexity leads to the formation of turbulent fluctuations at increasingly small scales as Re_ℓ increases, resulting in the creation of large spatial gradients in velocity and other quantities (e.g., temperature and chemical species concentrations). These large gradients, in turn, lead to rapid molecular transport of thermochemical scalars (e.g., temperature and chemical species concentrations), as compared to variations due to chemical reactions alone.

It is this mixing property of turbulence that makes it particularly attractive for many combustion systems. For non-premixed combustion, turbulence accelerates the rate-limiting process of fuel and oxidizer mixing. For premixed combustion—in which reaction rates are not limited by the rate of fuel and oxidizer mixing—turbulence increases the rate at which energy and species are mixed between the products and reactants, ultimately leading to an increased reaction rate compared to laminar flames. We note that "mixing" in this context refers to combined advective and diffusive processes; non-linear advective stirring increases the magnitude and spatial extent of scalar and velocity gradients, which then lead to rapid molecular diffusion. Together, the statistical effect of advective turbulent stirring and enhanced molecular diffusion is often referred to as "turbulent diffusion".

However, turbulence also complicates the design, analysis, and operation of combustion systems. The broad range of length and time scales at play in turbulent combustion—from the large integral scales to the Kolmogorov and chemical scales—precludes direct numerical simulations (DNS) of practical devices in engineering contexts; models must therefore be employed. For example, in the context of large eddy simulations (LES), models are required to describe the influence of unresolved subfilter scale (SFS) phenomena on resolved scale

behaviors. In highly turbulent flames, much of the turbulence-induced thermochemical complexity and the flame-induced turbulence dynamics exist in the subfilter scales and must be modeled. In order to create physics-based models, it therefore is critical to understand the various interactions between the flame and turbulence that can occur at highly turbulent conditions.

In this review, we address the following overarching questions:

1. What are highly turbulent flames, how are they characterized, and what are some of their macro-scale behaviors?
2. How are the thermochemical structure and dynamics of the flame modified by the presence of intense turbulence?
3. How are turbulence structure and dynamics modified by premixed flames at highly turbulent conditions?

The first items are addressed primarily in Section 2, while the second and third questions are addressed in Sections 3 and 4, respectively. An outlook for future research directions is provided in Section 5.

2. Preliminary Comments and Global Characteristics

We will often discuss the effects of turbulence on premixed flames by differentiating the turbulent flame "structure" and "dynamics" from that which would occur under laminar flow conditions. The expected impact of turbulence on the flame is typically described through various dimensionless parameters constructed using characteristic length, time, and/or velocity-scales, which may be visualized through regime diagrams. We therefore begin this review with a brief discussion of laminar flame structure, dimensionless parameters, regime diagrams, and the locations of some engineering-relevant devices in the regime diagrams. We also include a brief discussion of experimental and DNS configurations commonly used to study highly turbulent combustion, as well as the turbulent flame speeds observed in these configurations. Several practical and theoretical challenges are highlighted, and some best practices are recommended.

2.1. Governing equations

In general terms, turbulent combustion is characterized by highly irregular fluid motions that are coupled with reactive scalar dynamics, both of which vary in space and time in a complicated manner. The fluid density (ρ), velocity vector (u_i), total energy (e_0, sum of thermal, chemical, and kinetic energy), and species mass fractions[1] (Y_β, where $\beta = 1, \ldots, n_\mathrm{s}$ for n_s total chemical species), evolve according to the system of equations

$$\frac{\mathrm{D}\rho}{\mathrm{D}t} = -\rho\frac{\partial u_k}{\partial x_k}\,, \tag{1}$$

$$\frac{\mathrm{D}u_i}{\mathrm{D}t} = -\frac{1}{\rho}\frac{\partial p}{\partial x_i} + \frac{1}{\rho}\frac{\partial \tau_{ij}}{\partial x_j} + \mathcal{F}_i\,, \tag{2}$$

$$\frac{\mathrm{D}e_0}{\mathrm{D}t} = -\frac{1}{\rho}\frac{\partial (u_j p)}{\partial x_j} + \frac{1}{\rho}\frac{\partial}{\partial x_j}\left(\kappa\frac{\partial T}{\partial x_j}\right) + \frac{1}{\rho}\frac{\partial (u_i \tau_{ij})}{\partial x_j} + u_i\mathcal{F}_i\,, \tag{3}$$

$$\frac{\mathrm{D}Y_\beta}{\mathrm{D}t} = \frac{1}{\rho}\frac{\partial}{\partial x_k}\left(\rho\mathcal{D}_\beta\frac{\partial Y_\beta}{\partial x_k}\right) + \dot{\omega}_\beta\,, \tag{4}$$

where summation over Greek indices in Eq. (4) is not implied. Here, $\mathrm{D}/\mathrm{D}t \equiv \partial/\partial t + u_j\partial/\partial x_j$ is the material, or Lagrangian, derivative that represents advection following a fluid element. Other quantities in these equations are the pressure (p), temperature (T), volumetric (or body) force ($\mathcal{F}_i$), thermal conductivity (κ), and molecular transport coefficient for Y_β ($\mathcal{D}_\beta$). We have assumed gradient diffusion, ignoring Soret and Dufour effects. Radiant energy transfer is also neglected in Eq. (3). The Newtonian viscous stress tensor τ_{ij} is expressed as

$$\tau_{ij} = 2\mu S_{ij} - \frac{2}{3}\delta_{ij}\mu_\mathrm{B}S_{kk}\,, \tag{5}$$

where μ and μ_B are the dynamic viscosity and bulk viscosity, respectively, and

$$S_{ij} = \frac{1}{2}\left(\frac{\partial u_i}{\partial x_j} + \frac{\partial u_j}{\partial x_i}\right)\,, \tag{6}$$

is the rate-of-strain tensor. Sources of Y_β (i.e., due to chemical reactions) are represented by $\dot{\omega}_\beta$ and may take on positive or negative values. All of the transport coefficients (i.e.,

[1]Eq. (4) can also be written in terms of species mole fractions. Indeed, it can be viewed as a general equation for any reactive scalar with gradient diffusion, given an appropriate diffusion coefficient. For clarity, we will largely treat chemical scalars in terms of mass fractions in this paper.

κ, $\mathcal{D}_\beta$, μ, and μ_B) appearing in the above equations depend on the local temperature and fluid composition, and are not constant in reacting flows. A full description of the system dynamics therefore requires auxiliary relations to represent the chemical reactions, transport coefficients, and the thermodynamic equation of state. From a Lagrangian point of view, Eqs. (1)–(4) state that the change in thermodynamic, flow, and chemical properties following a fluid element at location $\boldsymbol{x}$ at time t is a result of the balance between diffusive (molecular transport) effects and various source terms.

For chemical species, the source term is generally local, depending only on the local composition and temperature-dependent reaction rate coefficient. By contrast, diffusion processes are non-local, being driven by gradients (e.g., $\chi_j \equiv \partial Y/\partial x_j$) that couple adjacent dissimilar fluid states. In laminar flames, the competition between advection, reaction, and molecular diffusion ultimately determines the structure and evolution of the scalar field. This also holds true in turbulent flames, but with turbulent advection leading to a broader range of scalar gradients than are found in laminar flames (thereby affecting the diffusion process) and, consequently, a wider range of thermochemical states (affecting the reaction process).

2.2. Laminar premixed flames

2.2.1. Deflagrations and auto-ignition

Turbulent flames may exhibit local behaviors ranging from being similar to laminar premixed deflagrations—in which energy and species diffusion are necessary to sustain the reactions—to being similar to autoignition[2]. While laminar deflagrations are most common, as will be discussed in Section 3, turbulence may create local gas mixtures that should be viewed as auto-igniting fronts [13–16]. Hence, this distinction will become important for discussions in Section 3, although devices that rely on auto-ignition as the major combustion mode (e.g. some sequential gas turbine combustors [17]) are not the main focus of this review.

[2]Detonation waves occur when the combustion wave travels at a supersonic speed. Although this mode of combustion can occur in many engineering and natural contexts, the focus of the present review is on subsonic, non-detonative, combustion.

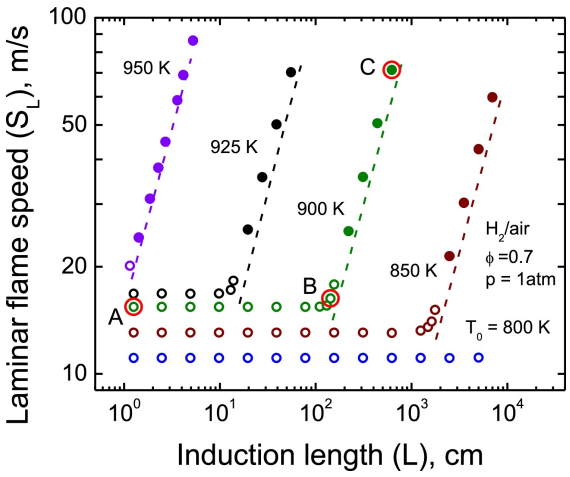

Figure 1: Unstretched laminar flame speed (s_{L}^0) as a function of the induction length (L). Reprinted from [12] with permission of Elsevier.

To illustrate these combustion modes, consider a one-dimensional (1D) linear domain with a steady laminar flame in the observer reference frame. Hence, the speed of the gas upstream of the flame is the "laminar flame speed", denoted s_{L}^0 (the superscript '0' indicates that the flame is 'unstretched'). In cases where the ignition delay time (or induction time, τ_{i}) of the reactant mixture is long compared to the residence time of the unburnt mixture in the system (i.e., L/s_{L}^0, where L is the characteristic induction length), reactions are sustained by diffusion of energy and species from the products to the reactants (a deflagration). The laminar flame speed is then an intrinsic property of the reactant mixture that can be solved through an eigenvalue problem [18] and is independent of the ignition delay time.

For reactant mixtures in which the ignition delay is short compared to the residence time of the gas in the domain, the reactants will auto-ignite in the absence of any external source and without the need for diffusion from the products. The flame then stabilizes after an induction length $L = s_{\mathrm{L}}^0 \tau_{\mathrm{i}}$. Whereas τ_{i} is a unique function of the reactant state, in this context, the "laminar flame speed" depends both on the reactants and the "desired" induction length; it is not a unique function of the mixture. These two limiting cases are demonstrated in Fig. 1, which shows the laminar flame speed (i.e., the reactant gas speed for a stationary flame) as a function of induction length for various atmospheric pressure

H_2/air flames at different reactant temperatures.

2.2.2. Laminar premixed deflagrations

We now turn briefly to laminar premixed deflagrations in order to define some quantities and concepts needed for the subsequent discussion. Figure 2 shows computed profiles of various quantities through laminar unstretched deflagrations with different fuels at a constant pressure of $p = 1$ atm and a reactant temperature of $T_\mathrm{r} = 500$ K[3]. The fuel consumption and heat release rates are shown, along with mass fractions of a few key species. Temperature is used to demarcate different regions of the laminar flame, and also to serve as a reasonable measure of the progress variable c (see Refs. [23, 24] for other methods of defining c). The origin of the physical space coordinates is at the peak heat release rate for each flame.

For the methane/air flame shown in Fig. 2(a), the exothermic reactions are confined to a relatively compact region at high temperature ($T \gtrsim 1200$ K) termed the "reaction zone". Upstream of this is a similarly compact region over which the reactants begin to breakdown, forming CH_2O, H_2, and other species. Species and energy diffuse further upstream in a relatively inert "preheat zone" that is dominated by molecular transport processes. Ultimately, however, the species profiles at all locations reflect the simultaneous effects of reaction, diffusion, and laminar convection, even as the relative balance of these effects varies throughout the flame.

The fuel consumption and heat release rates are co-located for the lean methane/air flame due to the relatively high temperatures required for methane-to-methyl initiation reactions. However, this relationship is compromised for the n-dodecane/air and hydrogen/air flames shown in Figs. 2(b)-(c). For the n-dodecane/air flame, fuel consumption precedes the heat release zone due to endothermic fuel pyrolysis. Such fuel cracking is expected for all heavy hydrocarbons [20, 21, 25]. For the hydrogen/air flame, the heat release zone overlaps with the fuel consumption region, although the peak of heat release precedes that of the fuel consumption. Heat release and fuel consumption both occur near the leading edge of the

[3]All laminar flame calculations in this work are done in PREMIX [19] using the HyChem approach [20–22] with multi-component and Soret diffusion.

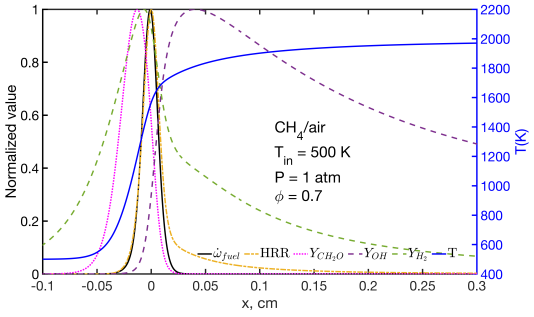

(a) CH_4/air

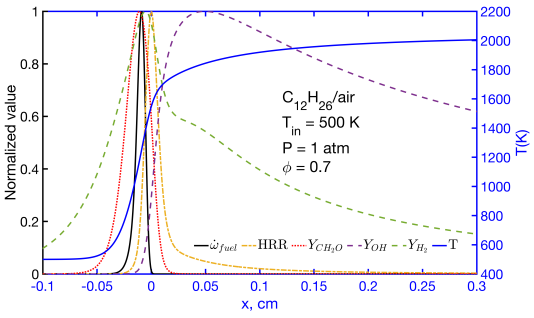

(b) n-dodecane/air

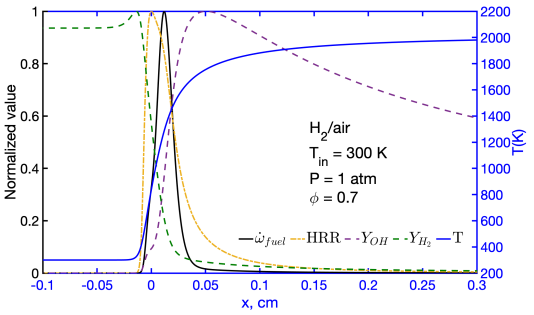

(c) H_2/air

Figure 2: One-dimensional unstretched laminar flames in physical space for lean methane/air, n-dodecane/air and hydrogen/air flames at atmospheric pressure. All profiles are normalized by their respective peak values.

flame. Hence, a largely inert preheat zone and thin chemically-active reaction zone do not occur for these laminar flames (though the exothermic reactions are confined to a relatively thin region in the n-dodecane flame).

Important scales in these flames include a length characterizing the overall thermal thickness, $\delta_{\mathrm{L}}^0 \equiv (T_{\mathrm{p}} - T_{\mathrm{r}}) \max(|\nabla T|)^{-1}$, and a thickness characterizing the region of rapid exothermic reactions δ_{r}^0. The interpretation of δ_{L}^0 in terms of scalar field dynamics will be discussed in Section 3.1. In the hydrocarbon/air flames, $\delta_{\mathrm{r}}^0 = \mathcal{O}(10^{-1})\delta_{\mathrm{L}}^0$. However, δ_{r}^0 is larger relative to δ_{L}^0 in the H_2 flame. Characteristic flame time-scales are defined by dividing these length-scales by the laminar flame speed, viz. $\tau_\delta = \delta_{\mathrm{L}}^0/s_{\mathrm{L}}^0$ and $\tau_{\mathrm{r}} = \delta_{\mathrm{r}}^0/s_{\mathrm{L}}^0 = \mathcal{O}(10^{-1})\tau_\delta$. Hence, the range of length- and time-scales associated with an unstretched laminar premixed flame typically spans about one order of magnitude.

The unstretched laminar flame speed s_{L}^0 is a critical quantity for understanding turbulent premixed flames, as it is traditionally employed to define normalization chemical time scales for turbulent flames, both locally and globally. As previously mentioned, the unstretched laminar flame speed of a deflagration is a unique function of the reactant state, including composition, temperature, and pressure. The laminar flame speed is conventionally derived from 1D unstretched laminar flames where the least ambiguity is introduced in its definition/computation [26].

Figure 3 shows the laminar flame speed of n-dodecane as a function of temperature (from $T = 500$ K to 1100 K in 100 K intervals), equivalence ratios (from $\phi = 0.6$ to 1 in 0.05 intervals), and pressures (from $p = 28$ bar to 32 bar in 0.5 bar intervals). As predicted by combustion theory [27], the laminar flame speed has a weak negative correlation with pressure, as well as a weak dependence on equivalence ratio in the fuel-lean (i.e., $\phi < 1$) region. Temperature has a leading-order effect on the laminar flame speed; s_{L}^0 increases by approximately seven-fold as the reactant temperature is raised from 500 K to 1100 K. It is important to recognize this dependence, because local variations of the equivalence ratio and temperature are expected in highly turbulent flames, as discussed in Sec. 3.2.1. The temperature range in Fig. 3 is chosen to demonstrate the strong temperature dependence of laminar flame speed. However, it should be recognized that it is challenging to measure laminar flame speeds with preheat temperatures above 700 K, especially for heavy hydrocarbon fuels, due to fuel decomposition during the fuel heating and delivery process.

It is worth briefly mentioning that this discussion of laminar flame speed treats the

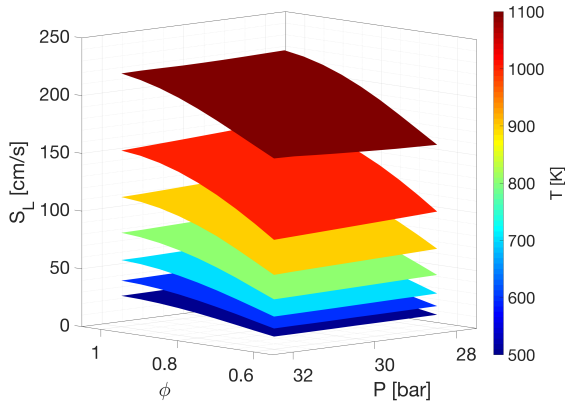

Figure 3: Unstretched laminar flame speed s_{L}^0 obtained at different temperatures T, equivalence ratios ϕ, and pressures p for an n-dodecane/air mixture.

deflagration as a coherent wave moving at speed s_{L}^0. However, due to gas acceleration normal to the flame and the corresponding decrease in density, different locations in the flame must move at different speeds in order to maintain a stationary flame. This leads to the definition of the displacement speed of a scalar isosurface (i.e., the surface of constant scalar value Y_β^*), defined as

$$s_{\mathrm{D}}|_{Y_\beta^*} = \frac{1}{|\nabla Y_\beta|} \frac{\mathrm{D}Y_\beta}{\mathrm{D}t}\bigg|_{Y_\beta^*}, \tag{7}$$

where $\mathrm{D}Y_\beta/\mathrm{D}t$ is given by Eq. (4). Hence, the displacement speed can be viewed as a field quantity that obeys a transport equation and obtains different values throughout both laminar and turbulent flames. This also highlights that, unlike the "laminar flame speed", the displacement speed is not a single value for a given reactant mixture. Indeed, for a steady laminar flame, the displacement speed varies between the gas speeds in the reactants and products in order to maintain a steady flame structure; care must be taken when evaluating the displacement speed to ensure that precise scalar isovalues are tracked.

The instantaneous and local thermochemical state of the reacting system can be expressed as the vector quantity $[T(\boldsymbol{x},t), \rho(\boldsymbol{x},t), \boldsymbol{Y}(\boldsymbol{x},t)]^\intercal \in \mathbb{R}^{n_\mathrm{s}+2}$, where n_s is the number of species. In a steady, unstretched laminar flame with a known reactant thermochemical state the thermochemical state at any point can be uniquely indexed to the progress variable; the thermochemical state is a surjective function with c that is an (n_s+2)-dimensional curve in

state space. Of course, Eqs. (4) and (7) show that the scalar field dynamics are controlled not only by the reaction rate, which depends on the local thermochemical state, but also by diffusive processes that depend on scalar gradients that couple dissimilar fluid states. However, in a laminar premixed deflagration, the scalar gradients are also uniquely mapped by c. Hence, the dynamics of the scalar fields depend only on c.

The idea that the thermochemical and spatial structure of a 1D laminar premixed flame can be uniquely mapped to the progress variable has been very influential in the theory and modeling of turbulent premixed flames. In particular, laminar flamelet theory posits that, in cases where flame structures are thinner than the turbulence scales distorting the flame (or, equivalently, the flame time scales are shorter than turbulence time scales), the internal flame structure remains nearly constant while it moves in the flow [2, 28]. Hence, in such situations, the thermochemical structure and dynamics of a 3D turbulent flame can be mapped onto the structure of an ensemble of 1D laminar flame solutions based on a small number of parameters. This idea underlies a large number of reaction rate modeling strategies, such as flamelet prolongation of intrinsic low dimensional manifolds [29], flamelet generated manifolds [30], flame surface density methods [31], and level set (e.g., G-equation) methods [32].

Our focus here is on the structure and dynamics of turbulent premixed combustion at conditions where flame structures are thicker, potentially by a considerable amount, than some of the turbulent scales of motion. This includes both the local thermochemical structure of the scalar fields and their gradients, along with the structure and dynamics of the underlying turbulence that interacts with the thermochemical scalars. We note that the aim is not to evaluate the validity of different modelling paradigms that may be applied to turbulent flames, but rather to review current understanding of the physics and chemistry in these systems.

2.3. Configurations and other practical considerations

Before discussing the parameters and characteristics of highly-turbulent flames, it is helpful to briefly review some of the attributes of configurations—both experimental and

computational—that are used to study them. As the focus of this paper is on the underlying structure and dynamics of flames and turbulence, we exclude from consideration configurations that contain highly turbulent flames but have been used to study other aspects of combustion. For example, we do not consider studies or configurations focused on thermoacoustic instabilities or blow-out. Detailed reviews of these topics are provided elsewhere [33–35].

Experimental configurations that have been used to investigate turbulent flame structure and dynamics include rod-stabilized bluff-body flames [36–39], swirl flames (both low-swirl and high-swirl) [40–43], jet flames [44–50], Bunsen flames [51–59], expanding flame kernels [60–63], and propagating flames in tubes [64]. With few exceptions [64], these flames have been either unconfined by mechanical boundaries (i.e., combustion chambers), or the experiments ended before the flame interacted with the walls. This lack of confinement provides optical access for laser diagnostics without the complication of windows, but adds other complications that will be discussed below.

A common feature of jet and Bunsen flames[4] is that, in the absence of an open flame tip, the flame envelopes the reactants. Hence, the mass flow rate of reactants burnt by the flame is known, which allows calculation of the global consumption speed of the turbulent flame. In contrast, reactants may bypass the flame in bluff-body and swirl-flame configurations. A potential advantage of the latter flames is that they all involve a recirculation zone that helps anchor the flames, whereas jet and Bunsen flames require pilots in order to stabilize the flame base at highly turbulent conditions.

However, unconfined flames, whether piloted or not, add complications under highly turbulent conditions. To illustrate this, we consider the Lund University piloted jet (LUPJ) burner [47–50] and the Michigan Hi-Pilot Bunsen burner [56–58]. Schematics of these burners are shown in Fig. 4. Both burners involve central jets issuing into large co-flows containing

[4]Both jet and Bunsen flames involve a jet of reactants issuing from a nozzle. The difference between the two is that the turbulence that interacts with the flame in the jet configuration arises due to shear between the jet fluid and surroundings, whereas the turbulence that is meant to interact with a Bunsen flame is generated upstream of the reactants exiting the nozzle.

the products of the pilot flames. The pilots are meant to both stabilize the flame and isolate the reactants from the surrounding ambient air. In order to achieve high Karlovitz numbers, the jets are often operated fuel lean, whereas the pilots are operated at richer conditions to enhance stability.

Recently, the thermochemical structures of the LUPJ and Hi-Pilot burners have been assessed through DNS and Raman scattering measurements, respectively [59, 65]. At conditions where the the jet and pilot were at different equivalence ratios, rapid turbulence-induced mixing of the pilot and jet fluids drastically altered the composition of the reaction zones compared to what would occur purely from combustion of the reactants. For example, Fig. 5 shows the probability density function (PDF) of the measured atom-based equivalence ratio conditioned on fluid being in the primary reaction zone of the flame (taken to be $0.7 \leq c \leq 0.8$) [59]. The jet fluid was at $\phi = 0.65$ and the pilot was at $\phi = 0.90$. Figure 6 shows similar PDFs of the local equivalence ratio and conditionally-averaged heat release rates at different heights above the LUPJ burner from the DNS [65]. These figures clearly demonstrate that the reaction zone composition was not that of the jet, but a mixture of jet and pilot fluid. No evidence of local extinction was found in either the DNS or experiments, demonstrating that these flames are simultaneously mixing in surrounding fluid while burning; such flames are better classified as "stratified" than premixed.

It is therefore apparent that configurations that do not isolate the flame of interest from the ambient environment, or that isolate it using a thermochemically mismatched pilot, present challenges for analysis. That is, the effective composition that is burning in these flames is not entirely determined by the intended reactant flow. Instead, these flames are stratified by mixing of the surrounding fluid into the flame structure.

A major implication of this observation is that the chemical scales used to characterize the flames, place them on regime diagrams, normalize the turbulent burning velocity, etc. (see Sections 2.4 and 2.5), may not actually be characteristic of the chemistry occurring in the flame. Caution therefore must be applied when interpreting such results and comparing results across configurations. It is recommended that future configurations used to study highly turbulent flames be either isolated from the ambient environment or have large co-flow

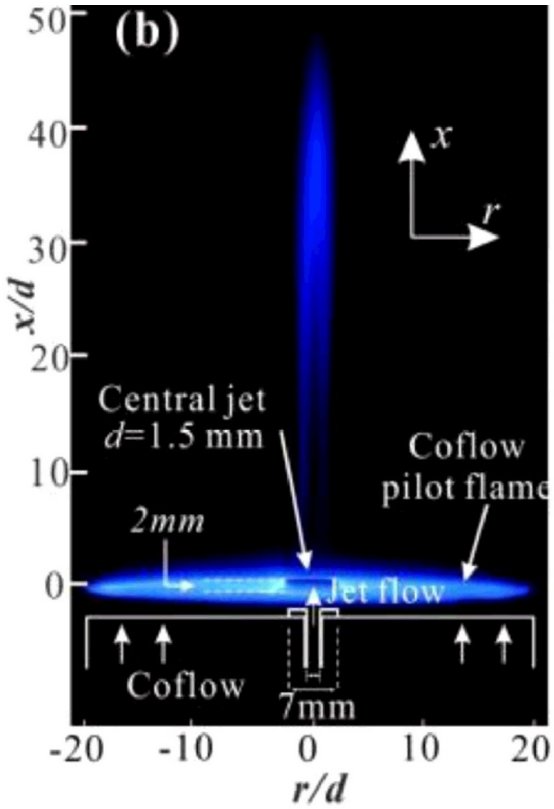

(a) Lund piloted premixed jet burner.

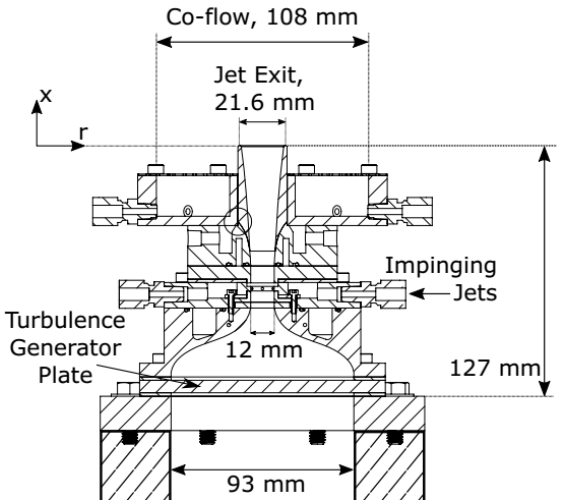

(b) Hi-Pilot Bunsen burner.

Figure 4: Example piloted flame configurations. Reprinted from Refs. [47] and [56] with permission of Elsevier.

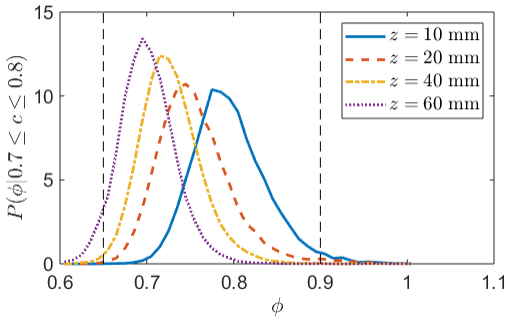

Figure 5: PDFs of the local measured equivalence ratio in the reaction zone (taken as $0.7 \leq c \leq 0.8$) at various axial locations above the exit of the Hi-Pilot burner. The premixed reactants are at $\phi = 0.65$ and the pilot flame has $\phi = 0.90$. Reprinted from Ref. [59] with permission of Elsevier.

pilots that are thermochemically matched to the reactants.

Contrary to the experimental configurations, the most popular computational configurations for DNS include the freely propagating planar flame (e.g., [66–71]) and expanding flame kernels (e.g., [72–76]), with the rare exception of piloted jet flames [77–79] and Bunsen flames [80]. The choice of configuration is mostly limited by the target range of dynamic scales (i.e., Re_ℓ), computational cost, complexities of boundary conditions, and robustness in numerical implementations. Direct comparisons with experiments have begun to emerge in recent years [81]. However, most DNS remain as theoretical tools to study the underlying governing physics or to extract *a priori* information for SFS modeling in LES or closure models for Reynolds averaged Navier Stokes (RANS) simulations.

With an estimated integral length-scale of approximately one-eighth the constraining dimension of the computational domain [82], the attainable integral length-scales of current DNS studies are still quite limited compared to laboratory-scale experiments; most DNS studies of highly turbulent flames have a computational domain of $\mathcal{O}(1 - 10$ mm). This also implies that the impact of large-scale motion, such as that seen in experimental investigations [56], is challenging to capture using DNS.

The most common remedy to create the desirable turbulence statistics in DNS include various schemes of numerical forcing or spectral nudging [66, 67, 83], which introduces modeling elements into DNS. Numerical forcing has also been employed to maintain statistically

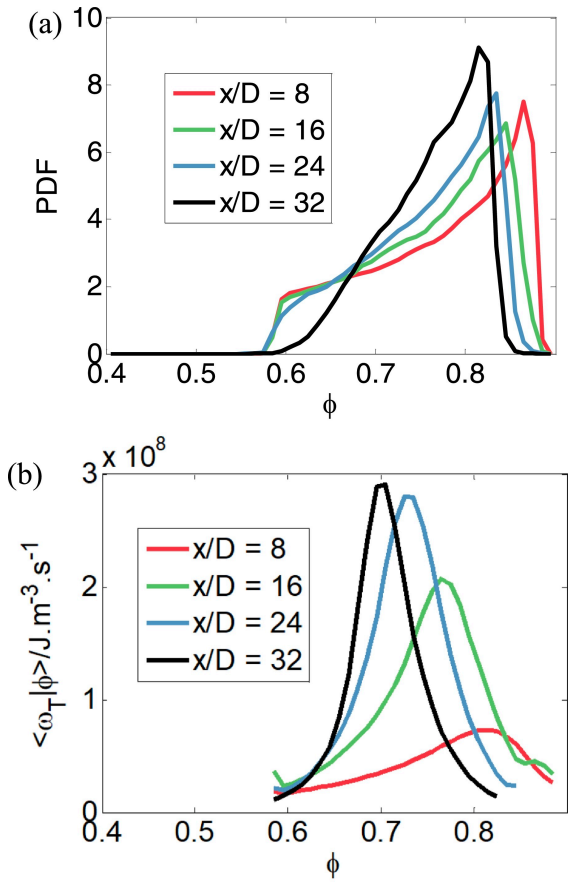

Figure 6: (a) PDFs of the equivalence ratio and (b) heat release rate conditionally averaged on the equivalence ratio at different heights above the LUPJ burner from DNS. Reprinted from Ref. [65] with permission of Elsevier.

steady-state turbulence (i.e., to compensate the decay of turbulence due to dissipation), although subtleties require extra caution whenever flames exist [84]. In addition to forcing, another category of treatment feeds the inlet of the computational domain with auxiliary homogeneous isotropic turbulence superimposed on a mean velocity field, leveraging Taylor's hypothesis [85]. The mean velocity field is often adjusted, based on the turbulent burning rate, to maintain a statistically stationary flame in space.

Recently, DNS has progressed beyond single-step global chemical models, with more studies employing reduced or skeletal chemical kinetic models, leveraging recent developments in compact kinetic models [20–22]. Carefully calibrated chemical kinetic models can account for the response to strain and curvature, as well as differential diffusion, more realistically.

Consequently, fuel-specific differential diffusion or pyrolysis effects can be studied [66, 69, 86]. Moreover, in the regime of highly turbulent premixed flames, the competition between elementary reactions becomes more prominent [87], which can lead to local or global limit conditions such as extinction [76]. It should be noted that DNS with global chemical kinetic models has the distinct advantage of readily enabling parametric studies, which can be particularly suitable to investigate problems involving scaling [71]. However, this review focuses mostly on studies with more detailed descriptions of chemistry, since the impact of turbulence on chemistry is of particular interest here.

2.4. Turbulent flame characterization

One goal of understanding the physics and chemistry of turbulent flames is the ability to predict *a priori* what flame structures will occur based on a few characteristic parameters, as this can inform proper model selection. Indeed, considerable research effort has been devoted to correlating characteristic dimensionless parameters with observed flame structures [8, 11]. Traditionally, the focus has been on whether certain scalar fields are observed to be "broadened" relative to a laminar counterpart, the correlation of different scalars relative to laminar flames, or the correlation of scalars and scalar gradients (see Section 3 for a detailed discussion). This section reviews some of the basic principles used to characterize turbulent flames, highlights challenges with this characterization, discusses recent attempts to classify turbulent flames into regimes, and presents some suggestions for future regime classifications. Open questions from this Section (and Section 2.5) motivate the discussion of flame thermochemistry and turbulence dynamics in Sections 3 and 4.

2.4.1. Characteristic scales and dimensionless parameters

Turbulent fluid motions are characterized by a wide range of scales, from the larger integral scales (i.e., length-scale ℓ, time-scale $\mathcal{T}$, and velocity-scale u_ℓ) where kinetic energy input occurs, to the Kolmogorov microscales (i.e., length-, time-, and velocity-scales λ_K, τ_K, and u_K, respectively) where kinetic energy is dissipated into heat by viscous processes. The integral length- and time-scales for a particular quantity are defined based on the integral under the autocorrelation function for that quantity in either space or time, with $u_\ell \equiv \ell\mathcal{T}^{-1}$.

Physically, these scales indicate the spatial and temporal extents required for turbulent fluctuations to become de-correlated, or de-coherent. There are different integral scales for different flow properties and spatial autocorrelation directions, as well as for different locations in the flow. However, for the purposes of characterizing turbulence/flame interactions, the integral length-scale is often represented by some large-scale geometric feature of the system, such as a nozzle diameter, shear layer width, or DNS domain size. The integral velocity-scale is often approximated as $u_\ell \approx (u_i' u_i')^{1/2}$, where $(\cdot)'$ represents a fluctuation about an appropriately defined mean.[5]

The Kolmogorov scales are defined based on dimensional arguments in constant density turbulence as

$$\lambda_\mathrm{K} = \left(\frac{\nu^3}{\varepsilon}\right)^{1/4}, \; \tau_\mathrm{K} = \left(\frac{\nu}{\varepsilon}\right)^{1/2}, \; u_\mathrm{K} = (\nu\varepsilon)^{1/4} \tag{8}$$

where ν and ε are the local values of the kinematic viscosity and mean kinetic energy dissipation rate, respectively. It should be noted that the Kolmogorov scales are defined statistically. This presents challenges in turbulent flames, wherein the local temperature at a point (and hence viscosity) can fluctuate widely as the flame structure moves across the point. As such, the Kolmogorov scales computed from mean properties at a point may not be representative of the turbulence with which the flame interacts at any instant in time (see, e.g., [67, 84, 88]). Physically, the Kolmogorov length-scale is proportional to the scale at which the effects of viscous diffusion and turbulent straining on the evolution of the velocity field balance. When characterizing a particular experiment or simulation, turbulence is often described at a user-selected location in the reactants where $\nu = \nu_\mathrm{r}$ is a constant.

The integral and Kolmogorov length-scales are related by $\ell/\lambda_\mathrm{K} = c_\mathrm{K}\mathrm{Re}_\ell^{3/4}$ where $\mathrm{Re}_\ell = u_\ell \ell/\nu$ is the integral-scale Reynolds number and c_K is an $\mathcal{O}(1)$ constant. Hence, for high Reynolds number turbulence (i.e., $\mathrm{Re}_\ell \ggg 1$), there is a large range of scales in the flow. In contrast, a laminar flame involves steep gradients over a relatively small range of scales, corresponding to one order of magnitude between the characteristic length-scale of rapid

[5]We will interpret the mean as an ensemble mean taken over a large number of realizations of nominally identical simulations/experiments, even if spatial or temporal means are employed in practice.

exothermic reactions ($\delta_{\rm r}^0$) and the overall thermal structure of the flame (i.e., $\delta_{\rm L}^0 = \mathcal{O}(10\delta_{\rm r}^0)$) in hydrocarbon/air flames.

Common practice is to construct dimensionless groups characterizing turbulence/flame interactions based on (a) the ratio of the integral velocity-scale to laminar flame speed $u_\ell/s_{\rm L}^0$; (b) the ratio of the integral length-scale to flame thermal thickness $\ell/\delta_{\rm L}^0$; (c) the ratio of flame time-scale to Kolmogorov time-scale,[6] which defines a Karlovitz number ${\rm Ka}_{\delta,{\rm K}} = \tau_\delta/\tau_{\rm K}$; and (d) the ratio of the integral time-scale to flame time-scale, which defines a Damköhler number ${\rm Da}_{\ell,\delta} = \mathcal{T}/\tau_\delta$. Based on dimensional arguments, $s_{\rm L}^0 = c_s\bar{\alpha}/\delta_{\rm L}^0$, where $c_{\rm s}$ is a scaling factor and $\bar{\alpha}$ is an appropriate thermal diffusivity. Hence, the resulting dimensionless groups can be written as

$$ {\rm Ka}_{\delta,{\rm K}} = \left(\frac{\delta_{\rm L}^0}{\lambda_{\rm K}}\right)^2 \frac{\nu_{\rm r}}{\bar{\alpha}c_{\rm s}}\,, \tag{9} $$

$$ {\rm Da}_{\ell,\delta} = \left(\frac{\ell}{\delta_{\rm L}^0}\right)^2 \frac{\bar{\alpha}c_{\rm s}}{\nu_{\rm r}} {\rm Re}_\ell{}^{-1}\,, \tag{10} $$

$$ {\rm Re}_\ell = c_{\rm K}^{-4}{\rm Ka}_{\delta,{\rm K}}{}^2{\rm Da}_{\ell,\delta}{}^2\,. \tag{11} $$

We note that $\bar{\alpha}$ can be manually selected for a given flame such that $c_{\rm s} = 1$ [58, 89]. Peters [89] recommends that it should correspond to the diffusivity in the "inner reaction layer" for atmospheric methane/air flames, at a temperature between 1600-2000 K. Alternatively, one may define $\bar{\alpha}$ at the mean temperature between the reactants and products, at the peak of the heat release rate, or at some other point. We therefore choose to explicitly leave $c_{\rm s}$ as a variable in these equations.

As is common practice, we have chosen to characterize the turbulence in the reactants. Hence, ${\rm Re}_\ell$ is measured based on u_ℓ, ℓ, and $\nu = \nu_{\rm r}$ in the unburnt reactants. The group $\nu_{\rm r}\left(\bar{\alpha}c_{\rm s}\right)^{-1} = \nu_{\rm r}\left(s_{\rm L}^0\delta_{\rm L}^0\right)^{-1}$ is often taken to be unity. That is, the kinematic viscosity in the reactants is taken to be equal to the characteristic thermal diffusivity, which may be determined at the peak of the heat release rate. However, laminar flame calculations indicate that $\nu_{\rm r}\left(s_{\rm L}^0\delta_{\rm L}^0\right)^{-1}$ is between 0.1 and 0.2 for hydrocarbon/air flames.

[6] The definition of Karlovitz number based on $\tau_{\rm K}$ and Damköhler number based on $\mathcal{T}$ is historical. One could equally define ${\rm Da}_{{\rm K},\delta} = {\rm Ka}_{\delta,{\rm K}}{}^{-1}$ and ${\rm Ka}_{\delta,\ell} = {\rm Da}_{\ell,\delta}{}^{-1}$.

Furthermore, c_{K} is often taken to be unity, whereas many measurements show that $c_{\mathrm{K}} \approx 0.5$ and, hence, $c_{\mathrm{K}}^{-4} \approx 16$ [90–93]. Nevertheless, Karlovitz and Damköhler numbers based on Eqs. (9) and (10) are often reported with unity factors. Moreover, due to the difficulty in measuring λ_{K}, experiments may use Eq. (11) to estimate the Karlovitz number, again with a unity factor. While we do not advocate that $c_{\mathrm{K}} \approx 0.5$ is a fundamental result that should be used universally moving forward, the resultant order-of-magnitude ambiguity mandates that caution be taken where comparing turbulence conditions across different studies and that the method of computing $\mathrm{Ka}_{\delta,\mathrm{K}}$ be clearly reported. Recommendations on the latter are provided below.

It is useful to describe how the Karlovitz and Damköhler numbers vary with the physical operating parameters of a combustor. To this end, these dimensionless groups can be re-written as

$$\mathrm{Ka}_{\delta,\mathrm{K}} = c_{\mathrm{K}}^2 \overbrace{\left(\frac{u_\ell^{3/2}}{\ell^{1/2}}\right)}^{I_{\mathrm{Ka}}} \overbrace{\left(\frac{\delta_{\mathrm{L}}^0}{s_{\mathrm{L}}^0}\frac{1}{\nu_{\mathrm{r}}^{1/2}}\right)}^{II_{\mathrm{Ka}}}, \tag{12}$$

$$\mathrm{Da}_{\ell,\delta} = \underbrace{\left(\frac{\ell}{u_\ell}\right)}_{I_{\mathrm{Da}}} \underbrace{\left(\frac{s_{\mathrm{L}}^0}{\delta_{\mathrm{L}}^0}\right)}_{II_{\mathrm{Da}}}. \tag{13}$$

The I-quantities represent terms that depend on the flow conditions and geometry (e.g., the bulk velocity, turbulence generation, and scale) of the system. These terms can be varied independently of the II-quantities, which depend on the thermodynamic state and chemical composition (e.g., the reactant pressure, temperature, and composition) in a complex manner.

Figure 7 shows how II_{Ka} and II_{Da} vary with pressure, reactant temperature, and equivalence ratio for n-dodecane/air flames. High Karlovitz numbers are associated with lower reactant temperatures, lower equivalence ratios, and higher pressure, with the largest sensitivity to preheat temperature. Unsurprisingly given the definitions of II_{Ka} and II_{Da}, high Damköhler numbers follow a generally opposite trend, being associated with higher temperatures and higher equivalence ratios. However, II_{Da} also increases with pressure due to the lack of dependence on kinematic viscosity, as compared to II_{Ka}.

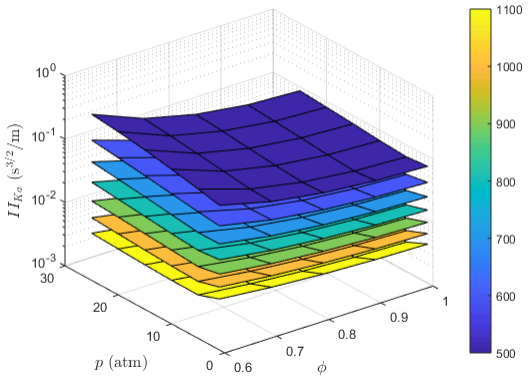

(a) II_{Ka}

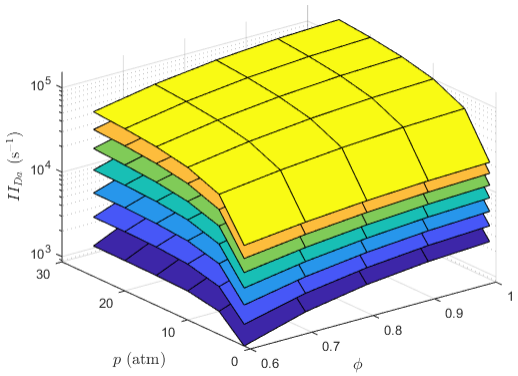

(b) II_{Da}

Figure 7: Variation of II_{Ka} and II_{Da} from Eqs. (12) and (13), respectively, with pressure, equivalence ratio, and preheat temperature (indicated by different colors, with the colorbar in (a) giving T in units of K) in unstretched laminar n-dodecane/air flames.

This analysis demonstrates a natural mitigation of extremely high Karlovitz numbers and low Damköhler numbers in terrestrial systems of engineering relevance. That is, adiabatic compression is associated with simultaneous increases in both pressure and temperature. Figure 8 shows how II_{Ka} and II_{Da} vary with isentropic compression up to 25 atm for a fixed equivalence ratio n-dodecane/air flame. The Karlovitz and Damköhler number responses are dominated by the temperature dependence, decreasing and increasing, respectively, as the temperature and pressure increase.

It should be noted that, under the assumption that $\nu_{\mathrm{r}} \approx s_{\mathrm{L}}^0 \delta_{\mathrm{L}}^0$, knowledge of any two of

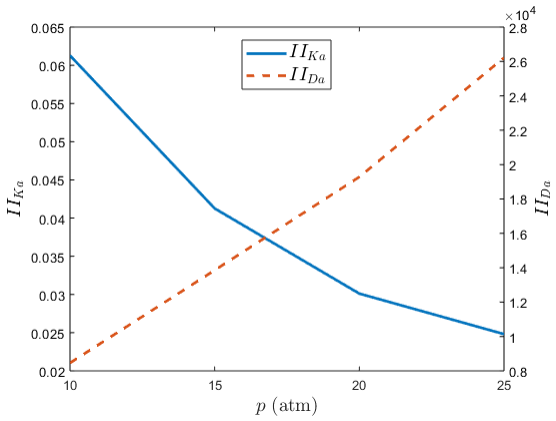

Figure 8: Variation of II_{Ka} and II_{Da} during isentropic compression for an n-dodecane/air flame at $\phi = 0.8$.

the aforementioned dimensionless parameters (i.e., u_ℓ/s_{L}^0, $\ell/\delta_{\mathrm{L}}^0$, $\mathrm{Ka}_{\delta,\mathrm{K}}$, $\mathrm{Da}_{\ell,\delta}$, or Re_ℓ) uniquely defines all other parameters. Furthermore, under this condition and with $c_{\mathrm{K}} = 1$, Eq. (12) can be written in the popular form

$$\mathrm{Ka}_{\delta,\mathrm{K}} = \left(\frac{u_\ell}{s_{\mathrm{L}}^0}\right)^{3/2} \left(\frac{\delta_{\mathrm{L}}^0}{\ell}\right)^{1/2} . \tag{14}$$

It is interesting to note that Eqs. (12) and (14) differ by a factor of $c_{\mathrm{K}}^2(s_{\mathrm{L}}^0\delta_{\mathrm{L}}^0/\nu_{\mathrm{r}})^{1/2}$, which has an $\mathcal{O}(1)$ value. Hence, through a convenient cancellation of factors, Karlovitz numbers calculated by these two equations will be approximately equal. However, this may differ by a factor of $\mathcal{O}(10)$ compared to calculations based on Eq. (9), depending on how λ_{K} is calculated and whether $\nu_{\mathrm{r}}/(\bar{\alpha}c_{\mathrm{s}})$ is taken to be unity. *For consistency, it is thus recommended that Eq.* (14) *be used when reporting Karlovitz numbers.*

Finally, we note that turbulent flames are generally characterized at a single point, often in the unburnt reactants at the exit of a nozzle or inlet of a DNS domain. However, practical flames exhibit widely varying turbulence properties with position. Furthermore, local flame structures may not correlate directly with local turbulence due to the finite interaction time and advection parallel to the flame surface [78, 79, 94]. These issues are discussed more in Section 2.4.2.

2.4.2. Expected parameters for highly turbulent flames

Theoretical expectations regarding the parameter space at which different flame structures occur are graphically expressed using regime diagrams. The two most popular regime diagrams are those proposed by Williams [95] and by Borghi [96], which was later modified by Peters [2]; for compactness, we will refer to the former as the "Williams" diagram and the latter as the "Borghi/Peters" diagram. The former uses Re_ℓ and $\mathrm{Da}_{\ell,\delta}$ as abscissa and ordinate measures, respectively. The latter uses ℓ/δ_L^0 and u_ℓ/s_L^0. As mentioned above, in the case of premixed combustion and assuming $c_\mathrm{K} = \nu_\mathrm{r}\left(\overline{\alpha}c_\mathrm{s}\right)^{-1} = 1$, any two dimensionless groups establish the other groups; the two diagrams are conceptually equivalent in this case, though different regime labels are traditionally used[7].

The regime diagrams are shown in Fig. 9, with some significant lines and regime labels indicated. The points shown in Fig. 9 correspond to typical operating conditions of gas turbine main combustors, gas turbine afterburners, and ramjet engines, which are summarized in Table 1 and described in more detail below. Note that the Borghi/Peters diagram typically includes lines at constant values of $\mathrm{Ka}_{\delta,K}$, whereas the Williams diagram shows lines at constant $\lambda_\mathrm{K}/\delta_\mathrm{L}^0$. However, under the assumptions above, $\mathrm{Ka}_{\delta,\mathrm{K}} = \left(\lambda_\mathrm{K}/\delta_\mathrm{L}^0\right)^2$ (see Eq. (9)) and lines are labeled as constant $\mathrm{Ka}_{\delta,K}$ on both diagrams.

The line $\mathrm{Ka}_{\delta,\mathrm{K}} = 1$ is known as the Klimov-Williams (K-W) condition [95, 97, 98], which represents $\lambda_\mathrm{K} = \delta_\mathrm{L}^0$ and $u_\mathrm{K} = s_\mathrm{L}^0$. Hence, at such conditions, the Kolmogorov scale in the reactants is smaller than the thermal thickness of the flame and the magnitude of the associated velocity fluctuations is greater than the laminar flame speed. The flame is expected to retain the internal structure of a laminar flame, corresponding to thin "reaction sheets" or "flamelets", which is supported by numerous studies [8].

The main focus of this review is on turbulence intensities well above the K-W criterion, i.e. $\mathrm{Ka}_{\delta,K} \gg 1$, where the internal flame structure and turbulence mutually interact in complicated ways. Indeed, the parameter space beyond the K-W criterion is described differently in the different regime diagrams. In the Borghi/Peters diagram, an additional

[7]The Williams diagram also describes non-premixed combustion.

line is drawn at $\mathrm{Ka}_{\delta,\mathrm{K}} = 100$, corresponding to $\lambda_\mathrm{K} = 0.1\delta^0_\mathrm{L}$; in methane/air flames this gives $\lambda_\mathrm{K} \approx \delta^0_\mathrm{r}$. That is, the Kolmogorov length-scale (in the reactants) is smaller than $1/10^{\mathrm{th}}$ the laminar flame thermal thickness, which is the approximate thickness of the exothermic reaction layer in laminar methane/air flames. Correspondingly, the Kolmogorov time-scale (in the reactants) becomes shorter than the characteristic reaction time-scale. This boundary has been proposed as the lower limit at which turbulence would modify the "reaction zone" structure of a methane/air flame. The region $1 \lesssim \mathrm{Ka}_{\delta,\mathrm{K}} \lesssim 100$ is proposed to have flames exhibiting broadening of the "preheat zone", but not the "reaction zone". Note that this boundary does not account for any affect of the flame on the turbulence (Section 4)

Williams [28] does not specify a label for the parameter space immediately beyond $\mathrm{Ka}_{\delta,K} > 1$, but does propose a regime of "distributed reactions" or "stirred reactors" at $\ell/\delta^0_\mathrm{L} < 1$, corresponding to Damköhler's second hypothesis regarding small-scale turbulence [99]. We note that the intervening parameter space is sometimes labelled "flamelets in eddies", following a modification to the Williams diagram by Turns [100]. Furthermore, Williams [101] adds additional lines and labels corresponding to the "thin reaction zone" and "broken flamelet" regimes in the Borghi/Peters diagram.

Section 2.4.3 discusses limitations of—and recent proposed modifications to—regime diagrams and regime boundaries. Nevertheless, regardless of these limitations, it is instructive to demonstrate where some typical combustion systems—in which "highly turbulent" flames may be expected—operate in terms of the regime diagram. Hence, for illustrative purposes, we consider a gas turbine combustor, afterburner, and ramjet. In every case, the fuel is represented as n-dodecane. While other fuels could be considered (e.g., more realistic jet fuels, methane, hydrogen, etc.), we do not expect a qualitative change in the parameter space encompassed on the regime diagrams[8]. In the gas turbine combustor and ramjet, the fuel is mixed with fresh air; in the afterburner, fuel is mixed with appropriately diluted combustion products. Even though these devices would be partially premixed in reality, we represent them as perfectly premixed. We take 10 mm $\leq \ell \leq$ 20 mm to represent a

[8]Hydrogen may shift the parameter space to lower Karlovitz numbers for the flows specified here, but may also accommodate higher flow speeds.

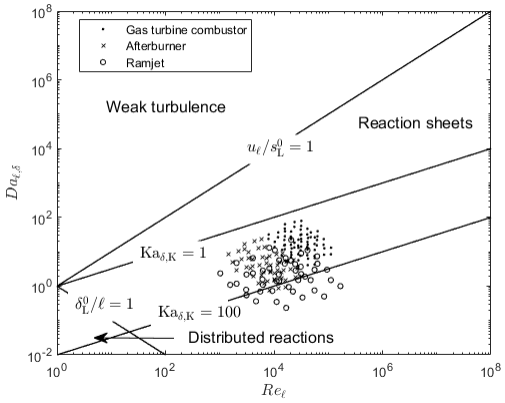

(a) Regime diagram of Williams [95]

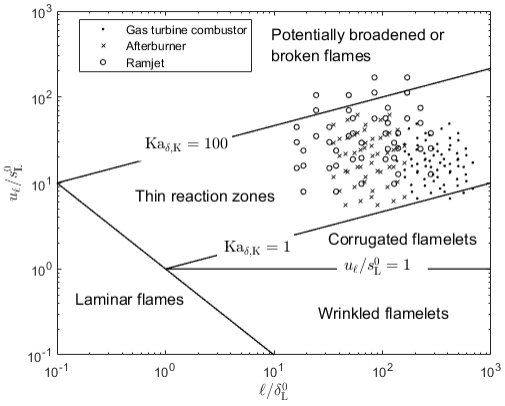

(b) Regime diagram of Borghi [96] and Peters [2]

Figure 9: Regime diagrams with estimated conditions for various engines.

characteristic integral scale in each device. The other properties used in these calculations are provided in Table 1 and are based on typical approximate operating parameters, e.g., Ref. [102].The specific operating points shown in Fig. 9 are taken from a uniform sampling of conditions over the range shown in the table. While other parameters could be selected, they are not expected to make qualitative changes to the results. We note that there is a minor discrepancy between the location of the engine points relative to the constant $\mathrm{Ka}_{\delta,\mathrm{K}}$ lines in Fig. 9(a) versus Fig. 9(b). This arises because Re_ℓ is calculated using ν_r, whereas the constant $\mathrm{Ka}_{\delta,\mathrm{K}}$ lines are calculated assuming that ν_r is equal to both the molecular and thermal diffusivity.

Table 1: Properties used for calculation of engine conditions. All calculations used n-dodecane fuel and 10 mm $\leq \ell \leq$ 20 mm. All parameters are based on approximate typical operation, e.g. portions of the inflow condition range specified in Ref. [102].

	p (bar)	T_r (K)	ϕ	u_ℓ (m/s)
Gas turbine combustor	$10 \leq p \leq 20$	$500 \leq T_\mathrm{r} \leq 700$	$0.7 \leq \phi \leq 0.8$	$5 \leq u_\ell \leq 15$
Afterburner	$2 \leq p \leq 4$	$900 \leq T_\mathrm{r} \leq 1100$	$0.7 \leq \phi \leq 0.8$	$10 \leq u_\ell \leq 40$
Ramjet	$1 \leq p \leq 5$	$500 \leq T_\mathrm{r} \leq 900$	0.7	$20 \leq u_\ell \leq 60$

The majority of the conditions lie between $1 \leq \mathrm{Ka}_{\delta,\mathrm{K}} \leq 100$. No conditions approach the range $\mathrm{Ka}_{\delta,\mathrm{K}} > 1000$. All configurations have $\ell \gg \delta_\mathrm{L}^0$ and, therefore, do not approach the distributed reaction regime predicted by Williams. Such conditions would require very broad flames (e.g., low pressures or highly diluted preheated reactants) and/or small integral scales. Combustion of highly diluted premixed reactants is associated with moderate or intense low-oxygen dilution (MILD), flameless, or colorless combustion systems, which are reviewed elsewhere [103, 104]. The focus here is largely on combustion in the parameter space around the points shown in Fig. 9, though we also include some studies at higher $\mathrm{Ka}_{\delta,\mathrm{K}}$ and lower ℓ/δ_L^0, which may be of interest to devices not considered in Fig 9.

2.4.3. Comments on regimes

Despite the placement of the various points on the regime diagrams, it is not clear that the parameters employed or the lines drawn are sufficient to fully characterize the mutual interactions between turbulence and flames for several reasons. This section discusses these issues and recent results, and provides some recommendations on the use of regimes and regime diagrams.

To begin, a comment is warranted regarding lines based on $\mathrm{Ka}_{\delta,\mathrm{K}}$ or λ_K. The Kolomogrov length-scale is obtained purely from dimensional arguments. However, measurements and simulations in constant density turbulent flows have shown that the actual observed smallest scales (denoted λ_ν due to their connection to the kinematic viscosity ν) are proportional to λ_K, but several times larger (values in the range of $\lambda_\nu \approx 5\lambda_\mathrm{K}$ are often reported) [90–

93]. Such a difference would significantly impact the parameter space at which different regimes/behaviors are expected. For example, if the K-W condition is modified to be $\lambda_\nu \leq \delta_{\mathrm{L}}^0$ with $\lambda_\nu \approx 5\lambda_{\mathrm{K}}$, this would indicate that modification of the flame structure could be expected around $\mathrm{Ka}_{\delta,\mathrm{K}} \approx 25$. Furthermore, if $c_{\mathrm{K}} = 0.5$, this would be $\mathrm{Ka}_{\delta,\mathrm{K}} \approx 50$. If $\nu_{\mathrm{r}} \left(s_{\mathrm{L}}^0 \delta_{\mathrm{L}}^0\right)^{-1} \approx 0.2$, this would instead correspond to $\mathrm{Ka}_{\delta,\mathrm{K}} \approx 5$ or 10. Similar to the K-W criterion, it can be argued that the effects of small scale turbulence on the reaction zone structure should occur at considerably higher Karlovitz numbers than $\mathrm{Ka}_{\delta,\mathrm{K}} = 100$ because $\lambda_\nu > \lambda_{\mathrm{K}}$. The purpose of this discussion is not to propose moving the K-W line to $\mathrm{Ka}_{\delta,\mathrm{K}} = 5$, 25, or some other number, but simply to highlight a potential order-of-magnitude disagreement between the physical reasoning behind some regime boundaries and the practical realization of the effects in experiments and simulations. One, therefore, should not be surprised when experimental or DNS results do not show transitions between regimes at the conditions predicted by the theoretical arguments underlying regime diagrams (or even within an order of magnitude).

In addition to this ambiguity, it is not clear that turbulence characterized at a single point (typically in the reactants) is sufficient to predict a combustion regime, for several reasons. Practical combustion devices exhibit considerable variation in both turbulence conditions and flame structures. For example, Fig. 10(a), shows how u_ℓ/s_{L}^0, $\ell/\delta_{\mathrm{L}}^0$, and $\mathrm{Ka}_{\delta,\mathrm{K}}$ vary with downstream distance (x/D) in DNS of a highly turbulent jet flame in the LUPJ configuration [78, 79, 94]. The local values of $\mathrm{Ka}_{\delta,\mathrm{K}}$ decrease with downstream distance, which would indicate a decreased effect of small-scale turbulence. However, the visual appearance of the scalar fields (see Fig. 10(b)) indicates the opposite, with increased corrugation and broadening of the CH_2O contours with downstream distance. The scalar fields observed in the DNS are consistent with experiments of the same configuration [47, 48]. Hence, using a single value of dimensionless parameters to characterize a practical turbulent flame is insufficient and the local flame structure may not reflect the local characteristics of the turbulent flow.

It is worth noting that the apparent broadening of the CH_2O regions at downstream locations in Fig. 10(b) involves both the effects of local turbulence and the advection of turbulence-influenced CH_2O from further upstream (which has also been affected by the

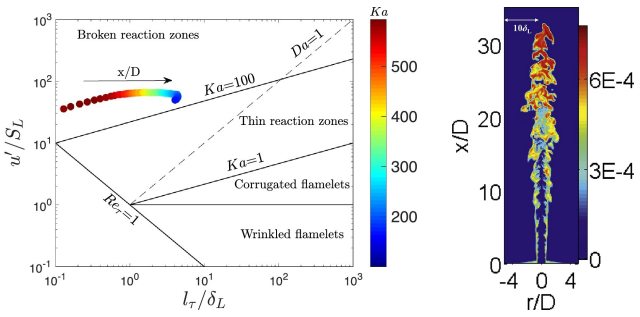

(a) Variation of local conditions with downstream position.

(b) Typical instantaneous CH_2O field.

Figure 10: Results from DNS of a highly turbulent jet flame showing an inverse relationship between the local conditions and physical appearance of the flame. Reprinted from Refs. [94] and [79] with permission of Elsevier.

turbulence). Since the jet flow speed in these flames is much higher than the laminar flame speed, the turbulence and flame simultaneously advect a considerable distance downstream before turbulence in the reactants passes into the products. Near the flame base, the turbulence and flame have not interacted for long and the flame retains a laminar-like structure; towards the flame tip, the flame has "consumed" more turbulence. Hence, the flame structure observed at higher axial locations may be more consistent with the expected consequence (i.e., flame structure) arising from the turbulence/flame interactions than near the flame base. This is somewhat analogous to the temporal evolution of a laminar flame initial condition to the fully turbulent state during DNS of planar flames, which requires a certain number of flow-through times to establish the statistically steady flame structure.

Moreover, the traditional turbulence characterization does not account for the influence of the flame on the turbulence or the detailed distribution of kinetic energy amongst scales in turbulence (see Section 4 for a detailed discussion). Several researchers have introduced new parameters or modifications to regime diagrams to account for these effects. For example, Lapointe *et al.* [67] propose to use a "reaction zone" Karlovitz number—based on the Kolmogorov scale in the reaction zone and 1–2 orders of magnitude lower than $\mathrm{Ka}_{\delta,\mathrm{K}}$ due to the increased viscosity—to characterize whether turbulence will disrupt the inner flame struc-

ture. Aspden *et al.* [105] argue that, at sufficiently high Karlovitz numbers ($\mathrm{Ka}_{\delta,\mathrm{K}} \gg 100$), λ_K scale structures are too small compared to the thermochemical gradients to enhance mixing. Instead, a metric is proposed that is similar to a Karlovitz number, but uses the turbulence time-scale at δ_L^0.

Recent evidence, reviewed by Driscoll *et al.* [11], also has brought into question the conventional regime diagrams and boundaries. In particular, they indicate that experiments and DNS at $\mathrm{Ka}_{\delta,\mathrm{K}} \geq 1$ may or may not exhibit preheat zone broadening, depending on Re_ℓ. This is demonstrated in Fig. 11 from Skiba *et al.* [58], which shows that $\mathrm{Ka}_{\delta,\mathrm{K}} \geq 1$ is necessary but not sufficient for broadening of the preheat zone to occur. In the experimental data, the division between broadened preheat zones/thin reaction zones (BP-TR) and thin flamelets requires an effective "turbulent diffusivity" ($\mathcal{D}_\mathrm{T}$) of 180 times the characteristic molecular diffusivity ($\mathcal{D}^*$). Based on scaling arguments, Driscoll *et al.* [11] proposed that this corresponds to a boundary of $\mathrm{Re}_\ell \gtrsim 2800$ and that this value was necessary to observe preheat layer broadening (this value assumes unity scaling factors in all relationships). However, the DNS studies in Fig. 11 indicate broadened preheat zones for lower $\mathcal{D}_\mathrm{T}/\mathcal{D}^*$, but only at $\mathrm{Ka}_{\delta,\mathrm{K}} \gtrsim 60$. We note that "turbulent diffusivity" is a modeling concept that is meant to statistically reflect the increased molecular mixing rate generated by turbulence; it is not a physical process affecting the instantaneous dynamics of velocity or scalar according to Eqs. (1)-(4).

Broadened reactions are observed for DNS and some experiments, although other experiments do not observe broadened reactions at similar Karlovitz numbers. In particular, broadened reactions in Fig. 11 (black and blue stars) occur at smaller ℓ/δ_L^0 than the experimental BP-TR points at similar Karlovitz numbers (filled red squares). The majority of the black stars were obtained in the LUPJ burner with $\ell/\delta_\mathrm{L}^0 \lesssim 10$ [47], whereas the red dots were obtained in the Michigan Hi-Pilot burner with $\ell/\delta_\mathrm{L}^0 \gtrsim 10$ [58]. Indeed, broadened reactions occur for $\mathrm{Da}_{\ell,\delta} \lesssim 1$ and BP-TR occur for $\mathrm{Da}_{\ell,\delta} \gtrsim 1$, at least to $\mathrm{Ka}_{\delta,\mathrm{K}} \approx 550$ in the Hi-Pilot burner. We note that the DNS and experimental cases with broadened reactions were omitted from the regime diagram in Driscoll *et al.* [11], although the other data in Ref. [11] is identical to that of Skiba *et al.* [58].

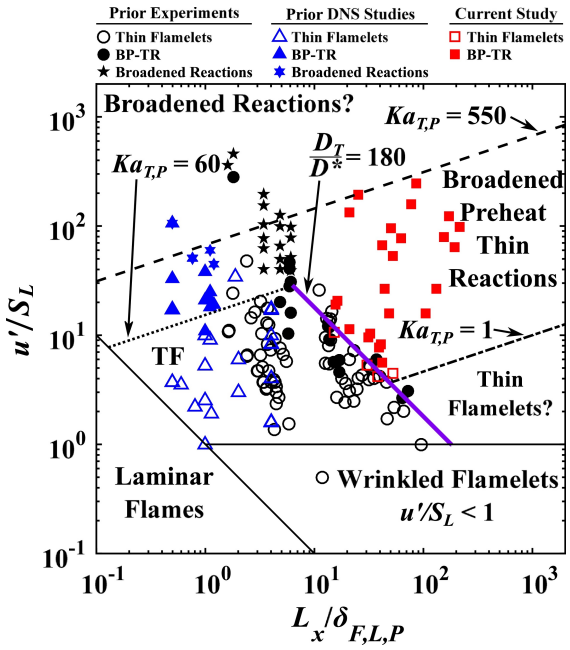

Figure 11: Regime diagram compiled by Skiba *et al.* [58]. 'BP-TR' indicates that broadened preheat zones and thin reactions were observed. Reprinted from Ref. [58] with permission of Elsevier.

As a final comment, the terms "broadened preheat", "thin reaction", "broadened reaction", etc. in the Borghi/Peters diagram are somewhat limiting. These terms apply most readily to flames that posses a relatively broad and inert preheat zone, followed by a thin reaction zone. Figure 2 demonstrates that this structure is most relevant to flames for relatively simple hydrocarbon fuels (e.g., CH_4); hydrogen flames possess an exothermic structure throughout, whereas large hydrocarbon flames possess an endothermic fuel pyrolysis zone coincident with the "preheat" zone. The Williams diagram avoids these issues by not prescribing labels to the parameter space between flame sheets and broadened reactions.

More broadly applicable labels could be applied to the various regions of the regime diagrams. As mentioned above and discussed in more detail in Sections 3 and 4, a laminar-like flame structure implies a correlation between different scalar values and between values of a scalar and its gradient. The boundary $\mathrm{Ka}_{\delta,\mathrm{K}} \gtrsim 1$ may more generally be conceived as the conditions at which turbulence in the reactants has scales that can disrupt the correlation of scalars that are distributed over lengths similar to $\mathcal{O}(\delta_{\mathrm{L}}^0)$, whether or not reactions are

occurring. Similarly, $\mathrm{Ka}_{\delta,\mathrm{K}} \gtrsim 100$ may more accurately be considered the condition at which turbulence in the reactants has scales that could disrupt the correlation of scalars that are distributed over lengths similar to $\mathcal{O}(0.1\delta_{\mathrm{L}}^0)$.

In total, the observations described above highlight some of the limitations of regime diagrams, namely: (a) the scale-based arguments used to prescribe regime boundaries may have order-of-magnitude quantitative differences with the physical scales present in turbulent flames; (b) they do not account for spatial inhomogeneity and the advection of flame structures; (c) they do not account for the influence of the flame on the turbulence; (d) regime labels that distinguish between preheat and reaction zones are restrictive in terms of fuels; and (e) additional length/velocity/times scales may be needed to predict regimes. Despite these limitations, regime diagrams provide a useful conceptual/academic aid for understanding and articulating the general influences of turbulence on flames as a function of conditions (it can be argued that this was their original intent). They can also provide conservative *a priori* guidance on appropriate/efficient modelling paradigms for closing reaction source terms for a given configuration/condition, although recent developments on adaptive modeling provide an alternative path (e.g., Ref. [106]). However, the utility of comparing the detailed regime transitions between different configurations is limited.

2.5. Turbulent flame speed

We close this introductory section with a brief review of the current understanding of the turbulent flame speed in highly turbulent flames. The turbulent flame speed is a convenient overall metric of a flame that captures the net effects of the complicated turbulence/flame interactions. Comparisons of turbulent flame speeds to theoretical expectations—e.g., based on a collection of thin propagating flame surfaces—can be used to assess theories and help identify open questions. Models for the turbulent flame speed can also be used to close the reaction rate source term, as reviewed by Lipatnikov and Chomiak [6].

Driscoll [8] presents a review of the turbulent flame speed, its definitions, ambiguities in these definitions, and measurements/simulations in the flamelet regime. Of particular

relevance here is the global consumption speed

$$s_{\mathrm{T,GC}} \equiv \frac{\bar{\dot{m}}_{\mathrm{r}}}{\rho_{\mathrm{r}} A_{\bar{c}=0.5}} \,, \tag{15}$$

where $\bar{\dot{m}}_{\mathrm{r}}$ is the mean mass flow rate of reactants consumed by the flame and $A_{\bar{c}=0.5}$ is the area of the surface corresponding to a mean reaction progress variable of $\bar{c} = 0.5$. This surface roughly represents the midpoint of the flame brush. Experimentally, envelope flames (e.g., jet and Bunsen flames) without local extinction allow direct calculation of $s_{\mathrm{T,GC}}$ because $\bar{\dot{m}}_{\mathrm{r}}$ and ρ_{r} are known, and $A_{\bar{c}=0.5}$ can be reasonably measured. In DNS, $s_{\mathrm{T,GC}}$ can be calculated directly from the simulated reaction rates and/or from reactant mass flow rates.

Under the assumption that a turbulent premixed flame consists of a collection of thin 1D propagating flame structures that are similar to stretched laminar deflagrations, we obtain

$$\bar{\dot{m}}_{\mathrm{r}} = \rho_{\mathrm{r}} s_{\mathrm{T,GC}} A_{\bar{c}=0.5} = \rho_{\mathrm{r}} \bar{I}_0 \bar{s}_{\mathrm{L}}^0 \bar{A}_{\mathrm{T}} \,, \tag{16}$$

where $\bar{A}_{\mathrm{T}}$ is the mean area of a selected c isosurface and $\bar{I}_0$ is an $\mathcal{O}(1)$ factor that accounts for the effects of stretch of the flame speed. Hence,

$$\frac{s_{\mathrm{T,GC}}}{s_{\mathrm{L}}^0} = I_0 \frac{\bar{A}_{\mathrm{T}}}{A_{\bar{c}=0.5}} \,, \tag{17}$$

where we have taken $A_{\bar{c}=0.5}$ to characterize the area of an "equivalent" laminar flame (i.e., one with the same area as the mean flame brush, which would be exactly true for statistically 1D flames).

It is common practice to plot $s_{\mathrm{T,GC}}$ versus u_ℓ, both normalized by s_{L}^0. However, as discussed above, caution must be applied when considering the laminar flame properties attributed to highly turbulent combustion experiments due to the tendency to mix surrounding fluid into the reaction zone [59, 65]. Unless this ambient fluid is thermo-chemically matched to the products of the reactants, the laminar flame speed of the reactants may not properly characterize the flame.

The data of Wabel *et al.* [56] were acquired in the Hi-Pilot Bunsen flame across a range of turbulence conditions (up to $u_\ell / s_{\mathrm{L}}^0 \approx 150$), all with equal jet and pilot equivalence ratios of $\phi = 0.75$. Figure 12 summarizes their findings, which also includes the results of Yuen and

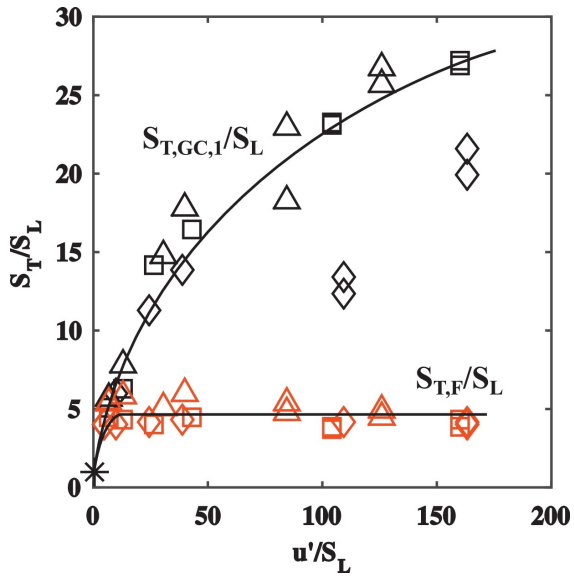

Figure 12: Experimentally measured turbulent flame speed versus turbulence intensity. $S_{\mathrm{T,F}}/S_{\mathrm{L}}$ is equivalent to $\bar{A}_{\mathrm{T}}/A_{\bar{c}=0.5}$ in our notation. Reprinted from Ref. [56] with permission of Elsevier.

Gülder [52] for $u_\ell/s_{\mathrm{L}}^0 \lesssim 25$. The mean progress variable field was estimated by binarizing instantaneous OH planar laser-induced fluorescence (PLIF) images and then taking the average. The turbulent flame surface area was estimated from the instantaneous PLIF images.

Values of $s_{\mathrm{T,GC}}/s_{\mathrm{L}}^0 > 25$ were observed. These increased continuously, but at a decreasing rate with increasing u_ℓ. The maximum in $s_{\mathrm{T,GC}}$ from previous studies at lower turbulence intensities was not observed [107], which is attributed to the large co-flow of hot pilot fluid that prevented local flame extinction. In contrast to the continuously increasing $s_{\mathrm{T,GC}}$, measured values of $\bar{A}_{\mathrm{T}}/A_{\bar{c}=0.5}$ (denoted $S_{\mathrm{T,F}}/S_{\mathrm{L}}$ in Fig. 12) increased for low u_ℓ but plateaued at $\bar{A}_{\mathrm{T}}/A_{\bar{c}=0.5} \approx 5$.

We note that comparing the measured $\bar{A}_{\mathrm{T}}/A_{\bar{c}=0.5}$ with $s_{\mathrm{T,GC}}/s_{\mathrm{L}}^0$ via Eq. (17) requires consideration of the stretch factor I_0. However, the $\phi = 0.75$ methane/air flame studied has a near-zero Markstein length, resulting in $I_0 \approx 1$ and indicating that the laminar flame speed should decrease slightly with increasing stretch rate due to turbulence [108]. Hence, flame stretch would increase the discrepancy between the measured turbulent flame speed and the consumption rate expected from the flame area and stretched laminar flame speed.

Imaging of CH_2O and OH using PLIF in these flames demonstrated broadened regions of CH_2O, but topologically thin and connected regions of exothermic reactions (identified from the overlap of CH_2O and OH). There was thus no evidence of broken or broadened reaction zones. Hence, these experiments provide evidence of increased reaction rates while maintaining a reaction zone spatial structure that qualitatively remains similar to that of a laminar flame. This is consistent with the observations of Osborne *et al.* [55], who experimentally showed increased local flame speeds in regions of thickened preheat zones and thin reaction zones.

Other experimental evidence supports this general conclusion. For example, Wang *et al.* [50] reported $s_{\mathrm{T,GC}}/s_{\mathrm{L}}^0$ measurements in the LUPJ jet burner. If the area of the turbulent flame was calculated using the area of the CH_2O surface, their data corresponded very well with that of Wabel *et al.* [56]. However, the flames used in this study had mismatched pilot and jet equivalence ratios. There consequently may be some ambiguity in the proper s_{L}^0 normalization factor.

Another study by Sosa *et al.* [64] presented turbulent flame speeds in a planar flame propagating into a heated flow at a sufficient velocity for fluid compressibility to have an influence. Since the flame was stationary in the laboratory frame, the turbulent flame speed was determined directly from the velocity of the oncoming reactants. They reported $s_{\mathrm{T,GC}}/s_{\mathrm{L}}^0$ values above 60. While flame surface areas were not measured, it is expected that $\bar{A}_{\mathrm{T}}/A_{\bar{c}=0.5}$ is considerably less than $s_{\mathrm{T,GC}}/s_{\mathrm{L}}^0$.

In contrast to the experiments, most DNS of flames in boxes of homogeneous isotropic turbulence find much lower $s_{\mathrm{T,GC}}/s_{\mathrm{L}}^0$ values than experiments at similar u_ℓ/s_{L}^0. Furthermore, the DNS studies often find that $s_{\mathrm{T,GC}}/s_{\mathrm{L}}^0$ is very similar to $\bar{A}_{\mathrm{T}}/A_{\bar{c}=0.5}$ [71, 109]. Typical results are shown in Fig. 13. It should be noted that the studies shown in Fig. 13 utilized single-step chemistry, which may be insufficient to describe the effects of stretch on the flame speed. Nevertheless, the simulations of Nivarti and Cant [71] utilized a $\phi = 1.0$ methane/air flame that should be relatively insensitive to stretch.

Regarding the higher values of $s_{\mathrm{T,GC}}/s_{\mathrm{L}}^0$ for a given $\bar{A}_{\mathrm{T}}/A_{\mathrm{L}}$ measured in experiments, one potential explanation is that the experiments are over-measuring $s_{\mathrm{T,GC}}$ or under-measuring

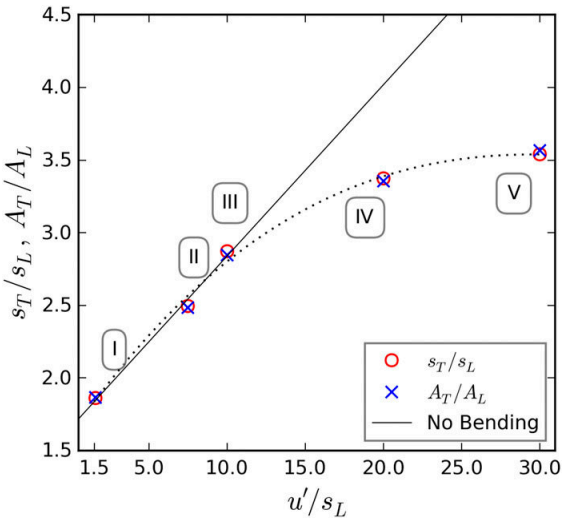

(a) Normalized flame speed and flame area versus turbulence intensity in $\phi = 1.0$ methane/air flames. Reprinted from Ref. [71] with permission of AIP Publishing.

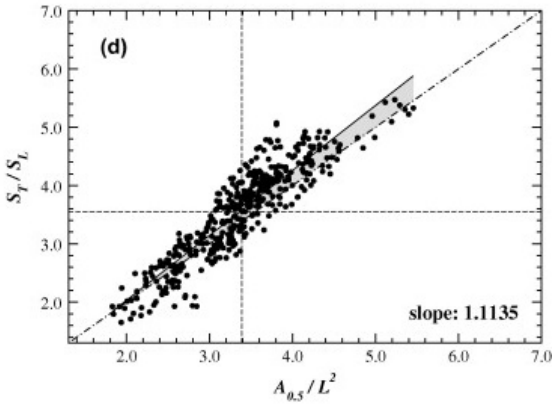

(b) Normalized flame speed versus flame area in $\phi = 1.0$ H_2/air flames. Reprinted from Ref. [110] with permission of Elsevier.

Figure 13: DNS results indicating correspondence between turbulent flame speed and flame area.

$\bar{A}_T$. The former is unlikely since the mass flow rate of reactants and reactant density can generally be well controlled in experiments. As long as there is not substantial local extinction—which is prevented by the large co-flow of hot products in most configurations—$\bar{m}_r$ is known. The use of the $\bar{c} = 0.5$ isosurface area to normalize the reactant flux in Eq. (16)

is arbitrary and affects the reported values of $s_{\mathrm{T,GC}}$. Given that the density of the unburnt reactants is used to compute the reactant volume flux, it may be more appropriate to use a $\bar{c}$ isosurface towards the reactant side of the flame brush. However, in the jet and Bunsen flames studied, this would reduce the normalizing surface area and further increase the reported $s_{\mathrm{T,GC}}$.

While it is likely that experiments are under-estimating $\bar{A}_{\mathrm{T}}$, this cannot account for the large discrepancy between $s_{\mathrm{T,GC}}/s_{\mathrm{L}}^0$ and $\bar{A}_{\mathrm{T}}/A_{\bar{c}=0.5}$ (nor the much higher values of $s_{\mathrm{T,GC}}/s_{\mathrm{L}}^0$ in the experiments compared to the DNS). Such under-estimation arises primarily due to resolution limitations and the use of two-dimensional (2D) measurements to estimate 3D flame areas. These effects have been evaluated in several recent studies. For example, Wabel *et al.* [111] post-processed DNS data to mimic the experimental signal collection process. They found that the measurement process decreased the measured area, but the decrease was limited to about a 10-30% under-estimation over a reasonable range of experimental parameters. Similarly, Wang *et al.* [112] showed that 2D measurements tend to under-predict flame areas by about 30%. Wang *et al.* [50] post-processed their experimental data in the LUPJ burner using two different effective pixel sizes. While they did find some sensitivity of the measured flame area to the pixel size, this was insufficient to compensate for the difference between $s_{\mathrm{T,GC}}/s_{\mathrm{L}}^0$ and $\bar{A}_{\mathrm{T}}/A_{\bar{c}=0.5}$. Skiba *et al.* [113] experimentally demonstrated that a six-fold decrease in resolution reduced the measured flame area by approximately 30%. Klein *et al.* [114] used DNS of H_2/air flames and showed some sensitivity of flame area calculated using scalar isosurfaces to that deduced by the generalized flame surface density, depending on the choice of scalar, progress variable level, and number of dimensions considered. Similar to the other studies, these sensitivities were insufficient to explain the discrepancy between the experimentally observed turbulent flame speed and flame area. Hence, while experiments may under-measure the flame area, this is insufficient to account for the differences between $s_{\mathrm{T,GC}}/s_{\mathrm{L}}^0$ and $\bar{A}_{\mathrm{T}}/A_{\bar{c}=0.5}$.

The experiments therefore show an increase in the local flame propagation speed, such that a given amount of area consumes more reactants per unit time than would be expected in a laminar flame, which does not occur in the DNS. This allows the turbulent flame speed

to increase by more than would be possible based on flame surface area. One potential explanation is that there is a large-scale (geometry dependent and/or high Reynolds number) effect that is not captured in the DNS. For example, flame merging has been shown to cause an increase in the local consumption rate [115–118], which would be more prevalent in jet and Bunsen flames (see Fig. 10(a)) and in flames with larger integral-scale corrugations than in most DNS configurations.

Another potential explanation is based on enhanced mixing due to flame-scale turbulence. A recent study by Nivarti *et al.* [119] has investigated whether the $s_{\mathrm{T,GC}}$ discrepancy can be attributed to the simultaneous action of increased turbulent diffusivity and flame area increase (i.e., if Damköhler's first and second hypothesis [99] are acting concurrently), which is similar to the arguments made by Osborne *et al.* [55]. Using a model spectrum, they showed that the increase in $s_{\mathrm{T,GC}}/s_{\mathrm{L}}$ relative to $A_T/A_{\tilde{c}=0.5}$ in experiments could be reconciled by an increase in the "turbulent diffusivity", essentially leading to a faster local flame speed. However, this does not reconcile the discrepancy between the experiments and DNS, as DNS should predict the local flame behavior if the chemistry and transport are sufficiently modelled. Thus, understanding the reasons for this discrepancy remains an area of active research and is discussed further in Section 3.

2.6. Summary

The main takeaways from the discussion in Section 2 are:

1. The idealized separation of laminar premixed deflagrations into inert preheat zones and chemically active reaction zones is only appropriate for a limited range of fuels (e.g., methane). Conceptualizations of turbulent flames that rely on this separation may face challenges for other fuels, such as hydrogen or large hydrocarbons.
2. Experimental configurations to study highly turbulent flames should isolate the region being investigated from the surroundings using either physical confinement or a co-flow that is thermochemically matched to the environment. Otherwise, rapid turbulence-induced mixing can stratify the reaction zones with fluid from the surroundings.

3. DNS can provide valuable insights into flame structure and dynamics at highly turbulent conditions, and modern calculations now routinely use multi-step reduced or skeletal chemical kinetic models. Caution must, however, be used when developing insights from such studies, since DNS still requires substantial simplifications as compared to experiments and often includes models for large-scale kinetic energy input.
4. Significant ambiguity can exist in the calculation of the dimensionless parameters used to characterize turbulent flames, depending on where certain parameters are measured and what assumptions are made. We recommend the use of Eqs. (13) and (14) to calculate $\mathrm{Da}_{\ell,\delta}$ and $\mathrm{Ka}_{\delta,\mathrm{K}}$, respectively.
5. There is a natural mitigation of extremely high Karlovitz numbers and low Damköhler numbers in terrestrial systems of engineering interest due to the linkage between system temperature and pressure.
6. While regime diagrams provide a useful academic and conceptual aid for understanding the effects of turbulence on flame structures, their utility for accurately predicting the flame structure in real flames based on a small number of characteristic parameters is questionable. Ambiguities arise due to the parameters used to define regime boundaries (particularly in flames with spatially varying turbulence and flame structures), the impact of the flame on the turbulence, the lack of inert preheat zones when burning many fuels, the smallest turbulence scales being much smaller than the smallest thermochemical scales, etc.
7. Despite significant progress in both experiments and DNS, phenomenological disagreements still exist in the relationship between turbulent flame speed and flame surface area that are not explained by experimental uncertainty.

3. Thermochemical Structure and Dynamics

The objective of this section is to report current information regarding the thermochemical structure and dynamics of highly turbulent premixed flames. Extending Eq. (4) for chemical scalars to a generic scalar ψ (which could also include, e.g., temperature or

progress variable) yields

$$\frac{\mathrm{D}\psi}{\mathrm{D}t} = \frac{1}{\rho}\frac{\partial}{\partial x_k}\left(\rho D \frac{\partial \psi}{\partial x_k}\right) + \dot{\omega}\,. \tag{18}$$

Hence, the Lagrangian evolution of ψ is dictated by both the scalar gradient $\chi_k = \partial\psi/\partial x_k$ and the corresponding source term. For chemical scalars, the source term is generally a local quantity, whereas the gradients are inherently non-local.

The major focus of this section is on characterizing the local thermochemical state and associated source terms during highly turbulent premixed combustion. Although we discuss the spatial structure of the flame—and, hence, the scalar gradients and molecular transport—where appropriate, scalar gradient dynamics are closely linked to turbulence dynamics. As such, much of the discussion regarding scalar gradient dynamics in turbulent flames is deferred to Section 4.2.

From the perspective of the thermochemical state space, the attainable states in a highly turbulent premixed flame are more varied than in a laminar flame, due to the larger range of scalar gradients and associated time scales. To investigate their effects, in Section 3.1 we first describe the structure of highly turbulent premixed flames from the perspective of their characteristics in physical space. The thermochemical states observed in highly turbulent premixed flames, and the associated reaction rates, are subsequently described in Section 3.2. Given the impacts of turbulence on thermochemical states in highly turbulent flames, we discuss potential deviations from the chemical pathways observed in laminar flames in Section 3.3. Chemical pathways are closely related to local combustion modes, and we discuss the classification and quantification of these modes in Section 3.4. A brief summary is provided in Section 3.5.

3.1. Flame structure in physical space

In studies that focus on high Karlovitz number premixed flames, the flame structure is frequently probed and described; Fig. 1 in Ref. [120] provides a comprehensive summary of these studies and their corresponding Karlovitz numbers. Both computational and experimental studies [53, 55, 56, 66, 67, 78, 86, 105, 113, 121–127] have compared turbulent premixed flames at high $\mathrm{Ka}_{\delta,\mathrm{K}}$ to corresponding laminar flames in physical space, with the

primary goal of assessing whether "flame broadening" is observed under highly turbulent conditions. This topic is comprehensively reviewed in Ref. [11] and, hence, is not discussed in detail here.

A challenge when considering turbulent flame spatial structure is that phenomenological observations of thinning or broadening are often qualitative and depend on the definitions of "preheat" and "reaction" zones. Such definitions are often not unified across studies, as is evident by the various isolines or radical layers employed in Refs. [56, 67, 127].

To avoid complications arising from such different definitions, the physical structure of flames can be re-cast into a consideration of scalar field dynamics. In particular, for a scalar that characterizes the location of the flame (e.g., the temperature), a scalar field with dimensions of length can be defined based on the local scalar gradient magnitude $\chi \equiv (\chi_k \chi_k)^{1/2}$ as [128, 129]

$$\delta_\mathrm{t} = \frac{(\Delta\psi)_\mathrm{ref}}{\chi}\,, \tag{19}$$

where $(\Delta\psi)_\mathrm{ref}$ denotes a reference change in ψ (e.g., the difference in product and reactant temperatures when $\psi = T$). In the case of an unstretched laminar flame where $\psi = T$ and χ is evaluated at the location of the maximum gradient, $\delta_\mathrm{t} = \delta_\mathrm{L}^0$. A primary advantage of the scalar gradient approach to understanding flame structure is that ψ and δ_t are both field quantities that have exact, physics-based governing equations. Such equations directly reveal the dynamics of the fields – both globally and locally – even for highly turbulent conditions where the concept of a quasi-laminar coherent flamelet may be lost (see Section 4.2.1).

Figure 14 shows examples of probability density functions and conditional statistics of δ_t evaluated at different locations in highly turbulent premixed flames, as characterized by a progress variable, $\psi = c$, or reactant mass fraction, $\psi = Y$. These results show that a wide range of δ_t—both thinner and thicker than the corresponding laminar flame—can occur at any position within the flame for highly turbulent conditions. As the turbulence intensity increases, the fluid dynamic strain rate locally increases thermochemical gradients and decreases the width of high-gradient structures, resulting in broad regions of reduced gradients; that is, the dynamics lead to small regions of intense scalar gradients with inter-

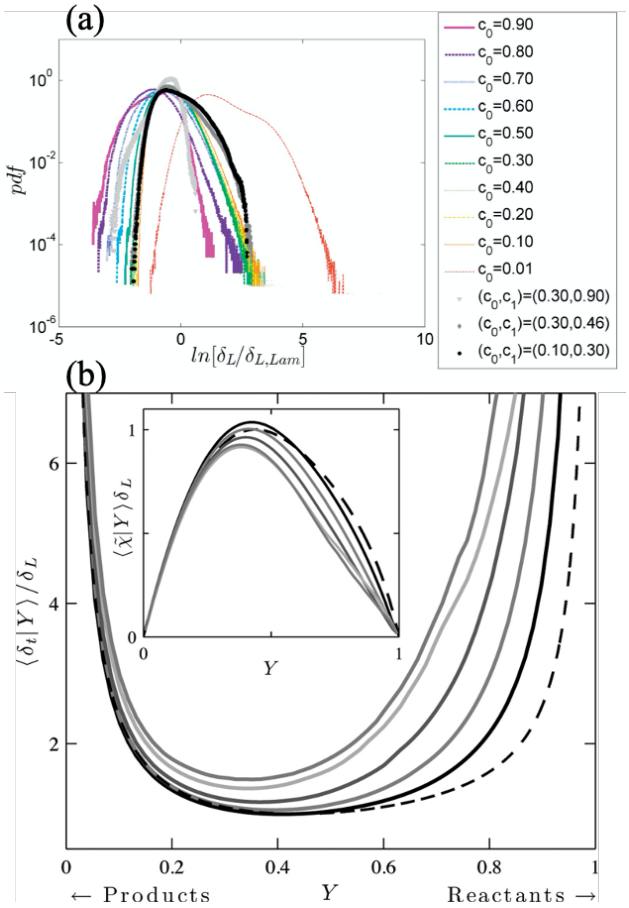

Figure 14: Statistics of the local flame thickness δ_t from DNS. (a) Reprinted from Ref. [129] with permission of Elsevier; (b) Reprinted from Ref. [128] with permission of AIP Publishing.

vening broad regions of low gradients. Hence, the overall flame width increases while strong gradients—higher than those found in laminar flames—are concentrated. This behavior is demonstrated in Fig. 15 from both experiments and DNS [78, 130], and is likely due to a combination of two related effects. In particular, for the larger Reynolds numbers found in many highly turbulent configurations, internal intermittency, which is associated with the concentration of velocity gradients into an increasingly small volume of the flow, becomes more pronounced. At the same time, the turbulent velocity field itself has an increasingly dominant effect on the scalar dynamics, and the scalar field begins to reflect the intermittent properties of the turbulence. Although disentangling the relative contributions of these effects on the scalar intermittency remains a subject of active research, both are responsible

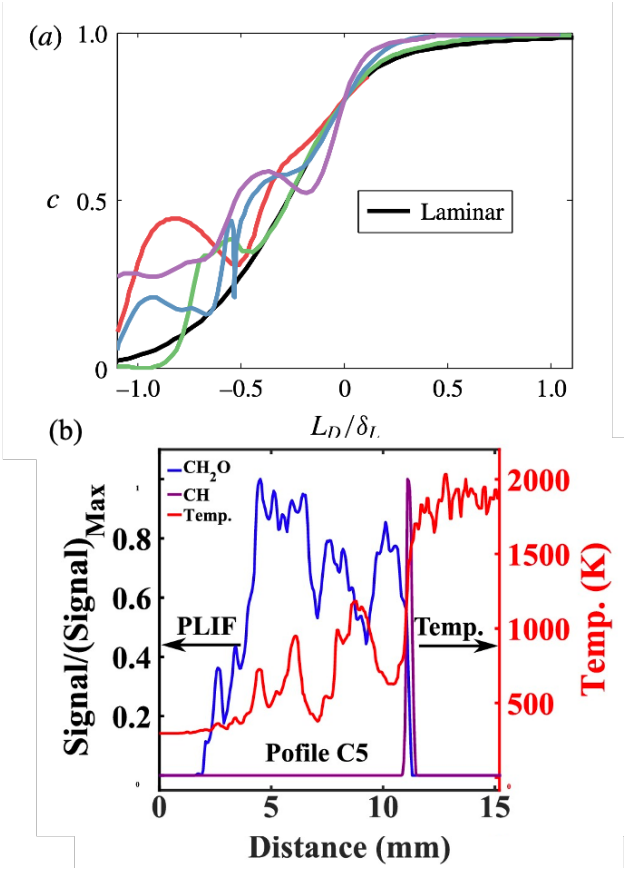

Figure 15: Instantaneous temperature profiles across the flame brushes obtained (a) from DNS of the LUPJ burner, reprinted from Ref. [78] with permission Cambridge University Press; (b) experimental measurements of instantaneous temperature, CH_2O-PLIF and CH-PLIF signals across the flame brush for the Hi-Pilot burner, reprinted from Ref. [130] with permission from Elsevier.

in some measure for the increasing concentration of strong scalar gradients noted above. Internal intermittency in the context of turbulence structure and dynamics is discussed in more detail in Sections 4.2.3 and 4.3.

Another factor complicating the structure of a turbulent flame is the potential for reactions occurring throughout the flame, (i.e., the lack of chemically inert preheat zones). As demonstrated by the profiles of the unstrained laminar flames in Fig. 2, an inert region of diffusive mixing generally does not occur upstream of highly exothermic reactions when considering detailed elementary chemical reactions. For example, significant endothermic fuel cracking reactions (due to pyrolysis) occur in the preheat zone for dodecane/air flames.

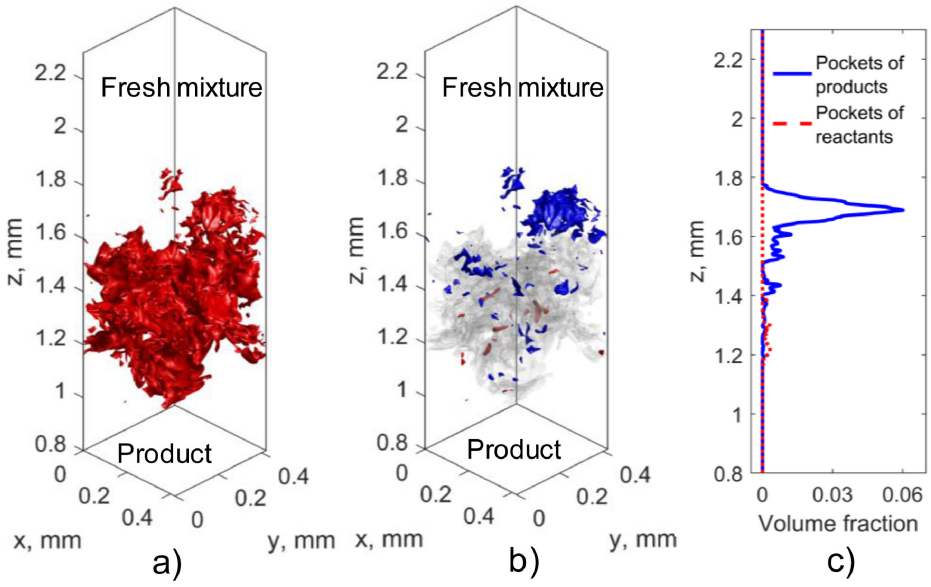

Figure 16: (a) 3D isosurfaces identified by zero crossing of the maximum positive eigenvalue of the chemical Jacobian, (b) the reactant (red) and product (blue) pockets, for $\mathrm{Ka}_{\delta,\mathrm{K}}$=1000, and (c) volume fractions of the two types of pockets in the streamwise direction. The grey isosurface in panel (b) indicates the continuous main reaction front. Reprinted from Ref. [66] with permission from Elsevier.

Exothermic reactions can also take place throughout hydrogen/air flames, in a region that is broader than the fuel consumption region due to differential diffusion.

Strong turbulence can further complicate the concept of a preheat zone if flames locally extinguish. In such situations, turbulent advection can rapidly stir hot products into the preheat zone, from which enthalpy and species subsequently diffuse. One manifestation of this is the presence of product "pockets" that are separated from reactants by extinguishing flame surfaces (i.e., isosurfaces with zero or negative displacement speed). Such pockets were observed in all DNS of n-dodecane/air flames at Karlovitz numbers from 100 to 10,000 [66], as visualized by the blue regions in Fig. 16(b). The presence of pockets complicates the physical space structure of the flame, as well as the thermochemical structure and reaction rates (see Section 3.3.2). We also note that reactant pockets can be formed in the products, as visualized by the red regions in Fig. 16(b).

As mentioned in Section 2.4.3, the distinction between the preheat zones and reaction zones becomes unhelpful for highly turbulent flames, particularly when considering fuels

other than methane. Terminologies such as "volumes of reacting fluids" or "volumes of packed flame filaments" may be more appropriate [70, 121]. Consequently, traditional experimental and computational diagnostics and models can be insufficient and/or inappropriate in describing the flame structures under these challenging conditions where clear interfaces between fresh mixture and products cease to exist. We will further elaborate on this point in Sections 3.2 and 3.3.1.

3.2. Flame structure in thermochemical space

The ability of turbulence to alter the spatial distribution of scalars in physical space is associated with changes in scalar gradients. This, in turn, alters the rate of molecular transport processes responsible for scalar mixing, ultimately resulting in changes to scalar source terms (i.e., chemical reaction rates). This section reviews changes in the thermochemical states observed in highly turbulent premixed flames.

3.2.1. Non-unity Lewis number effects

Molecular transport is the fundamental process that mixes scalars at the molecular level, which is necessary for chemical reactions. Turbulent advection alters the gradients that drive this process, but any differences in transport properties between different scalars remain. Nevertheless, there is a phenomenological understanding that differences in transport properties become less significant, in a practical sense, as turbulence intensity increases. Physically, this should be interpreted as the creation of a state that appears to have uniform transport properties in some statistical sense (i.e., in an average or filtered field), due to rapid spatio-temporal variations in the magnitude and orientation of scalar gradients. Therefore, statistically, differences between diffusion coefficients for various species and heat are expected to become less significant under highly turbulent conditions. With such an expectation, effects due to varying Lewis number ($\mathrm{Le} = \alpha/\mathcal{D}$) are frequently examined and discussed in the literature on highly turbulent premixed flames [67, 69, 83, 86, 122, 131, 132].

Before we discuss the relevant findings, we wish to clarify some terminology commonly employed to describe molecular and thermal transport; namely, preferential diffusion, differential diffusion, and Lewis number effects. Preferential diffusion is conventionally em-

ployed to indicate different molecular diffusivities for different species (i.e., $\mathcal{D}_\mathrm{A} \neq \mathcal{D}_\mathrm{B}$) in a multi-component chemical system [5]. Similarly, the term "non-unity Lewis number effect" conventionally indicates that the molecular diffusivity of species A is different from the thermal diffusivity of the local gas mixture (i.e., $\mathcal{D}_\mathrm{A} \neq \alpha$). For a multi-component reacting mixture, the global Lewis number is often defined based on the deficient species in the fresh mixture [5], although an individual Lewis number can be defined for each species. Consequently, the term "non-unity Lewis number effect" alone can be ambiguous and more clarification is usually needed to elucidate its exact meaning. Differential diffusion, similar to "non-unity Lewis number effects", is also used liberally in the literature; it has been used as a synonym to "preferential diffusion" [133, 134] or "non-constant non-unity Lewis number effects" [67, 83, 122, 132].

To avoid ambiguity, we recommend explicit specification of the transport models where possible, so that readers can have a precise understanding of the meaning. During discussion, more specific descriptions are suggested, such as "differential species diffusion" or "differential diffusion between species and heat", or consistently reserving "non-unity Lewis number effect" for the description of differential heat and species transport.

Physically, a multi-component chemical system always has non-constant non-unity Lewis number (i.e., $\mathcal{D}_\mathrm{A} \neq \mathcal{D}_\mathrm{B} \neq \alpha$). Hence, the issues mentioned above are mostly observed in computational studies. However, physical systems can "appear" or "behave" as if the Lewis number were unity or no differential diffusion existed, to the extent observable by the experiment. Recognizing physical conditions that lead to such observations is beneficial for modeling studies.

Although non-unity Lewis number effects are expected to decrease in importance with increasing turbulence intensity, they can remain significant even at quite high turbulence intensities [69, 83, 86, 131, 135]. Aspden *et al.* [69] reported the distribution of local (atom-based) equivalence ratios versus temperature through DNS of hydrogen/air flames from $\mathrm{Ka}_{\delta,\mathrm{K}} = 10$ to 1.6×10^3 with inlet equivalence ratios of $\phi_0 = 0.31$ and 0.40 (see Fig. 17). Similar variations in mean equivalence ratio versus temperature were observed between the $\mathrm{Ka}_{\delta,\mathrm{K}} = 10$ turbulent flames and corresponding laminar flames for both inlet equiva-

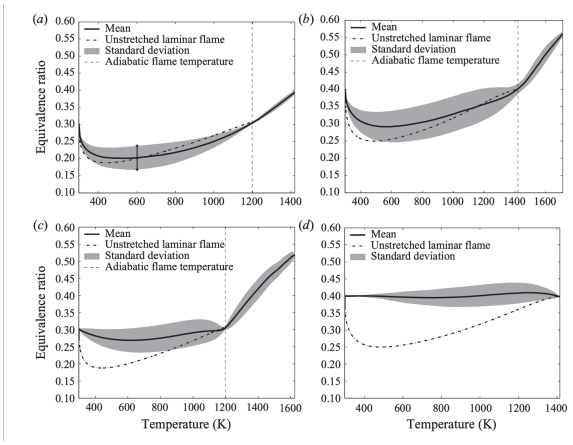

Figure 17: Conditional mean (solid line) and standard deviation (shaded area) of local equivalence ratio as a function of temperature for: (a) $\phi_0 = 0.31$ and $\mathrm{Ka}_{\delta,\mathrm{K}} = 10$; (b) $\phi_0 = 0.4$ and $\mathrm{Ka}_{\delta,\mathrm{K}} = 10$; (c) $\phi_0 = 0.31$ and $\mathrm{Ka}_{\delta,\mathrm{K}} = 1.6 \times 10^3$; and (d) $\phi_0 = 0.4$ and $\mathrm{Ka}_{\delta,\mathrm{K}} = 1.6 \times 10^3$. The dashed line indicates the corresponding unstrained laminar flame solutions. The vertical dashed line denotes the adiabatic flame temperature at ϕ_0. Reprinted from Ref. [69] with permission from Cambridge University Press.

lence ratios, indicating the continued importance of differential diffusion. Additionally, the $\mathrm{Ka}_{\delta,\mathrm{K}} = 10$ flames exhibited locations with mean equivalence ratios greater than ϕ_0 and temperatures above the adiabatic flame temperature as a result of differential diffusion. At $\mathrm{Ka}_{\delta,\mathrm{K}} = 1.6 \times 10^3$, both flames have different mean equivalence ratio profiles that remain close to ϕ_0, indicating a statistically decreased significance of differential diffusion. Nevertheless, the standard deviation around the mean remains significant compared to the $\mathrm{Ka}_{\delta,\mathrm{K}} = 10$ cases, particularly at $\phi_0 = 0.31$. Interestingly, the $\phi > \phi_0$ branch beyond the adiabatic flame temperature was only observed for $\phi_0 = 0.31$ at $\mathrm{Ka}_{\delta,\mathrm{K}} = 1.6 \times 10^3$.

Barlow *et al.* [135] measured C/H, C/O and C/N ratios for the Cambridge bluff-body stabilized burner with both streams comprised of methane/air mixtures at $\phi = 0.75$ (Case SwB1). The Reynolds numbers for the inner and outer jets were 5,960 and 11,500, respectively. They observed varying atomic ratios across the turbulent premixed flame as shown in Fig. **??**, which suggests the role of differential species diffusion in these turbulent premixed flames. The same trends of atomic ratios were observed in an LES/PDF study [136], where mixture-averaged molecular transport was invoked to account for molecular transport on

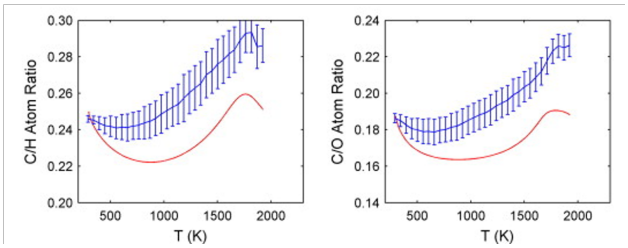

Figure 18: Comparison of measured results for selected atomic ratios at $z = 10$ mm above the bluff body surface in the turbulent flame plotted versus temperature (blue) and compared with calculated results for an unstrained laminar flame at $\phi = 0.75$ (red). Reprinted with permission from [135].

the resolved grid only. However, the subgrid differential diffusion remains unaccounted for in this study, which could contribute to the reported discrepancy between experiments and computation.

Non-unity Lewis number effects have also been delineated by comparing simulations conducted with different molecular transport models [67, 83, 122, 127, 132]. For example, Lapointe *et al.* [67] conducted 3D DNS of forced turbulent planar n-heptane/air flames. The Karlovitz number based on the unburnt gases up to 1050 were studied, which corresponds to 237 when defined based on the properties in the reaction zone. For each Karlovitz number, two transport models were compared, namely a unity Lewis number model and a non-unity Lewis number model that was obtained from an unstrained laminar premixed flame simulation using full transport.

The different transport models showed differences in the peak temperature corresponding to the maximum fuel consumption rate. However, such differences decreased with increasing Karlovitz number, indicating a weakened role of Lewis number effects. Lapointe *et al.* [67] observed higher levels of local extinction with non-unity Lewis number transport, which is expected because the response to strain and curvature can be significantly impacted by transport properties [5], thereby modifying the local extinction behavior. The scalars were more scattered in state space with the non-unity Lewis number model. However, the mean mass fractions of C_2H_4 (and other scalars) versus temperature agreed better with laminar solutions obtained using unity Lewis number, as opposed to those obtained with

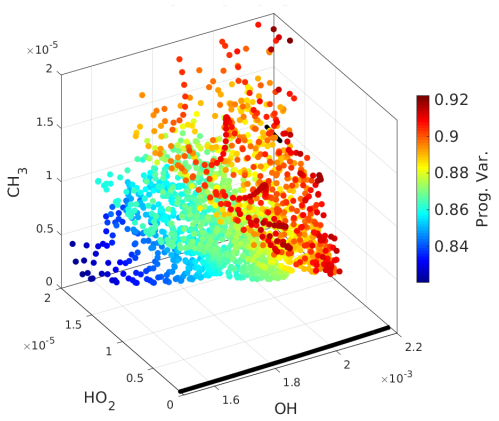

Figure 19: Scatter plot in the OH-CH_3-HO_2 mass fraction space in a 3D turbulent premixed flame, colored by progress variable. The solid (black) line corresponds to the laminar flame solution. Reprinted from Ref. [87].

non-unity Lewis number. This supports the phenomenological observation of decreased effects of differential diffusion on the mean state when turbulence is intense.

Hence, the aforementioned studies point to a reduced influence of non-unity Lewis numbers on the mean thermochemical state with increased turbulence intensity. Nevertheless, differential diffusion can significantly influence the mean state at highly turbulent conditions, and also influences the distribution of states around the mean. We note that non-unity Lewis number effects have predominantly been studied in canonical configurations with relatively simple fuels. The impact of differential diffusion may change with composition/thermal stratification and with more complicated fuels.

3.2.2. Scalar distributions in thermochemical space

Ultimately, the combination of molecular diffusion with turbulence-induced scalar gradients and chemical reactions results in more varied thermochemical states compared to laminar flames. Scatter plots or joint PDFs of two or three thermochemical variables are frequently employed to examine the extent to which turbulence impacts the flame in thermochemical space. The conditional means of key thermochemical variables in turbulent flames are subsequently compared with profiles extracted from corresponding laminar flames. Com-

parison between conditional statistics in turbulent flames with laminar solutions have been comprehensively discussed in Section 3.1 of Ref. [11]. Hence, we only present some typical results that are useful for motivating/understanding the subsequent discussion of reaction rates and chemical pathways.

Figure 19 shows scatter plots of the mass fractions of HO_2, OH, and CH_3 obtained from a 3D simulation of a premixed Jet-A/air flame kernel subjected to intense turbulence [87]. The scatter plots are colored by a temperature-based progress variable in the range between 0.84 and 0.92, representing the transition from the preheat to the reaction zone. Compared to the corresponding laminar solution, which is essentially a 1D manifold, the OH-CH_3-HO_2 mass fraction space for the turbulent flame is larger and 3D. In particular, CH_3 penetrates into the reaction zone in the turbulent flames, while there is zero CH_3 beyond $c = 0.84$ in the corresponding laminar flame. Reactions such as CH_3 + OH = CH_2^* +HO_2 are expected to have faster reaction rates with CH_3 exposed to higher temperatures, which can potentially impact the global burning rate and chemical pathway.

The thermochemical space also has been explored in the experiments and DNS of the LUPJ burner over the range $\mathrm{Ka}_{\delta,\mathrm{K}} = \mathcal{O}(10) - \mathcal{O}(1,000)$ [47, 78]. In the experiments, OH and CH_2O were measured by PLIF, and temperature was measured by Rayleigh scattering. Substantial amounts of OH were observed in the low-temperature regions of the flame (i.e., $T <$ 1200 K), which is absent in the corresponding laminar flame. The temperature-conditioned mean OH mass fractions gradually deviated from the laminar flame as $\mathrm{Ka}_{\delta,\mathrm{K}}$ was increased. Scatter plots of a few important species from both the experiments and DNS are shown in Fig. 20. The DNS showed good qualitative agreement with the experiments, although there were notable differences in the shape of the scatter plots. For example, the simulations show more samples at low concentrations of HCO and at high concentrations of CH_2O and OH. The experimental results are generally more scattered in the plots due to noise in the measurements. Clearly, this degree of scatter deviates significantly from the profiles that would occur in laminar flames. Such wide variations in species-species and species-temperature correlations are ubiquitous in highly turbulent flames. Despite the wide variation in thermochemical states, conditional mean profiles generally resemble those of laminar flames at

"appropriate" conditions (i.e., with a particular strain-rate and transport model) [79, 132], although a large standard deviation around the conditional mean is always observed.

The wide variation of thermochemical states can challenge the assumptions of existing turbulent combustion closures, including both flamelet-like and non-flamelet-like models. For example, the LUPJ burner has been used for *a priori* and *a posteriori* assessment of a flamelet model [137], a thickened-flame approach [138], and a transported PDF approach [139]. Five different flamelet tabulation methods (i.e., "chem-tables") are compared [137], including one obtained using the conditional statistics from DNS, two obtained from counterflow stratified premixed 1D flames with and without differential diffusion, one from freely propagating premixed 1D flames, and one from zero-dimensional autoigniting plug-flow reactors. All of the flamelet tables capture the mean and root-mean-squared fluctuation profiles of the flow and major species well, with more discrepancies observed in predicting CH_2O. However, the flamelet table based on counterflow stratified premixed 1D flames with differential diffusion shows better agreement with DNS upstream near the inlet, while the flamelet table based on auto-igniting plug flow predicts CH_2O and the instantaneous flame structure the best further downstream. That is, the flamelet tables need to be adjusted in order to capture the local flame structure.

Similarly, the thickened flame model also needs to be adapted to account for the local variation of thermochemical states when constructing the thickening factor. Compared to the traditional approach, where the thickening factor is estimated based on unstrained laminar flames at corresponding boundary conditions, the thickening factor in Ref. [138] accounts for variations in the local hydrodynamic strain and adjusts the reference flame thickness based on the heat release rate layer thickness, subject to different strains. Similar adjustments have also been implemented in the context of transported PDF methods with a power-law based mixing frequency model [139]. One additional model constant is multiplied in the expression for thermal thickness of an unstrained laminar flame in the proposed power-law scaling function, compared to an earlier version of the power law model; the new mixing model yields better agreement with DNS in predicting scalar mixing rates. Based on these three studies, all three traditional models are applicable to the high Karlovitz

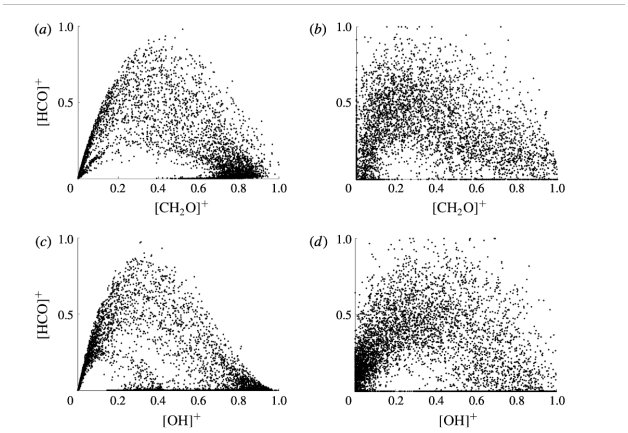

Figure 20: Normalised scatter plots of (a,b) [HCO] versus [CH_2O] and (c,d) [HCO] versus [OH], where [X] denotes the concentration of species X. The left-hand plots show the species concentrations from the DNS and the right-hand plots show the species PLIF signals of the experiment. Reprinted from Ref. [78] with permission of Cambridge University Press.

number LUPJ jet flame. However, the wide distribution of thermochemical states arising from strong turbulence-chemistry interactions requires modifications (e.g., estimates of the reference flame thickness) in all three models. A future challenge lies in how to obtain the knowledge of thermochemical states and model their diversity *a priori*, when no DNS or experimental insights are available.

3.3. Chemical reactions in the enlarged thermochemical space

Responding to the enlarged thermochemical space in turbulent flames, local reaction rates are also more varied than in laminar flames. Indeed, the exponential relationship between reaction rate and temperature means that relatively small temperature variations can result in large reaction rate variations. In the following section, we review the impact of thermochemical states on combustion chemistry.

3.3.1. Chemical pathways

One of the major questions concerning highly turbulent combustion is whether turbulence alters the chemical pathway of a given reactant mixture [65, 87, 126, 140–144]. Here "chemical pathway" indicates a network of key elementary reactions, which could be the

complete collection of elementary reactions for specific reactive mixtures at certain specific initial conditions, or a certain subset thereof. For example, when heat release rates are targeted, the relevant chemical pathway is tightly connected to fuel oxidation processes. For hydrocarbon fuels, the oxidation pathway is equivalent to tracking the major carbon flow.

Understanding such chemical pathways under highly turbulent conditions has practical implications for the optimization/reduction of chemical kinetic models. With hundreds or thousands of model parameters, chemical kinetic models (detailed or global) require experimental or theoretical measurements to anchor the optimization of model parameters. The experiments are mostly canonical, including data from flow reactors, laminar flame speed experiments, rapid compression machines, or shock tubes. For example, the GRI-Mech mechanisms are optimized based on a collection of reliable experiments that relate to natural gas combustion, including NO formation and re-burn [145]. Turbulent conditions are rarely included in the experimental data sets that support the development of kinetic models. Therefore, it is of primary interest to understand whether optimizations based on non-turbulent data are sufficient to describe turbulent flames.

We note that many chemical pathway studies are constrained by the fact that a particular chemical mechanism was used to conduct the analysis; if a certain chemical pathway is missing from the particular chemical mechanism, such studies are not designed to identify these. Meanwhile, conclusive comparisons between different chemical mechanisms that have different reactions are also difficult, because of the above-mentioned optimization of chemical kinetic models. Therefore, caution must be taken regarding statements that the same reactions are at play when comparing two chemical mechanisms with different lineages.

The chemical pathways reproduced in Fig. 21 track the carbon flow resulting from relevant chemical reactions in the DNS of the LUPJ burner [65]. The numbers and thickness of the arrows indicate the fraction of carbon flow through each route, and the values obtained from the turbulent flame (black) are compared to those obtained from corresponding laminar flames (red). Similar dominant paths are observed between laminar and turbulent flames; the black and red numbers are, for the most part, similar. The relative rates of the different reactions change with position; e.g., the CO-CO_2 conversion is shifted downstream

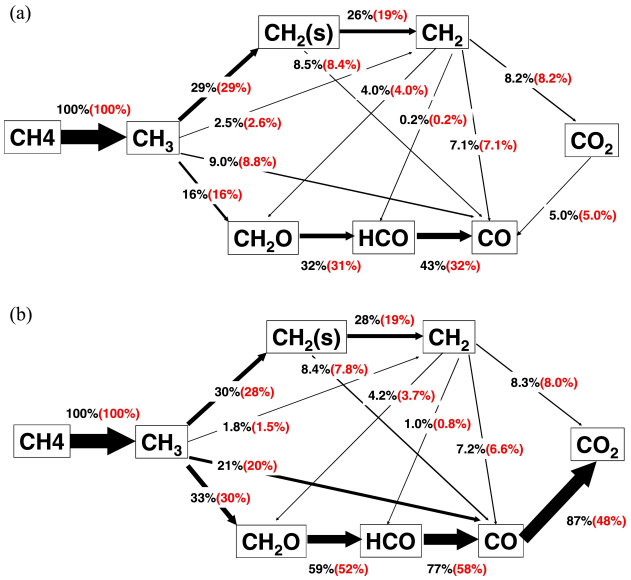

Figure 21: The main C1 reaction path for carbon flow at two downstream locations of a piloted jet flame: (a) $x/D = 8$; (b) $x/D = 32$. The numbers in red are based on unity Lewis number laminar flames at the corresponding mean strain rate and temperature. The thickness of the arrows is weighted with the fraction of the carbon flow. Reproduced from Ref. [65] with permission form Elsevier.

due to the accumulation of CO further downstream and longer residence times required for this process.

A few recent DNS studies at high Karlovitz numbers have discussed the impact of turbulence on reaction pathways through analyses of reaction fluxes [65, 140, 142, 143]. Dasgupta *et al.* [140] analyzed a recent series of DNS of lean hydrogen-air flames at different Karlovitz numbers [86] by analyzing integrated reaction fluxes along local flame normal directions. They also examined methane/air flames [142] and n-dodecane/air flames [143] using corresponding DNS datasets [121, 123]. For all three flames, the conclusions remain that the fractional contribution from each reaction to the overall heat release is not significantly altered by turbulence. Therefore, they conclude that kinetic models that are optimized using laminar targets are adequate for describing chemistry in turbulent flows.

Recognizing the uncertainties that exist in the elemental rate parameters, Zhao *et al.* [87] systematically examined the possible change of chemical pathways through sensitivity analysis using 620 2D DNS of flame kernels in decaying isotropic turbulence. Global first-order

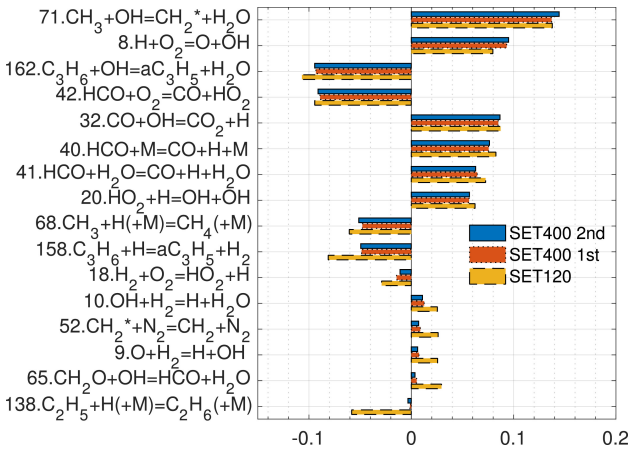

Figure 22: Reprinted from Fig. 8 in Ref. [87]. Ranked composite impact factors obtained using (from left to right): SET400 with second order regression (blue solid); SET400 with first-order regression (red dotted); and SET120 with first-order regression (yellow dashed) for Case2ms. The impact factor is defined as the product of sensitivity coefficient and uncertainty factor. A negative impact factor results from a negative sensitivity coefficient, which indicates that the heat release rate decreases with increasing reaction rate constant.

and second-order sensitivity analyses [146] of target quantities, such as heat release rates and CO mass fraction, were performed. They found that the top ten reactions that contributed to the overall heat release rate stay comparable between laminar and turbulent conditions, although more reactions are sensitive in the turbulent flame. In particular, the chain branching reaction H+O_2=OH+O and the oxidation reaction CO+OH=CO_2+H are consistently predicted to be the most significant reactions impacting heat release rates.

Based on quantified uncertainties in the reaction rates, this study also provides a ranked list of important reactions for further study/refinement based on their impact factor, defined as the product of the sensitivity coefficient and the uncertainty factor for each reaction. The sixteen most impactful reactions are shown in Fig. 22. Although H+O_2=OH+O is the most sensitive reaction, $CH_3 + OH = CH_2^* + H_2O$ is the most impactful reaction since it is less studied experimentally compared to H+O_2=OH+O and has a larger uncertainty factor. Such a ranked list can provide guidance in setting priorities for obtaining more precise experimental/theoretical data of chemical reaction rates.

When pollutant formation is the primary concern (e.g., soot [87] or NOx [144]), the

reaction rates of key species (e.g., C_2H_2, N_2O, and NO_2) are often employed as the quantities of interest; reactions leading to production and consumption of these targeted species are considered components of the chemical pathways. Karimkashi *et al.* [144] examined chemical pathways for NO production in turbulent premixed methane/air flames using 2D DNS of freely propagating planar flames for increasing turbulence intensities and with a reduced mechanism based on GRI-Mech 3.0 [145]. They reported a negative net contribution of the prompt NO pathway under highly turbulent conditions, leading to a reduction of NO compared to the expected prompt NO production under low turbulence intensity and laminar conditions. The negative contribution was attributed to turbulent transport of the unburnt intermediate species, such as CH_3 and CH_2, to the high-temperature reaction zone.

Zhao *et al.* [87] studied the sensitivity of the integrated mass of C_2H_2 to gas-phase reactions, as C_2H_2 is on the critical path to soot formation. They observed that the top ranked reactions contributing to the production of C_2H_2 are very similar between turbulent and laminar conditions. Interestingly, they also reported accumulated CH_3 radicals in the reaction zone under turbulent conditions, which is absent in the laminar counterpart.

A common conclusion from all of the above studies with different fuels and methods is that, although the same underlying reactions are at play, the relative importance of these reactions can be altered under highly turbulent conditions. This conclusion also indicates that calibration of chemical kinetic models should take into account the effects of the turbulence-enlarged thermochemical state space.

3.3.2. Reaction rates

As seen in the previous section, relevant reactions for high-temperature heat release are similar between laminar and turbulent flames. Consequently, certain similarities in thermochemical state space are expected even when turbulence is intense, at least in the statistical sense. Driscoll *et al.* [11] review evidence and discuss this statistical similarity in detail. Here, a few examples are introduced to provide a perspective on this topic. In addition, we highlight a few physical scenarios at which this laminar/turbulent similarity does not hold (e.g., product/reactant mixing at extinction locations).

Different influences of turbulence on reaction rate have been reported, depending on the fuel. For example, Aspden *et al.* [69, 86] reported strong variations in the local hydrogen consumption rates for a series of hydrogen/air flames, which resulted in an overall increase in the mean consumption rate compared to freely propagating 3D laminar flames. Here, 3D freely propagating premixed laminar flames are employed as reference flames to include effects of thermodiffusive instabilities that are not captured by idealized flat laminar premixed flames with low Lewis number [147]. Lapointe *et al.* [67] also observed strong variations in local fuel consumption rate for n-heptane/air flames, although the mean fuel consumption rates were lower than the laminar counterpart. Sankaran *et al.* [80] examined the mean reaction rate of CH_4, CO and OH at several downstream locations of a turbulent premixed methane/air Bunsen flame in the thin reaction zone regime. The mean reaction rates, conditioned on progress variable, were bounded by solutions obtained from an unstrained laminar flame and a strained laminar flame with a strain rate matching that of the mean tangential strain in the turbulent flame. More recently, Savard *et al.* [132] examined the conditional mean reaction rates of three rich n-dodecane/air premixed flames (ϕ = 3, 5, and 7) at a constant pressure of 60 atm, matching the Karlovitz number from the Engine Combustion Network Spray A condition. The heat release rate and reaction rates of n-$C_{12}H_{26}$, $C_{12}H_{15}O_2$, CH_2O and C_2H_2 were compared against laminar flame solutions using unity and non-unity Lewis number solutions. As shown in Fig. 23, there is a broad spread of reaction rates around the corresponding laminar solutions. The mean reaction rates in progress variable space match more closely with the unity Lewis number laminar solutions than the non-unity Lewis number solutions.

Most studies of reaction rates in highly turbulent flames have shown that conditional means resemble those of laminar flames at "appropriate" conditions (i.e., with a particular strain-rate and transport model), although a large standard deviation around the conditional mean is always observed. However, such a resemblance may be compromised by mixing of hot radical-rich products with the reactants directly, for example through the pocket flames shown by Fig. 16 in Section 3.1. When these pockets fail to ignite the surrounding fresh mixture, the enthalpy and species in the pocket flame gradually mix with the surrounding

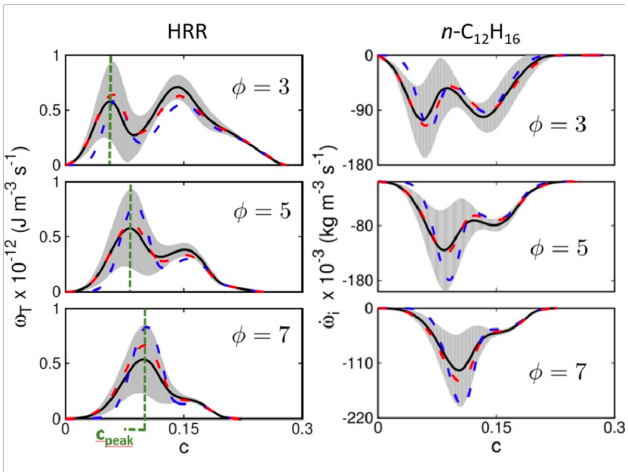

Figure 23: Turbulent flame structure in progress variable space from [132]. Left: heat release rates. Right: reaction rates of n-$C_{12}H_{16}$. Black solid lines: conditional means. Gray-shaded areas: plus/minus one conditional standard deviation. Blue dashed lines: laminar flames with non-unity Le. Red dashed line: laminar flames with unity Le. The location in c space of the first peak in HRR, denoted c_{peak}, is shown by green dashed lines. Reprinted from Ref. [132] with permission from Elsevier.

fresh mixture. Such mixing can be highly consequential for large hydrocarbons because, in laminar flames, endothermic fuel cracking processes are segregated from oxidation reactions (see Fig. 2(b)). However, if the fresh reactants mix with the products without reacting, the subsequent reaction rates can be enhanced. This was demonstrated by Smolke *et al.* [148] using calculations from a series of isobaric and adiabatic pyrolytic reactors with initial temperatures at 1100 K, 1200 K and 1300 K. They found that the laminar flame speed and the extinction strain rates were increased when the reactants employed in these calculations were obtained from the partially "reformed" products in the pyrolytic reactors.

3.3.3. Decorrelated fuel consumption and heat release rates

Whether the fuel decomposition rate is correlated (or decorrelated) with heat release rate in the same manner as in a corresponding laminar flame is a potentially useful metric for assessing the influence of turbulence on chemistry. As shown in Fig. 2, the location of fuel consumption relative to heat release rate in laminar flames depends on the fuel/air mixture. Indeed, despite being the most investigated fuel, methane is rather an exception in

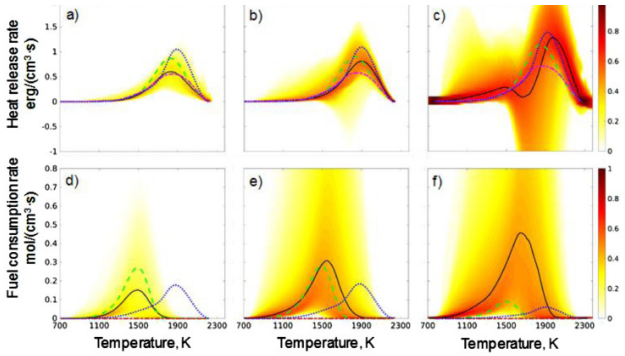

Figure 24: Joint PDFs (contour) and conditional mean (black solid lines) of heat release rate (a–c) and fuel consumption rate (d–f) versus temperature, for $\mathrm{Ka}_{\delta,\mathrm{K}} = 100$ (a, d), 1000 (b, e), and 10000 (c, f), in comparison with solutions from zero-dimensional auto-ignition (red dash-dotted-dash lines), perfectly stirred reactors (blue dotted lines), and 1D freely propagating premixed flames (green dashed lines). Color of each pixel indicates the logarithmic number of computational cells within the pixel normalized by the maximum value. In panel (f), the fuel consumption rate is scaled by 1/4. Reproduced from Ref. [66].

terms of the co-location of fuel consumption and heat release. Unsurprisingly, the enlarged thermochemical space induced by strong turbulence can alter these relationships in a fuel-dependent manner.

Aspden *et al.* [69, 86, 131] reported an increasing de-correlation between fuel consumption and heat release rates with increasing Karlovitz numbers in H_2/air flames. They suggested that differential diffusion of the highly mobile hydrogen atom, in conjunction with turbulent advection and molecular mixing, contribute to the observed de-correlation.

Xu *et al.* [66] observed a de-correlation between fuel consumption and heat release rates for a series of DNS of n-dodecane/air flames at 30 bar. As shown in Fig. 24, the fuel consumption rate peaks around 1500 K and the heat release rate peaks around 1900 K at a relatively modest Karlovitz number of 100. Similar de-correlations have been reported in a few other heavy-hydrocarbon based DNS studies [67, 123], and have also been observed in corresponding unstrained laminar flames (e.g., as shown in Fig. 2(b)), as an expected consequence of fuel cracking [148]. However, the fuel consumption peak is brought closer to the heat release peak in temperature space with increasing Karlovitz numbers (i.e., Fig. 24(b) and (c) for $\mathrm{Ka}_{\delta,\mathrm{K}} = 1{,}000$ and 10,000, respectively). That is, the de-correlation of fuel

consumption and heat release rates found in laminar n-dodecane/air flames is statistically reduced in intense turbulence due to the rapid turbulence-induced mixing. Fuel consumption rates are much larger than in corresponding laminar flames at $\mathrm{Ka}_{\delta,\mathrm{K}} = 10{,}000$, because the endothermic fuel cracking process is exposed to temperatures up to 1800 K.

Although the limit of a perfectly stirred reactor (PSR) is employed in Fig. 24, PSR-like behaviors are rarely observed in the reviewed literature, except under the extreme conditions around Karlovitz numbers of 10,000 as shown in Fig. 24. As reflected in Fig. 9(a), conditions relevant to practical combustors reside outside the "distributed reactions" regime. The irrelevance of the PSR limit is partly due to the fact that practical devices are designed to avoid detrimental limit conditions. As observed in the previous sections, transition to extinction, autoignition and compressible regimes occur more frequently with increasing turbulence intensity. Such limit phenomena might be precursors to global flame extinction or the onset of combustion instability [33], which are undesirable in practical combustors.

For methane/air flames, the normally co-located fuel consumption and heat release rates in a laminar flame can become de-correlated due to hydrodynamic effects. As noted by Wabel *et al.* [111], heat release rates in the LUPJ burner do not completely coincide with methane consumption. Their study post-processed DNS of two high Karlovitz number flames to assess experimentally accessible heat release rate markers, accounting for experimental factors. They reported the existence of a spatially distributed low-intensity heat release zone that makes up approximately 30% of the total heat release rate, due to slow oxidation of CO that is convected downstream to CO_2 due to insufficient residence time upstream. We note that this distributed heat release region is fundamentally different than that hypothesized to occur due to rapid turbulent stirring in the main heat release zone of a methane/air flame. The low-intensity heat release zone cannot be detected by common flame markers, because these markers are designed to detect key chemical reactions in the process of transitioning from hydrocarbon fuels to CO, instead of CO oxidation.

Wang *et al.* [65] also reported "two-stage" combustion in DNS of stratified flames. They found that the temperature-conditioned mean reaction rate of the recombination reaction $\mathrm{CO + OH = CO_2 + H}$ is lower than in a laminar flame in the upstream regions with low

residence time. Further downstream, the conditional mean of the reaction rate becomes comparable to, or higher than, corresponding laminar flames, indicating that CO is not completely oxidized upstream and significant CO oxidation occurs further downstream. As a result of the low residence time upstream, fuel fragments such as CO and H_2 are not allowed sufficient time to be converted to CO_2 or H_2O. Consequently, they are convected downstream and fully oxidized at the flame tip.

3.4. Local combustion mode and its diagnostics

To understand the dynamics of flame propagation in highly turbulent premixed flames, diagnosis of the local combustion mode is vitally important [15, 134, 149, 150]. Here, we aim to distinguish between the different modes of premixed combustion described in Section 2.2.1, as opposed to whether local flame segments are premixed, non-premixed, or partially premixed. Knowledge of whether a local mixture is a diffusion-enabled premixed deflagration or a chemistry-driven auto-ignition front is critical for developing physics-based combustion models. For a chemistry-driven auto-ignition front, its propagation is more sensitive to the local composition and details of finite-rate chemistry, compared to a conventional deflagration wave.

3.4.1. Budget analysis

Quantitative diagnostics of the local combustion mode are related to the balance between advection, diffusion, and reaction, as these are the three driving processes for chemical scalar dynamics. Transport budget analysis of advection, diffusion, and reaction has been widely adopted to differentiate various local dynamics [13, 70, 149, 151]. The quantity of interest in these studies is usually a scalar, such as mass fraction of a species or progress variable, or the scalar gradient. The analysis is conventionally conducted in physical space. For example, through transport budget analysis, Krisman *et al.* [152] demonstrated that advection is balanced by reactions under autoignitive conditions, while diffusion is balanced by reactions for deflagration waves.

However, this form of budget analysis can be ambiguous under certain complicated conditions (e.g., turbulent stratified flames). Other quantities, such as the scalar dissipation

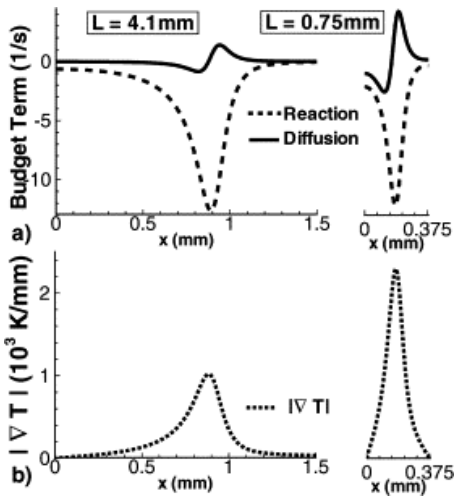

Figure 25: Reprinted from Fig. 4 in Ref. [13] with permission of Elsevier. Transport budget analysis of Y_{H_2} for two one-dimensional hydrogen/air flames propagating into inhomogeneous temperatures. The L=4.1 mm case represents an auto-ignition front while the L=0.75 mm case represents a premixed front. Dashed line: reaction. Solid line: diffusion. Dotted line: temperature gradient.

rates or temperature gradients, need to be considered to clearly identify the mode. For example, Fig. 25 shows two different scenarios in a thermally stratified H_2/air flame where two one-dimensional hydrogen/air flames propagate into inhomogeneous temperature fields whose fluctuations are characterized by different wavelength L [13]; at $L = 4.1$ mm (large wavelength limit), reactions are much larger than diffusion, whereas reactions and diffusion are more balanced at $L = 0.75$ mm (small wavelength limit). However, there is no clear distinction between combustion modes and additional information (e.g., based on the temperature gradient in Fig. 25(b)), is required to more clearly identify the auto-igniting (lower gradient at L=4.1 mm) and deflagration (higher gradient at L=0.75 mm) fronts. Hence, although transport budget analysis can provide helpful insights for differentiating auto-ignition and deflagration fronts, its effectiveness is often configuration-dependent, and the comparison between diffusion, advection and reaction sources is rather qualitative.

3.4.2. Computational singular perturbation

A more quantitative method to quantify the contributions of chemistry and diffusion to scalar evolution employs the computational singular perturbation (CSP) method [153, 154]. A vector of modes can be defined for a nonlinear time-dependent ordinary differential equation (ODE) system. For a combustion system involving detailed chemistry, each element of the vector of modes is a linear combination of reaction rates for each species. The CSP method provides a refinement procedure to decouple the fast and slow modes, and subsequently identifies exhausted fast processes that can be algebraically related to other processes. It has been primarily applied in the analysis and reduction of stiff nonlinear ODE systems, to identify quasi-steady-state species, to eliminate unimportant species, and to remove stiffness.

For dynamic systems involving diffusion and advection, the CSP refinement procedure is extended to treat partial differential equations. For example, Valorani *et al.* [155] employed CSP to study the dynamic balances between chemistry, diffusion, and advection in a methane/air flame-vortex interaction simulation. The time scales of the local chemistry are represented by time scales of the fast and slow CSP modes, and the roles of diffusion, convection, and chemistry are compared in each CSP mode. They found that the cold reactant zone is driven by diffusion, where active chemical time scales are much slower than those of diffusion and convection. In the flame region, the driving time scales are those from chemical reactions, and the thermochemical manifold has a large dimension. Finally, downstream of the flame, the dynamics are locally controlled by slow transport processes and slow chemical kinetics.

In addition to understanding the flame structure, an importance index can be defined using the CSP concept to measure the relative importance of transport (convection and diffusion) and temperature [14]. The importance index was applied to the regions ahead of the reaction fronts in a series of HCCI-type syngas/air flames and successfully differentiated deflagration from auto-ignition. To further avoid the tolerance-based selection of individual chemical time scales, Valorani *et al.* [156] formulated a tangential stretching rate (TSR) method for reactive-diffusive systems, in which the relative importance of transport and

chemistry were compared in the direction of the most energy-containing mode.

3.4.3. Chemical explosive model analysis

Another quantitative approach to diagnose the local combustion mode is derived from chemical explosive mode analysis (CEMA) [157]. As described by Lu *et al.* [158], CEMA finds its premises and theoretical grounding in the CSP method, while devoting special attention to the role of eigenvalues of local chemical Jacobians. A variety of CSP tools and concepts are leveraged in CEMA, although the two methods are mathematically different; CEMA involves only the local chemical Jacobian (i.e., $\partial\dot{\boldsymbol{\omega}}/\partial\boldsymbol{\psi}$ following the notation in Eq. (20)), while CSP involves the full Jacobian of the right side of a thermochemical scalar transport equation (i.e., $\partial(\dot{\boldsymbol{\omega}}+\boldsymbol{s})/\partial\boldsymbol{\psi}$), considering both chemical and transport effects [159]. In CEMA, the zero-crossing of a single eigenvalue from a large set of candidates (e.g., a full set of eigenvalues, any vector of CSP data, or an arbitrary set of basis vectors) is identified as being strongly correlated to a variety of flame features, including the flame reaction fronts. As such, CEMA has been widely adopted in the analysis of turbulent reactive flows and other limiting phenomena in combustion, e.g., Refs. [66, 160–163].

CEMA is performed through the eigen-decomposition of the chemical Jacobian ($\boldsymbol{J}_{\boldsymbol{\omega}} \equiv \partial\dot{\boldsymbol{\omega}}/\partial\boldsymbol{\psi}$), as shown by

$$\frac{\mathrm{D}\dot{\boldsymbol{\omega}}}{\mathrm{D}t} = \frac{\partial\dot{\boldsymbol{\omega}}}{\partial\boldsymbol{\psi}}\frac{\mathrm{D}\boldsymbol{\psi}}{\mathrm{D}t} = \boldsymbol{J}_{\boldsymbol{\omega}}(\dot{\boldsymbol{\omega}} + \boldsymbol{s}) \ . \tag{20}$$

Here $\boldsymbol{\psi}$ is comprised of all species concentrations and temperature, and $\dot{\boldsymbol{\omega}}$ and $\boldsymbol{s}$ are two vectors containing the chemical and non-chemical (i.e., diffusion) source terms for all components of $\boldsymbol{\psi}$, respectively. A chemical mode is defined as an eigenmode of the chemical Jacobian $\boldsymbol{J}_{\boldsymbol{\omega}}$. Each chemical mode is associated with an eigenvalue (λ_{e}) and a corresponding pair of left ($\boldsymbol{b}_{\mathrm{e}}$) and right ($\boldsymbol{a}_{\mathrm{e}}$) eigenvectors. A chemical mode is further classified as a chemical *explosive* mode (CEM) if the real part of the associated eigenvalue, $\mathrm{Re}(\lambda_{\mathrm{e}})$, is positive [157]. The existence of a CEM indicates that the reaction rates of the mixture tend to grow exponentially along the direction of the eigenvector associated with the CEM, if the mixture is isolated in a lossless environment where all non-chemical sources are negligible; the existence of a CEM indicates that the mixture could undergo thermal runaway. How-

ever, the thermal runaway does not necessarily occur, particularly when other non-chemical effects, such as diffusion, are strong. To avoid ambiguity, the largest $\mathrm{Re}(\lambda_\mathrm{e})$ generally is taken to visualize the CEMs of the mixture.

Additional procedures have been developed in the past five years [12, 66] to introduce transport effects into CEMA-based methods. The objective is to distinguish different local combustion modes by measuring the contributions of diffusion (φ_s) and reaction (φ_ω) on the evolution of a (purley chemical) CEM. Both φ_s and φ_ω are defined based on the projection of the diffusion ($\boldsymbol{s}$) and reaction ($\dot{\boldsymbol{\omega}}$) source terms to the left eigenvector $\boldsymbol{b}_\mathrm{e}$ associated with CEM, respectively, namely

$$\varphi_\mathrm{s} \equiv \boldsymbol{b_e} \cdot \boldsymbol{s},\ \varphi_\omega \equiv \boldsymbol{b_e} \cdot \dot{\boldsymbol{\omega}}\ . \tag{21}$$

Comparison of φ_s and φ_ω systematically quantifies the competition between molecular diffusion and chemical reactions. Note that φ_ω is strictly positive. When $\varphi_\mathrm{s} > \varphi_\omega$, energy and radicals are transported in a manner that moves the mixture towards thermal runaway, at a faster rate than chemistry drives the mixture. This is termed (diffusion) "assisted ignition" in the CEMA literature. When $-\varphi_\omega < \varphi_\mathrm{s} < \varphi_\omega$, chemical kinetics dominate the local scalar dynamics compared to transport, which is termed "auto-ignition" in the literature. Finally, $\varphi_\mathrm{s} < -\varphi_\omega$ indicates that heat and radical loss through diffusion adjust the mixture away from ignition faster than the chemistry moves it towards ignition; this is termed "extinction". The ratio $\varphi_\mathrm{s}/\varphi_\omega$ then indicates the local combustion mode.

As an example, Fig. 26 shows CEMA of the combustion mode in the central plane of an upward-propagating n-dodecane/air planar jet flame at 30 atm and $\mathrm{Ka}_{\delta,\mathrm{K}} = 1{,}000$ [66]. The real part of the eigenvalue associated with the CEM is shown in the left panel, where the zero-crossing (i.e., the interface between positive and negative, or visually between red and blue in Fig. 26) indicates the location of ignition fronts. The local combustion modes (i.e., $\varphi_\mathrm{s}/\varphi_\omega$) are identified within the explosive region of the flame, as shown in the middle panel. The two diffusion-dominant modes (i.e., "extinction" mode and "assisted-ignition" mode) are frequently observed in the pre-ignition region of the turbulent flame brush, indicating a strong influence from diffusion on the ignition propensity in these flames. The integrated

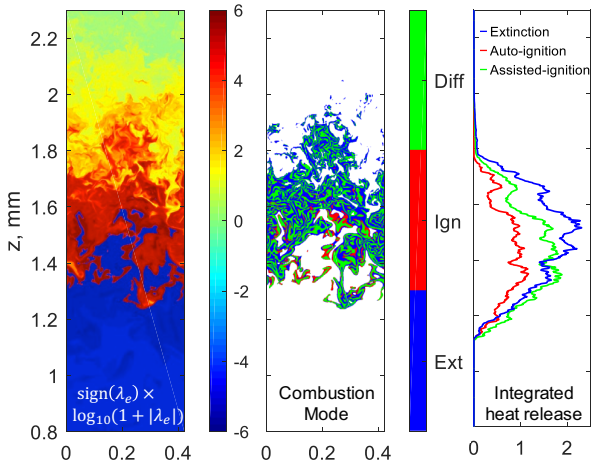

Figure 26: Distributions of the chemical explosive mode eigenvalue, local combustion modes, and integrated HRR per unit-length in the streamwise direction attributable to the different combustion modes. Colors in eigenvalue fields indicate the value of $\mathrm{sign}(\lambda_e) \times \log 10(1 + |\lambda_e|, 1/\mathrm{s})$. Colors on the combustion mode fields represent the assisted-ignition (green, Diff), auto-ignition (red, Ign), and extinction modes (blue, Ext), respectively. The product zone ($\lambda_e < 0$) and the fresh reactant zone ($T < 1000$ K) are truncated in the mode plots (the middle panel). Reproduced by permission of the Combustion Institute.

heat release rates, conditional on each local combustion mode and axial position, are shown in the right panel in Fig. 26. All three modes contribute significantly to the integrated heat release rate across the broad flame brush, demonstrating the intense competition between diffusion and reaction throughout this highly turbulent premixed flame.

We note that having significant heat release rate in regions identified as "extinction" is not paradoxical, given the definition of "extinction" used in this analysis. In fact, similar confusion might arise when relating the local "auto-ignition" mode with the conventional concept of "auto-ignition" in a mixture. The local "auto-ignition mode" and conventional "auto-ignition" share common characteristics in the sense that thermal runaway is a dominating factor compared to diffusion. Similarly, the "extinction mode" from CEMA describes a local and instantaneous condition where diffusion moves heat and radicals away from the ignition direction. Depending on the dynamics of the flame, the local extinction mode may or may not lead to extinction of the chemical reactions. The concepts of local extinction and local auto-ignition in turbulent flames are not unique to CEMA-based local mode analysis.

In fact, local extinction/auto-ignition has been constantly delineated in turbulent combustion literature using scatter plots and budget analysis (e.g., Fig. 25). CEMA-based local mode analysis only offers a specific mathematical definition.

An experimental approach for identifying CEMs (and heat release rate) has recently been proposed [164] and assessed using DNS of the LUPJ burner [165]. Raman/Rayleigh/OH PLIF measurements were simulated, providing information on the major species, temperature, and OH concentration. Promising agreement with computational predictions was shown in measuring the location of zero-crossing of the eigenvalues of the chemical Jacobian (i.e., the location of the ignition fronts) for both laminar and turbulent flames. This introduces the possibility of performing CEMA of local combustion modes in flames that are not accessible to DNS.

3.5. Summary

As a summary, the burning rates of flames are determined by reaction and transport (including both macroscopic transport through turbulence and microscopic transport through molecular diffusion) of the mixture. The competition between the processes intensifies with increasing turbulence intensity, and the resulting local combustion modes/states diversify in these highly turbulent flames. A few takeaway points are summarized below:

1. In physical space, highly turbulent premixed flames can be locally thinned or thickened. Preheat zones are shown to be reactive, enabled by pyrolysis reactions, differential diffusion, local extinction, and intense turbulent advection.
2. Non-unity Lewis number effects persist in these highly turbulent premixed flames, and are particularly noticeable in local flame dynamics, such as local heat release rates [69, 86] and responses to stretch [76], etc. Consequently, the choice of molecular transport models can have a significant impact, at least on local flame dynamics.
3. Reaction rates are more varied in highly turbulent flames compared to their laminar counterparts, for example as demonstrated in Refs. [67, 69, 86, 132], due to the enlarged thermochemical state space created by turbulence-chemistry interactions. Chemical pathways remain similar between different conditions, although more reactions are

consequential to a significant level for turbulent flames. Due to the optimization process used to develop chemical kinetic models, the task of identifying missing chemical pathways in reduced chemical mechanisms remains challenging.

4. Fuel consumption and heat release rates are not closely correlated in highly turbulent premixed flames, as a result of fuel pyrolysis [66, 67, 123], differential diffusion [69, 86, 131], local extinction [66], and turbulent advection [65, 111]. Caution should be taken when employing fuel consumption rates as a surrogate for heat release rate, either experimentally or computationally.
5. For high Karlovitz number turbulent premixed flames, local flame characteristics are diversified and adjusted to local turbulence and chemistry conditions. Such adjustments can manifest in terms of local flame thickness, flame surface density, and frequency of local limit conditions, etc. Consequently, many state-of-the-art turbulent combustion models can still provide reasonable predictions of flames in this regime, although prior knowledge of local conditions and the ability to adjust to these conditions are required to attain sufficient accuracy.

4. Turbulence Structure and Dynamics

The discussion in Section 3 focused on the impact of turbulence on flame structure and dynamics, primarily through the modification of scalar gradients controlling diffusion and, consequently, the complexity of the thermochemical state space and reaction rates. However, chemical reactions also influence the turbulent flow, both by altering fluid transport properties and by coupling thermal and mechanical energies. This section reviews current knowledge regarding the impact of combustion on turbulence structure and dynamics in highly turbulent premixed flames. In the following, we outline both *kinematic* and *dynamic* properties of turbulence. Kinematic properties pertain to *how* the flow is structured and moves, including both single and multi-point statistics of velocity (e.g., turbulence kinetic energy) and velocity gradient (e.g., vorticity and strain rate) quantities. Spectra and scale-dependent turbulence characteristics can also be considered kinematic properties. The

dynamics of turbulence provide an explanation for *why* the flow behaves as it does, in particular revealing the physical mechanisms by which the flame affects the turbulent flow. For example, dynamics encompasses the study of terms found in the turbulence kinetic energy transport equation, in either physical or spectral space, as well as the study of the coupled evolution of the vorticity and strain rate, including alignments between the vorticity and strain rate eigenvectors. We also discuss the status and outlook for universal theories of turbulence during highly turbulent premixed combustion, with a particular focus on the applicability of classical theories developed for non-reacting turbulence.

It should be noted that we focus here specifically on the properties of turbulence for highly turbulent premixed combustion. It has been established that there are substantial effects of the flame on turbulence at lower intensities, and an exhaustive review of knowledge in this area has been provided by Lipatnikov & Chomiak [9]. By contrast, we are just now beginning to understand the properties of turbulence at high intensities, and how these properties vary as the turbulence intensity (or Karlovitz number) increases. It should also be noted that, in the following discussion, we devote substantial attention to the properties of non-reacting (i.e., constant density and constant viscosity) turbulence. It will be seen from this review that properties of non-reacting turbulence are of more than simply academic interest since, in many respects, the characteristics of turbulence for highly turbulent combustion are similar to those found in non-reacting flows.

4.1. Turbulence kinetic energy, stresses, and fluxes

For any high-Re_ℓ turbulent flow, there is substantial spatial and temporal complexity, and fluid mixing is enhanced compared to laminar flows. This complexity can be quantified using second-order, single-point statistics, including the turbulence kinetic energy, turbulent stresses, and turbulent fluxes of various scalar quantities, such as the temperature and reactant mass fraction. In the following, we summarize the current understanding of these statistics in highly turbulent premixed reacting flows. It should be noted that these quantities, including their dynamics, are also frequently studied using multi-scale and spectral analyses; we will discuss these characteristics in Section 4.3.

4.1.1. Turbulence kinetic energy

The intensity of turbulence is often quantified using the turbulence kinetic energy $k \equiv (1/2)\overline{u_i' u_i'}$, where $u_i' = u_i - \overline{u}_i$ and $\overline{(\cdot)}$ is an appropriately defined average (e.g., an ensemble average). In many studies of premixed combustion, the ensemble averaged k is replaced instead by the Favre-averaged definition of turbulence kinetic energy, $\widetilde{k} \equiv (1/2)\widetilde{u_i'' u_i''}$, where $u_i'' = u_i - \widetilde{u}_i$ and $\widetilde{\psi} = \overline{\rho\psi}/\overline{\rho}$ denotes a Favre-average of a generic variable ψ. Favre averages are often used to simplify the analysis of governing equations in compressible and reacting flows, due to the considerable temporal and spatial variations in density found in such flows. In some cases, the turbulence intensity is quantified using a single component of u_i'', for example the root mean square intensity $\widetilde{(u_1'')^2}^{1/2}$.

The transport equation for $\widetilde{k}$ is obtained from the trace of the transport equation for the single-point momentum flux $\widetilde{u_i'' u_j''}$ as [166]

$$\frac{\partial}{\partial t}\left(\overline{\rho}\widetilde{k}\right) + \frac{\partial}{\partial x_k}\left(\overline{\rho}\widetilde{u}_k\widetilde{k}\right) = -\,\overline{\rho}\left(\widetilde{u_k'' u_i''}\right)\frac{\partial \widetilde{u}_i}{\partial x_k} - \overline{u_i''\frac{\partial p}{\partial x_i}} + \frac{\partial}{\partial x_k}\left[\overline{u_i''\tau_{ik}} - \frac{\overline{\rho}}{2}\left(\widetilde{u_k'' u_i'' u_i''}\right)\right] - \overline{\tau_{ik}\frac{\partial u_i''}{\partial x_k}}\,. \tag{22}$$

The first term on the right-hand side represents kinetic energy production by Favre-averaged velocity gradients, the second term represents the velocity-pressure gradient interaction, the third term represents viscous and turbulent transport, and the last term represents viscous dissipation. Although the production and dissipation terms are roughly equal in magnitude across a wide range of flows, the balance of the various terms Eq. (22) can nevertheless vary substantially, particularly in premixed reacting flows where the velocity-pressure gradient term can be significant. This term can be rewritten as

$$\overline{u_i''\frac{\partial p}{\partial x_i}} = \frac{\partial}{\partial x_k}\left(\overline{u_k'' p}\right) - \overline{p\frac{\partial u_k''}{\partial x_k}}\,, \tag{23}$$

where the second term on the right-hand side represents pressure-dilatation effects, which are present only in compressible flows where $\partial u_k''/\partial x_k \neq 0$. The first term on the right in Eq. (23) is present even in incompressible non-reacting flows and represents pressure transport; this term is often combined with the viscous and turbulent transport terms in Eq. (22).

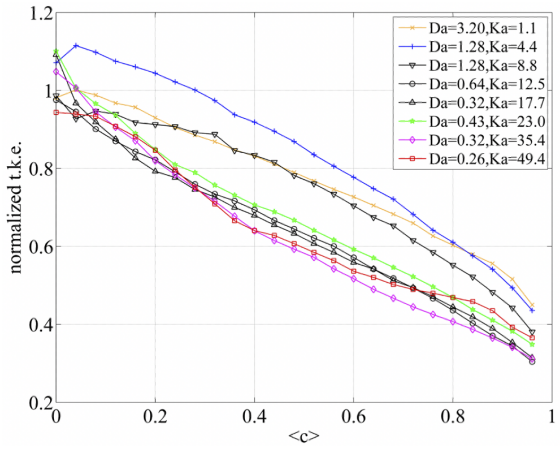

Figure 27: Favre-averaged turbulence kinetic energy $\widetilde{k}$ as a function of planar-averaged reaction progress variable for different $\mathrm{Ka}_{\delta,\mathrm{K}}$ and $\mathrm{Da}_{\ell,\delta}$ in a statistically planar lean methane-air premixed flame studied using DNS. Reprinted from Ref. [167] with permission from AIP Publishing.

A number of studies have examined the properties of the turbulence kinetic energy during premixed combustion spanning a wide range of turbulence intensities, including conditions characterized by high $\mathrm{Ka}_{\delta,\mathrm{K}}$. Using DNS of statistically planar flames, Chakraborty *et al.* [168] and Wang & Abraham [167] showed that $\widetilde{k}$ decreases monotonically across the flame brush at high $\mathrm{Ka}_{\delta,\mathrm{K}}$, where $\mathrm{Ka}_{\delta,\mathrm{K}} = 0.54$ and 13 in Ref. [168] and 1.1–49 in Ref. [167]. For example, Fig. 27 shows the decrease in $\widetilde{k}$ as a function of the planar averaged progress variable [167]. This decrease was found by both Chakraborty *et al.* [168] and Wang & Abraham [167] to be due to the dominance of viscous dissipation and viscous transport as the kinematic viscosity increases across the flame. Wang & Abraham [167] used a scaling analysis to further show that both viscous transport and dissipation vary as the square of $\mathrm{Ka}_{\delta,\mathrm{K}}$, with the production and pressure-dilatation terms having weaker scalings with $\mathrm{Ka}_{\delta,\mathrm{K}}$. For lower values of $\mathrm{Ka}_{\delta,\mathrm{K}}$, pressure-velocity coupling terms, including the pressure-dilatation, were found to be more significant in the overall dynamics, but the magnitudes of these terms weakened relative to the production and dissipation terms as $\mathrm{Ka}_{\delta,\mathrm{K}}$ increased. It is important to note, however, that there is no mean shear in these statistically planar flames that would lead to the production of turbulence kinetic energy via the first term on the right side of Eq. (22). These results are also statistical, and it is still possible to have

locally and instantaneously large values of the pressure-dilatation, even if the average effect is small.

Mean shear is present in jet flames, for example the planar premixed hydrogen-air jet studied using DNS by MacArt *et al.* [166, 169] and Lee *et al.* [170]. In these jet configurations, the stress components $\widetilde{u''_\alpha u''_\alpha}$ (summation over repeated Greek indices is not implied) were each shown to decrease across the flame as a whole, consistent with results for the planar configuration studied by Wang & Abraham [167]. However, there also was an increase in $\widetilde{u''_\alpha u''_\alpha}$ and, hence, $\widetilde{k}$ for intermediate values of the Favre-averaged progress variable $\widetilde{c}$ (see Fig. 28). This increase, which was present for both low and high values of $\mathrm{Ka}_{\delta,\mathrm{K}}$ (corresponding to in-flame Karlovitz numbers of 3.7 and 54, respectively), had different dynamical origins in each case, as shown in Fig. 29 [166]. In particular, for low $\mathrm{Ka}_{\delta,\mathrm{K}}$, each term in the transport equation for $\widetilde{k}$ was substantially non-zero, except for the turbulence and viscous transport terms, and the velocity-pressure gradient term was found to be dominant in the overall dynamics. However, for high $\mathrm{Ka}_{\delta,\mathrm{K}}$, the velocity-pressure gradient term was found to be negligible, with the dominant balance occurring between the production and viscous dissipation terms. This is the same balance observed in many non-reacting jet flows, where the mean shear results in large kinetic energy production that is primarily balanced by dissipation.

Consistent with the premixed jet cases examined by MacArt *et al.* [166, 169] and Lee *et al.* [170], the DNS study of a stratified premixed methane-air jet flame by Wang *et al.* [65] also shows that the turbulent velocity $u' \equiv (2k/3)^{1/2}$ is largest for intermediate values of the Favre-averaged progress variable $\widetilde{c}$, with the peak shifting to larger values of $\widetilde{c}$ with greater downstream distance (see Fig. 30). At all downstream locations, the final value of u' for $\widetilde{c} \to 1$ is smaller than the initial value for $\widetilde{c} \to 0$, and this disparity increases in magnitude with greater downstream distance. Although kinetic energy transport terms were not explicitly calculated in this study, it can again be inferred based on the results from MacArt *et al.* [166] that the increase in turbulence intensity for intermediate values of $\widetilde{c}$ corresponds to a dominance of shear-influenced production for intermediate values. It should be noted that Galeazzo *et al.* [171] show radial profiles of the axial velocity variance,

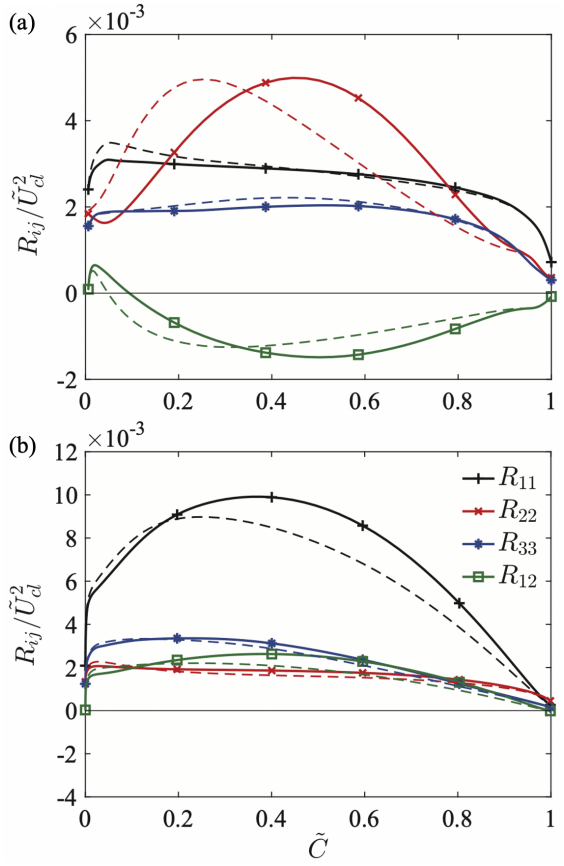

Figure 28: Turbulent stresses $\widetilde{u_i''u_j''}$ (solid lines) and $\overline{u_i'u_j'}$ (dashed lines) as a function Favre-averaged reaction progress variable for a planar premixed hydrogen-air jet flame at (a) low and (b) high $\mathrm{Ka}_{\delta,\mathrm{K}}$ (corresponding to in-flame Karlovitz numbers of 3.7 and 54, respectively). The ij component of the stress tensor is labeled as R_{ij}. Reprinted from Ref. [170] with permission from Elsevier.

which is connected to the turbulence kinetic energy, for the same high $\mathrm{Ka}_{\delta,\mathrm{K}}$ stratified premixed jet flame as that studied by Wang *et al.* [65]. The variance in this study peaks off the centerline of the jet, and results from LES with tabulated flamelets are shown to agree closely with corresponding DNS results for the same flow [65]. A similar peak in the variance was also observed experimentally by Coriton *et al.* [172] for a partially premixed dimethyl ether/air jet flame.

Taken together, these studies indicate that the turbulence intensity, reflected in the value of the turbulence kinetic energy, $\widetilde{k}$, generally decreases across premixed planar and jet flames at high $\mathrm{Ka}_{\delta,\mathrm{K}}$ conditions, due primarily to the increase in viscous dissipation resulting from

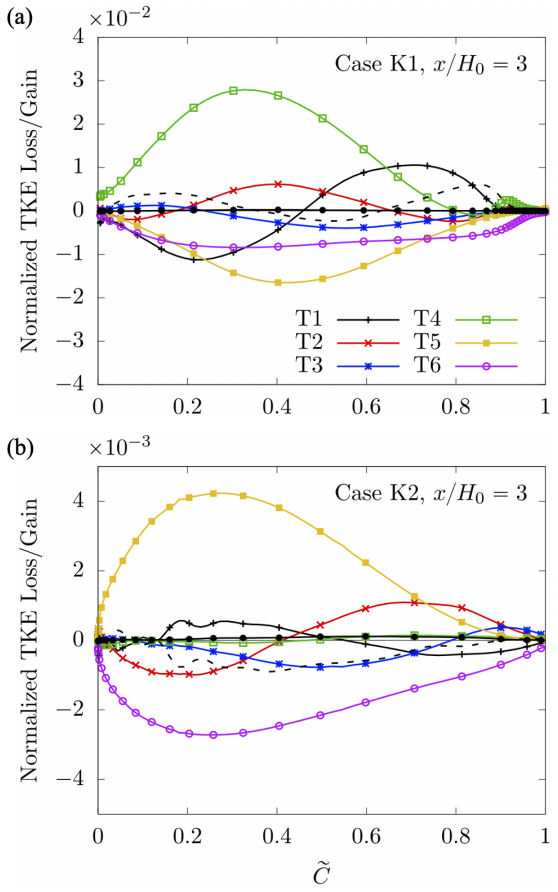

Figure 29: Terms in the transport equation for the turbulence kinetic energy $\widetilde{k}$ as a function Favre-averaged reaction progress variable for a planar premixed hydrogen-air jet flame at (a) low and (b) high $\mathrm{Ka}_{\delta,\mathrm{K}}$ (corresponding to in-flame Karlovitz numbers of 3.7 and 54, respectively). The terms shown are the mean convective transport (T1), turbulent transport (T2), viscous transport (T3), velocity-pressure gradient correlation (T4), production by the mean shear (T5), and viscous dissipation (T6). Black dashed lines in each panel indicate the residual. Reprinted from Ref. [166] with permission from Elsevier.

heat release and the corresponding increase in viscosity. In flows with strong mean shear, such as jets, dissipation is balanced primarily by production due to mean velocity gradients. A similar importance of mean shear has been observed for the propagation of flames in channels [173] and boundary layers [174]. Although velocity-pressure gradient effects can be dominant for low $\mathrm{Ka}_{\delta,\mathrm{K}}$, this effect contributes increasingly weakly to the overall dynamics, as compared to production and dissipation, with increasing $\mathrm{Ka}_{\delta,\mathrm{K}}$. As such, the dynamics of the turbulence kinetic energy increasingly approach that of a corresponding non-reacting

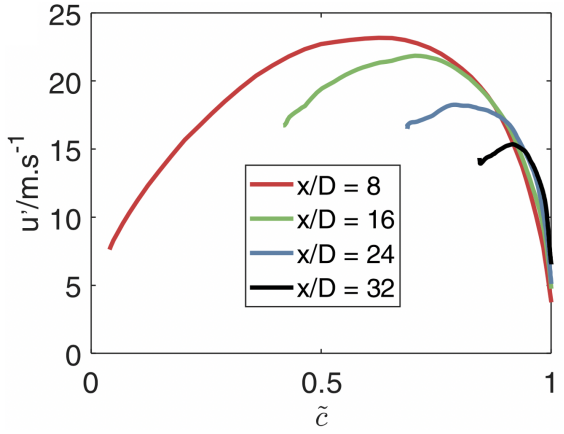

Figure 30: Turbulent velocity $u' \equiv (2k/3)^{1/2}$ as a function of the Favre-averaged reaction progress variable at different downstream distances, x/D, for DNS of a stratified premixed methane-air jet flame. Reprinted from Ref. [65] with permission from Elsevier.

flow as $\mathrm{Ka}_{\delta,\mathrm{K}}$ increases, although locally and instantaneously large magnitudes of heat release effects such as the pressure-dilatation correlation may still be present. This is particularly true for higher turbulence intensities where the internal intermittency (discussed more in subsequent sections) is greater, leading to potentially large values of gradient quantities relative to their means.

In contrast to these results for premixed planar and jet flames, in highly turbulent Bunsen flames relatively little change has been observed in the turbulence kinetic energy across the flame. In particular, despite the tendency for the turbulence kinetic energy to generally decrease across premixed planar and jet flames, Wabel *et al.* [175] did not observe a decrease in the turbulence kinetic energy across a highly turbulent premixed piloted Bunsen flame (see Fig. 31). This difference may be due to the higher free-stream turbulence levels in this case, although an increase in the integral scale was observed through the flame, suggesting that energy was shifted to larger scales, even if the overall kinetic energy was largely unaffected.

There is also evidence for a dependence on the fuel type in the kinetic energy dynamics. In particular, Paxton *et al.* [176] examined fuel effects on the turbulence kinetic energy and shear stress for premixed jet flames at high intensities, finding that these quantities decrease more rapidly along the jet centerline for methane-air mixtures than for mixtures with larger

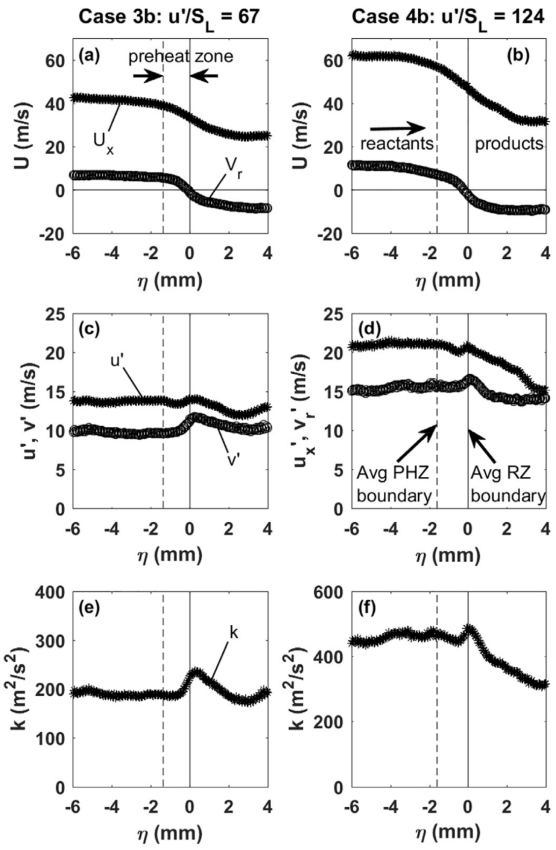

Figure 31: Turbulence statistics conditioned on distance from the reaction zone, η, showing the conditional mean velocity (a,b), conditional RMS velocity fluctuations (c,d), and the conditional turbulence kinetic energy k (e,f) for a highly turbulent premixed Bunsen flame. Preheat and reaction zone (PHZ and RZ, respectively) boundaries are indicated by dashed and solid vertical lines, respectively. Reprinted from Ref. [175] with permission from Elsevier.

hydrocarbon fuels. Moreover, the fuel dependence was found to become more pronounced as the Reynolds number increased. This study additionally showed that the effects of heat release can be partially accounted for in the scaling of the shear layer thickness when using a density-based momentum diameter, and that there is a fuel dependence of the shear layer structure. The underlying physical reasons for this fuel dependence, including the role played by changes in the diffusive transport of chemical species for different fuels, remains an important area for further research.

Finally, it should be noted that the comparison of ensemble- and Favre-averaged quanti-

ties in Fig. 28 from Lee *et al.* [170] indicates that the difference between these two types of averages becomes less pronounced as $\mathrm{Ka}_{\delta,\mathrm{K}}$ increases. Thus, not only are the kinetic energy dynamics increasingly similar to non-reacting flows as $\mathrm{Ka}_{\delta,\mathrm{K}}$ increases, but density weighting also becomes less significant such that $\widetilde{u_i'' u_j''} \to \overline{u_i' u_j'}$ as $\mathrm{Ka}_{\delta,\mathrm{K}}$ increases.

4.1.2. Turbulent stresses

The turbulent transport, or "flux", of a generic quantity ψ can be quantified using the single-point, second-order statistic $\overline{u_i' \psi'}$ (in terms of an ensemble or other appropriately defined average) or as $\widetilde{u_i'' \psi''}$ (in terms of a Favre average). For example, $\widetilde{u_i'' u_j''}$ are turbulent fluxes of velocity u_j in the ith direction (this quantity is often referred to as the "turbulent stress"), and $\widetilde{u_i'' Y_\beta''}$ are turbulent fluxes in the ith direction of the Y_β mass fraction. These fluxes also appear as unclosed terms in the ensemble- or Favre-averaged governing equations for reacting flows. For example, from the Navier-Stokes equation in Eq. (2), the transport equation for the Favre-averaged velocity $\widetilde{u}_i$ is given by

$$\frac{\partial}{\partial t}\left(\overline{\rho}\widetilde{u}_i\right) + \frac{\partial}{\partial x_j}\left(\overline{\rho}\widetilde{u}_i\widetilde{u}_j\right) = -\frac{\partial \overline{p}}{\partial x_i} + \frac{\partial \overline{\tau}_{ij}}{\partial x_j} - \frac{\partial}{\partial x_j}\left(\overline{\rho}\widetilde{u_i'' u_j''}\right) , \tag{24}$$

where the last term on the right-hand side is the unclosed turbulent stress. A similar unclosed term appears in the transport equation for $\widetilde{Y}_j$.

Given the physical and modeling importance of turbulent stresses, substantial focus has been placed on quantifying their properties in different flows. Figure 28 shows four components of the stress tensor $\widetilde{u_i'' u_j''}$ for a premixed methane-air jet flame for both low and high $\mathrm{Ka}_{\delta,\mathrm{K}}$ [166, 170]. As noted in the previous section, the on-diagonal components of this tensor increase for intermediate values of $\widetilde{c}$ and decrease overall across the flame, but Fig. 28 further shows that the shear stress component $\widetilde{u_1'' u_2''}$ changes sign from being predominantly negative for low $\mathrm{Ka}_{\delta,\mathrm{K}}$ to predominantly positive for high $\mathrm{Ka}_{\delta,\mathrm{K}}$. Lee *et al.* [170] show that this change is due to differences in the velocity-pressure gradient effect through the flame. In particular, by decomposing this term into contributions from the fluctuating and mean pressure, Lee *et al.* [170] show that the fluctuating pressure component dominates at high $\mathrm{Ka}_{\delta,\mathrm{K}}$ and acts to isotropize the turbulence, whereas the mean pressure component

dominates for low $\mathrm{Ka}_{\delta,\mathrm{K}}$ where dilatation by the flame is significant relative to turbulence-induced fluctuations in the flow.

There are two primary implications of this result. The first is that the turbulence is expected to be more anisotropic due to effects from the flame at low $\mathrm{Ka}_{\delta,\mathrm{K}}$. This is a result that has been demonstrated in a number of reacting flow studies using a variety of metrics. In Section 4.2 we will comment on the generation of turbulence anisotropy in the context of vorticity characteristics, and a similar increase in the anisotropy within the flame was first observed for a premixed Bunsen flame by Steinberg *et al.* [177]. More recently, MacArt *et al.* [166] have shown using the Favre-averaged anisotropy tensor $\widetilde{a}_{ij} = \widetilde{u_i'' u_j''}/\widetilde{k} - 2\delta_{ij}/3$ that the turbulent stress tensor is anisotropic. Through an analysis of barycentric maps of $\widetilde{a}_{ij}$, MacArt *et al.* [166] show that turbulence is anisotropic within the flame for both low and high $\mathrm{Ka}_{\delta,\mathrm{K}}$, but after the flame, only the high $\mathrm{Ka}_{\delta,\mathrm{K}}$ case returns to an isotropic state. The tendency towards isotropy for high $\mathrm{Ka}_{\delta,\mathrm{K}}$ noted by MacArt *et al.* [166], was also demonstrated from an analysis of small-scale (i.e., SFS) stresses by Klein *et al.* [178] for a statistically planar hydrogen-air premixed flame. For lower $\mathrm{Ka}_{\delta,\mathrm{K}}$, increased anisotropy was again observed, which was once more attributed to the effects of dilatation by the flame.

The second primary implication of the change in stress behavior between low and high $\mathrm{Ka}_{\delta,\mathrm{K}}$ conditions is related to the applicability of the Boussinesq, or gradient transport, hypothesis that is the basis of many closure models for LES and RANS simulations. In the context of Favre-averaged quantities, this hypothesis states that $\widetilde{u_i'' \psi''} \propto -\partial\widetilde{\psi}/\partial x_i$. That is, the turbulent flux of an arbitrary quantity ψ in the ith direction occurs along the direction of decreasing $\widetilde{\psi}$ (given by the gradient). Through an examination of the alignments of velocity (i.e., turbulent stress) and scalar fluxes, MacArt *et al.* [166] showed that, at high $\mathrm{Ka}_{\delta,\mathrm{K}}$, the gradient transport hypothesis is approximately valid (or, at least, no less valid than in a corresponding non-reacting turbulent jet flow). Conversely, for low $\mathrm{Ka}_{\delta,\mathrm{K}}$, the turbulent scalar flux and turbulent stresses are substantially misaligned with the mean gradients, indicating counter-gradient transport and invalidating the Boussinesq hypothesis. This is reflected in conditional statistics of the turbulent shear stress, which reverses sign between the low and high $\mathrm{Ka}_{\delta,\mathrm{K}}$ cases [166, 169, 170] (see also Fig. 28).

It is emphasized that, although the Boussinesq hypothesis is approximately valid in premixed jet flames at high $\mathrm{Ka}_{\delta,\mathrm{K}}$, it should not be assumed that this hypothesis is valid across all high $\mathrm{Ka}_{\delta,\mathrm{K}}$ premixed reacting flows. The more appropriate understanding of this result is that the Boussinesq hypothesis becomes *as valid* in high $\mathrm{Ka}_{\delta,\mathrm{K}}$ flows as it is in a corresponding non-reacting flow. However, there are many non-reacting flows (e.g., rapidly strained flows or flows with high geometric curvatures) that also do not conform to the Boussinesq hypothesis [179]. It is unlikely that the addition of reactions to such flows would improve this agreement, particularly given the reduced applicability of the Boussinesq hypothesis observed in low $\mathrm{Ka}_{\delta,\mathrm{K}}$ premixed jet flames.

4.1.3. Turbulent scalar fluxes

As noted previously, the turbulent flux of a scalar quantity ψ, written as either $\overline{u_i'\psi'}$ or $\widetilde{u_i''\psi''}$ for ensemble and Favre averages, respectively, provides a quantitative measure of the strength of turbulent transport of ψ in the ith direction. In studies of turbulent premixed combustion across a range of turbulence intensities, it has been common, in particular, to study the turbulent transport of species mass fractions, Y_β, and the combustion progress variable, c. In addition to providing fundamental insights into the strength and direction of turbulent mixing, these fluxes also appear as unclosed terms in scalar model equations for RANS and LES (in the latter case, the average used to compute the scalar fluxes is replaced by an appropriate low-pass filter).

Due to their relevance to both RANS and LES, much of the research on scalar fluxes for highly turbulent conditions has, to date, focused primarily on the appropriate way in which to model these quantities, with a particular emphasis on determining the validity of the gradient transport, or Boussinesq, hypothesis for different flows and conditions. In general, the gradient transport hypothesis has been found to provide poor predictions for scalar fluxes in premixed flames at low $\mathrm{Ka}_{\delta,\mathrm{K}}$ (see, e.g., [180, 181]), but the agreement improves as $\mathrm{Ka}_{\delta,\mathrm{K}}$ increases. Klein *et al.* [178] examined SFS scalar fluxes (for species mass fraction scalars) in statistically planar hydrogen-air premixed flames across a range of both low and high $\mathrm{Ka}_{\delta,\mathrm{K}}$ (spanning Karlovitz numbers from 0.75 to 126), finding counter-gradient transport across

all $\mathrm{Ka}_{\delta,\mathrm{K}}$, although the correspondence with the gradient transport hypothesis increased as $\mathrm{Ka}_{\delta,\mathrm{K}}$ increased. It should be noted that Ranjan *et al.* [181] observed substantial counter-gradient transport even at high initial $\mathrm{Ka}_{\delta,\mathrm{K}}$, although for a statistically planar premixed flame interacting with decaying isotropic turbulence, where the local $\mathrm{Ka}_{\delta,\mathrm{K}}$ decreases in time as the turbulence decays.

MacArt *et al.* [166] showed that conditionally averaged cross-stream fluxes of the fuel mass fraction were generally positive for low $\mathrm{Ka}_{\delta,\mathrm{K}}$ and negative for high $\mathrm{Ka}_{\delta,\mathrm{K}}$, with the former corresponding to counter-gradient transport. Through an analysis of the transport equation for the flux $\widetilde{u_i'' Y_\beta''}$, it was shown that this change in behavior was due to the changing behavior of the mean scalar gradient and mean velocity gradient production terms as $\mathrm{Ka}_{\delta,\mathrm{K}}$ increased. MacArt *et al.* [166] additionally examined the variance of the scalar mass fraction, observing that the dynamics of $\widetilde{Y_{\mathrm{H_2O}}''^2}$ are dominated by heat release from the flame at low $\mathrm{Ka}_{\delta,\mathrm{K}}$, while the primary balance is between the production by the mean scalar gradient and dissipation at high $\mathrm{Ka}_{\delta,\mathrm{K}}$, in correspondence with non-reacting scalar variance dynamics.

Ultimately, although the properties of turbulent scalar fluxes do, in general, approach those of non-reacting passive scalar fluxes as $\mathrm{Ka}_{\delta,\mathrm{K}}$ increases, the gradient transport hypothesis remains of dubious validity at high $\mathrm{Ka}_{\delta,\mathrm{K}}$ and across all regions of a premixed flame. As such, further study of the dynamics of these fluxes, such as that performed by MacArt *et al.* [166], remains an important direction of research, particularly across different flows and spanning a wider range of conditions. The improved understanding resulting from such studies may result in the more widespread use in RANS and LES approaches of differential second-order moment closures that do not rely on algebraic gradient transport hypotheses.

4.2. Vorticity, strain rate, and scalar gradients

Velocity gradient quantities, and the vorticity and strain rate in particular, have received substantial focus in studies of both reacting and non-reacting turbulent flows. There are many reasons for this focus, including:

1. Due to the linear wavenumber weighting associated with gradients in spectral space, velocity gradient quantities more directly represent small-scale properties than veloc-

ities alone;

2. In many flows, vorticity and strain rate magnitude fields are punctuated by coherent and spatially localized structures (e.g., vortex "tubes" and "sheets") that provide potential building blocks of turbulence;
3. Statistics, and PDFs in particular, of the vorticity and strain rate reveal the internal intermittency associated with high Reynolds number turbulent flows;
4. The formation of small-scale fluid motions by nonlinear processes can be directly examined, in isolation from purely convective changes, through the vortex stretching term that appears in the vorticity transport equation;
5. The effects of chemical heat release on turbulence can be directly studied by examining dilatation and baroclinic torque terms in the vorticity transport equation;
6. The vorticity and strain rate have direct impacts on the dynamics of scalar gradients, which is particularly significant in reacting flows due to the connection between scalar gradients and flame structure (as was also discussed in Section 3).

Although each of these reasons provide motivation for the study of velocity gradients in premixed reacting flows, the last reason, in particular, allows the explicit study of interactions between turbulence and flame structure in highly turbulent premixed combustion. The local scalar gradient χ_i can be used to express a local flame normal direction as $n_i = \chi_i/\chi$, where χ is the scalar gradient magnitude, and the local flame width, δ_t can be expressed in terms of χ using Eq. (19). Given this connection between vorticity, strain rate, and scalar gradients, we begin this section with a discussion of the properties and dynamics of scalar gradients in highly turbulent premixed flames.

4.2.1. Scalar gradients

The gradients of thermochemical scalars are important for understanding the local, instantaneous structure of premixed flames, the influence of turbulence on the flame structure and dynamics, and the origins of thermochemical complexity under highly turbulent conditions. Thermochemical scalar gradients are also fundamental to understanding the scalar dissipation rate, which must be modeled in many RANS and LES approaches to simulating

premixed combustion. These gradients have consequently been extensively studied over a range of premixed flame conditions, including high turbulence intensities.

The orientation of n_i in highly turbulent premixed combustion has been explored in several studies, including those by Kim & Pitsch [182], Chakraborty *et al.* [183–185], Hartung *et al.* [186], and Hamlington *et al.* [128]. However, most such studies have focused primarily on the orientation of n_i with respect to the eigenvectors of the fluid dynamic strain rate tensor, S_{ij}, and relatively few have examined distributions of n_i or their connection to wrinkling. The alignments of n_i with the strain rate eigenvectors, as well as their physical significance, will be discussed in more detail below, but it is worth noting that distributions of observed orientations of n_i have been found to become more broad as the turbulence intensity increases [128]. For premixed flames in the presence of isotropic turbulence, in particular, the flame orientation becomes increasingly isotropic as the intensity increases [128], indicating that the flame increasingly reflects properties of the underlying turbulence.

The characteristics of δ_{t} have also been explored in a number of studies of highly turbulent premixed combustion. Kamal *et al.* [187] examined the scalar dissipation rate, which is related to the inverse of δ_{t}, in swirling bluff body stabilized premixed flames over a range of turbulence intensities, including high intensities. It was found that diffusive scalar structures become more broadly distributed as the turbulence intensity increases. This results, in particular, in higher probabilities of thin diffusive regions at low turbulence intensity, and broader distributions of diffusive widths at higher turbulence intensity; this range of widths was also discussed in Section 3.1. Similarly, Kamal *et al.* [188] examined temperature gradients and associated scalar dissipation rates in bluff-body stabilized stratified turbulent premixed methane-air flames, finding that gradients were reduced compared to the corresponding laminar flow, indicating a thickening of the flame (i.e., an increase in δ_{t}) compared to corresponding laminar strained and unstrained flames). Magnotti & Barlow [189] examined progress variable gradients and dissipation rates in a high-shear premixed methane-air bluff-body stabilized flame, revealing a decrease in gradient magnitudes through the flame and a corresponding increase in the flame thickness. For a fuel-lean flame this broadening was observed in the preheat zone only, but for a fuel rich flame the broadening was observed

in both the preheat and reaction zones.

Numerical studies have largely confirmed these experimental results. Kim & Pitsch [182], Sankaran *et al.* [80, 190], Chakraborty *et al.* [191], and Hamlington *et al.* [128] all found that δ_t was greater than the corresponding local laminar flame width in the preheat zone of premixed flames, as compared to the reaction zone, and that these values increased in all regions of the flame as the turbulence intensity increased. This is indicative of local flame broadening by turbulence, although the continued correspondence between the turbulent and laminar reaction zone widths, even for high turbulence intensities, was unexpected. This resilience of the reaction zone to strong turbulence has been explained [128, 184] by the reduction of vorticity and strain rate magnitudes by dilatation and the increase in viscous dissipation associated with heat release by the flame, as will be demonstrated in more detail in the next section. Distributions of the local flame width were also examined by Chaudhuri *et al.* [129] and Hamlington *et al.* [192], showing that a wide range of flame widths, both thinner and broader than the corresponding laminar flame, are found in highly turbulent conditions (see also Fig. 14).

The dynamics of n_i and δ_t are fundamentally governed by the dynamics of χ_i, which evolves according to the transport equation

$$\frac{\mathrm{D}\chi_i}{\mathrm{D}t} = -\chi_j S_{ij} - \frac{1}{2}\epsilon_{ijk}\chi_j\omega_k + \frac{\partial}{\partial x_i}\left(\frac{\mathrm{D}\psi}{\mathrm{D}t}\right) , \tag{25}$$

where $\mathrm{D}\psi/\mathrm{D}t$ appearing in the last term is obtained from Eq. (18). There are thus direct interaction terms between χ_i, the fluid dynamic strain rate S_{ij} given in Eq. (6), and the vorticity $\omega_i = \epsilon_{ijk}\partial u_k/\partial x_j$, where ϵ_{ijk} is the cyclic permutation tensor. The presence of the cross product of χ_i and ω_i means that the vorticity will act to rotate the flame surface normal, which is aligned with χ_i, in a direction that is orthogonal to ω_i. This explicit vorticity interaction term is, however, not present in the transport equation for χ, which is most directly connected to the flame width δ_t, namely

$$\frac{\mathrm{D}\chi}{\mathrm{D}t} = -\frac{\chi_i\chi_j}{\chi}S_{ij} + \frac{\chi_i}{\chi}\frac{\partial}{\partial x_i}\left(\frac{\mathrm{D}\psi}{\mathrm{D}t}\right) . \tag{26}$$

The vorticity ω_i does not explicitly appear in the above equation, indicating that only S_{ij} is responsible for direct changes in the scalar gradient magnitude. From these transport

equations, we can then derive transport equations for n_i and δ_t as

$$\frac{\mathrm{D}n_i}{\mathrm{D}t} = P_{ij}S_{jk}n_k - \frac{1}{2}\epsilon_{ijk}n_j\omega_k - \delta_\mathrm{t}P_{ij}\frac{\partial}{\partial x_j}\left(\frac{\mathrm{D}\psi}{\mathrm{D}t}\right) , \tag{27}$$

$$\frac{1}{\delta_\mathrm{t}}\frac{\mathrm{D}\delta_\mathrm{t}}{\mathrm{D}t} = n_iS_{ij}n_j - \delta_\mathrm{t}n_i\frac{\partial}{\partial x_i}\left(\frac{\mathrm{D}\psi}{\mathrm{D}t}\right) . \tag{28}$$

where $P_{ij} \equiv (n_in_j - \delta_{ij})$ corresponds to the plane parallel to the isosurface of ψ, or the plane for which n_i is the normal direction. The first terms on the right-hand sides of both of these equations account for the effect of the strain rate S_{ij} on n_i and δ_t. The last terms in each equation are also similar, but the effects of vorticity only explicitly appear in Eq. (27) for the evolution of n_i. This means that, in a conceptual field that is purely rotational and unstrained, the vorticity would cause changes to the direction of the flame surface normal without changing the flame width. Moreover, the presence of the cross product of the flame surface normal and the vorticity means that the vorticity vector will act to rotate the flame surface normal orthogonally to the direction of ω_i. Both S_{ij} and ω_i are properties of the turbulent flow in which the flame burns, and the interaction terms on the right-hand side of Eq. (25) represent the dominant terms leading to changes in n_i.

Prior studies of scalar gradient dynamics have shown that the dominant effects of turbulence on δ_t and χ are represented by the strain rate interaction terms found on the right-hand sides of Eqs. (26) and (28) [80, 128, 184, 185, 190]. In order to understand the sign and magnitude of this term for different conditions, it has been common to rewrite it in terms of the magnitude, eigenvalues, and eigenvectors of the strain rate S_{ij} as

$$n_iS_{ij}n_j = S\left(\lambda_1|\boldsymbol{e}_1\cdot\boldsymbol{n}|^2 + \lambda_2|\boldsymbol{e}_2\cdot\boldsymbol{n}|^2 + \lambda_3|\boldsymbol{e}_3\cdot\boldsymbol{n}|^2\right) , \tag{29}$$

where $S = (S_{ij}S_{ji})^{1/2}$ is the strain rate magnitude, λ_i are the eigenvalues of S_{ij}, with $\lambda_1 \geq \lambda_2 \geq \lambda_3$, and $\boldsymbol{e}_i$ are the corresponding eigenvectors. For $\lambda_1 > 0$ and $\lambda_3 < 0$, the most negative and positive eigenvalues are often referred to as the "compressional" and "extensional" eigenvalues, respectively. One effect of strain on a flame is to increase δ_t when n_i is more closely aligned with $\boldsymbol{e}_1$, and to decrease δ_t when n_i is more closely aligned with $\boldsymbol{e}_3$. That is, the sign of this turbulence interaction term is completely determined by the relative

magnitudes of the eigenvalues and the alignments of the local flame normal orientation with the strain rate eigenvectors.

In non-reacting turbulent flows where ψ is a passive scalar, the dominant alignment is between $\boldsymbol{n}$ and $\boldsymbol{e}_3$ [193–195], which would correspond to an increase in scalar gradient magnitude χ via Eq. (25) and to a decrease in the flame width δ_t due to the effects of fluid straining. By contrast, in non-premixed reacting flows, Boratav *et al.* [195, 196] found preferential alignment between the scalar gradient and most extensional strain rate eigenvector $\boldsymbol{e}_1$, indicating the destruction of the scalar gradient magnitude.

A number of studies of lower $\mathrm{Ka}_{\delta,\mathrm{K}}$ flows (outside of the highly turbulent regime that is the focus here, e.g., Refs. [186, 197]) have shown that there is preferential alignment between the scalar gradient and $\boldsymbol{e}_1$ in premixed reacting flows, contrary to results found in non-reacting turbulence. However, Chakraborty *et al.* [183] found that, in low $\mathrm{Da}_{\ell,\delta}$ statistically planar premixed flames (corresponding to $\mathrm{Ka}_{\delta,\mathrm{K}} = 11$) the scalar gradient is dominantly aligned with $\boldsymbol{e}_3$. This, in turn, indicates production of the scalar gradient magnitude and local thinning of the flame at these conditions. Consistent with prior studies, Chakraborty *et al.* [183] also found that, in high $\mathrm{Da}_{\ell,\delta}$ flames (with $\mathrm{Ka}_{\delta,\mathrm{K}} = 0.3$), the scalar gradient is aligned with $\boldsymbol{e}_1$, indicating reduction of the gradient magnitude and local flame broadening. It was noted, however, that even for the low $\mathrm{Da}_{\ell,\delta}$ premixed flame, significant regions of alignment with $\boldsymbol{e}_1$ were observed in regions with high local heat release.

Comparing with the high $\mathrm{Da}_{\ell,\delta}$ results of Swaminathan & Grout [197], which showed preferential alignment between $\boldsymbol{e}_1$ and scalar gradient, Kim & Pitsch [182] similarly noted that the alignment with $\boldsymbol{e}_3$ increases as $\mathrm{Ka}_{\delta,\mathrm{K}}$ increases, although this alignment weakens for intermediate values of the progress variable within the flame brush (see Fig. 32). These trends were further confirmed through a series of simulations with increasing $\mathrm{Ka}_{\delta,\mathrm{K}}$ by Hamlington *et al.* [128], where it was shown that there is increasingly dominant alignment between n_i and $\boldsymbol{e}_3$ as $\mathrm{Ka}_{\delta,\mathrm{K}}$ increases from 3.9 to 174.

Several studies have further examined the variation in alignments between the scalar gradient and strain rate eigenvectors at different locations within highly turbulent premixed flames. This is typically accomplished using conditional statistics based on a local progress

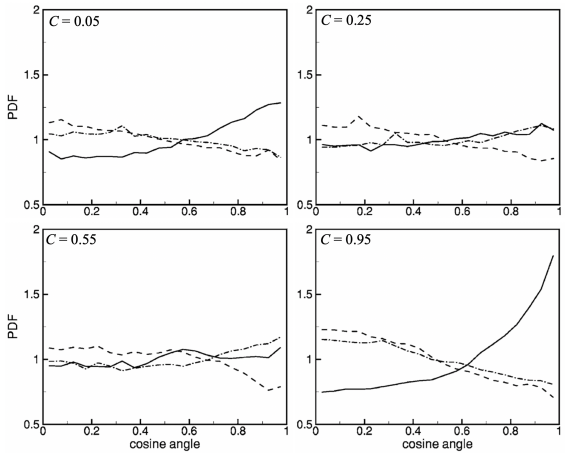

Figure 32: Alignment between $\boldsymbol{n}$ and the eigenvectors of the strain rate tensor at four different values of the reaction progress variable for a statistically planar premixed flame. Dash-dot lines show alignment with $\boldsymbol{e}_1$, dashed lines show alignment with $\boldsymbol{e}_2$, and solid lines show alignment with $\boldsymbol{e}_3$. Cosine angles close to 1 indicate better alignment, while those close to 0 indicate orthogonality. Reprinted from Ref. [182] with permission from AIP Publishing.

variable value. Both Kim & Pitsch [182] and Hamlington *et al.* [128] found that, over a range of different intensities, the alignment of $\boldsymbol{n}$ with $\boldsymbol{e}_1$ was most pronounced near locations of dominant heat release, approximately corresponding to the reaction zone. For both smaller and larger progress variable values, by contrast, preferential alignment was observed with $\boldsymbol{e}_3$.

Supporting the conclusions from these earlier numerical studies, Coriton & Frank [198] experimentally examined the effects of heat release on the eigenvalues and eigenvectors of S_{ij} for a premixed methane-air Bunsen flame. The flame normal was found to preferentially align with $\boldsymbol{e}_1$ close to the products, whereas alignment with $\boldsymbol{e}_3$ was observed in the preheat zone (see Fig. 33). In examining a high-intensity counter-flow premixed flame, Hampp & Lindstedt [199] similarly observed preferential alignment of the flame front normal with $\boldsymbol{e}_1$, as well as reduced vorticity magnitude for larger Da. These results are, correspondingly, consistent with a change in sign of the interaction term $n_i S_{ij} n_j$ through the flame for sufficiently weak turbulence intensities; when $\mathrm{Ka}_{\delta,\mathrm{K}}$ is large enough (e.g., over 100), this term was found to be negative for all locations in a statistically planar premixed flame, on average,

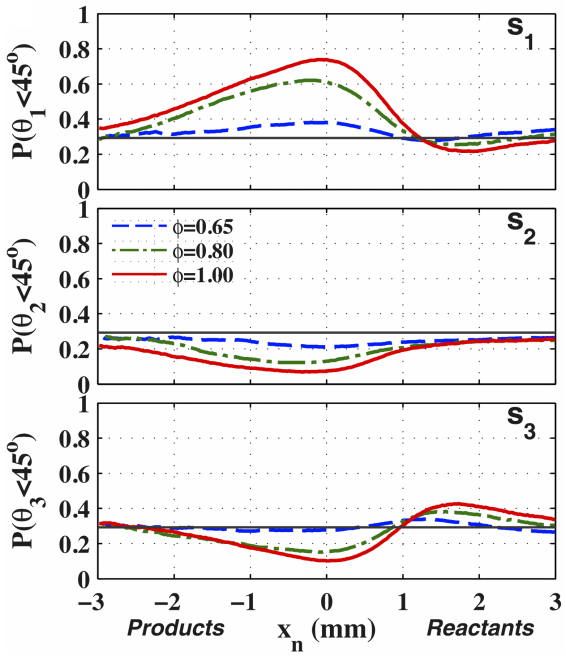

Figure 33: Flame-normal conditional probabilities as a function of the flame-normal coordinate, x_n for a premixed Bunsen flame. Reprinted from Ref. [198] with permission from Elsevier.

indicating a reduction in δ_t [128].

It should be noted, however, that these results obtained for statistically planar and jet premixed flames are not universal, and variations have been observed, particularly at low turbulence intensities. For example, Steinberg *et al.* [177] experimentally examined the alignment of the flame normal with the strain rate eigenvectors in a premixed methane-air slot Bunsen burner at low turbulence intensities. It was found that the flame normal and $\boldsymbol{e}_1$ were predominantly misaligned, and that this mis-alignment increased as turbulence structures approached the flame. Similarly, Zhou & Frank [200] experimentally examined the effects of heat release on strain rate eigenvectors in a counterflow flame at low turbulence intensities. They found that there is preferential alignment between $\boldsymbol{e}_3$ and $\boldsymbol{n}$ due to the effects of the bulk strain rate. Once again, dilatation from heat release promotes alignment between $\boldsymbol{e}_1$ and $\boldsymbol{n}$, although this alignment was not found to be dominant for this configuration.

With respect to other factors affecting scalar gradient alignment, Kim & Pitsch [182] examined the effects of flame curvature on alignment between the scalar gradient and strain

rate eigenvectors, finding that larger negative curvatures were associated with increased alignment between the scalar gradient and $\boldsymbol{e}_1$. Similarly, Chakraborty *et al.* [185] found that the alignment of n_i with $\boldsymbol{e}_1$ decreases as the mean curvature of spherically propagating flames decreases. In general, alignment between the scalar gradient and $\boldsymbol{e}_1$ was attributed to the importance of dilatation effects on the scalar dynamics. Chakraborty *et al.* [184, 185] also examined the effects of Lewis number (Le) and flow curvature on scalar gradient alignment. In Ref. [184], it was found for a range of high $\mathrm{Ka}_{\delta,\mathrm{K}}$ premixed flames (spanning roughly $\mathrm{Ka}_{\delta,\mathrm{K}} = 10 - 34$) that the alignment between the scalar gradient and $\boldsymbol{e}_1$ increases as Le decreases, indicating increased prevalence of flame broadening by turbulent straining.

Beginning with Kim & Pitsch [182] and Chakraborty *et al.* [183], several authors have made a distinction between flame-induced and fluid dynamic strain rates. The production term, $n_i S_{ij} n_j$, is equivalent to a flame normal strain rate, and accounts for the straining of the flame surface along its normal direction, leading to either flame broadening or thinning. By contrast, the tangential strain rate $(n_i n_j - \delta_{ij}) S_{ij}$ acting along the flame surface is generally assumed to be representative of changes in the flame surface area. The study of highly turbulent premixed jet flames by Wang *et al.* [112] showed that the magnitude of the production term is small near the jet exit due to preferential alignment of $\boldsymbol{n}$ with $\boldsymbol{e}_1$, but that this term becomes larger and positive due to the preferential alignment of $\boldsymbol{n}$ with $\boldsymbol{e}_3$ further downstream (see Fig. 34). Similar alignment results have been observed in many other studies spanning a range of turbulence intensities (e.g., [198, 201]).

In summary, in statistically planar and jet premixed flames at sufficiently low turbulence intensities, there is increased alignment between $\boldsymbol{n}$ and $\boldsymbol{e}_1$ in the reaction zone, corresponding to an increase in the local flame width δ_t by the fluid dynamic strain rate S_{ij}. However, as the turbulence intensity increases, this alignment is lost and there is an increasingly dominant alignment between the scalar gradient (or $\boldsymbol{n}$) and $\boldsymbol{e}_3$, consistent with the dynamics of a passive conserved scalar in non-reacting turbulence. The resulting creation of large scalar gradients is of leading-order importance for understanding many aspects of the thermochemical complexity noted in Section 3. In particular, the creation of large gradients, associated with the strain rate interaction term, leads to the increasing dominance of molecular trans-

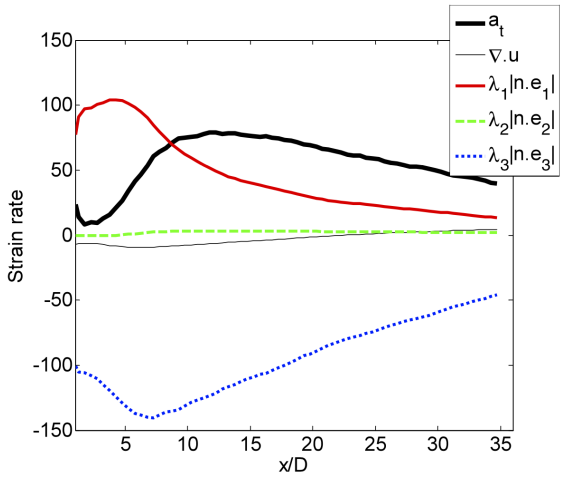

Figure 34: Average values of the scalar gradient magnitude production (a_t), the dilatation $\nabla \cdot \boldsymbol{u}$, and the components of the production due to the alignment of $\boldsymbol{n}$ with different strain rate eigenvectors $\boldsymbol{e}_i$ for the high Karlovitz premixed jet flame studied using DNS by Wang *et al.* [112].

port processes in the thermochemical dynamics. Moreover, since turbulence increases the magnitudes of both negative and positive gradients, resulting in both negative and positive values of transport fluxes, substantial non-monotonicity is found along thermochemical trajectories as the turbulence intensity increases [70]. It is cautioned, however, that these conclusions must be examined further in practical configurations where, for example, there are mean pressure gradients, as discussed in the next section.

4.2.2. Vorticity and strain rate

Given their central importance in the characterization and understanding of turbulence-flame interactions, the vorticity and strain rate are perhaps the most widely studied properties of turbulence in research on highly-turbulent premixed combustion. The dynamics of ω_i are governed by the transport equation

$$\frac{\mathrm{D}\omega_i}{\mathrm{D}t} = \omega_j S_{ij} - \omega_i S_{kk} + \frac{1}{\rho^2}\epsilon_{ijk}\frac{\partial \rho}{\partial x_j}\frac{\partial p}{\partial x_k} + \epsilon_{ijk}\frac{\partial}{\partial x_j}\left(\frac{1}{\rho}\frac{\partial \tau_{kl}}{\partial x_l}\right) , \tag{30}$$

where the first term on the right represents nonlinear vortex stretching associated with the fluid dynamic strain rate S_{ij}, the second term represents dilatation associated with compressibility (where $S_{kk} \neq 0$ in reacting flows), the third term is the baroclinic torque,

and the last term represents the effects of viscous transport. The corresponding transport equation for the enstrophy, $\Omega = (1/2)\omega_{\mathrm{i}}\omega_{\mathrm{i}}$, is obtained from Eq. (30) as

$$\frac{\mathrm{D}\Omega}{\mathrm{D}t} = \omega_i\omega_j S_{ij} - 2\Omega S_{kk} + \frac{\omega_i}{\rho^2}\epsilon_{ijk}\frac{\partial\rho}{\partial x_j}\frac{\partial p}{\partial x_k} + \omega_i\epsilon_{ijk}\frac{\partial}{\partial x_j}\left(\frac{1}{\rho}\frac{\partial\tau_{kl}}{\partial x_l}\right) . \tag{31}$$

Both of these transport equations include vortex-stretching terms that account for the interaction between the vorticity and the strain rate. These terms are associated with the nonlinear cascade process and the generation of small-scale features in turbulent flows. Transport equations can also be obtained for S_{ij} and its magnitude, explicitly revealing the nonlinear coupling between the dynamics of the vorticity and strain rate [202, 203].

In the above transport equations, there are three important reacting flow effects that are not present in constant density, constant viscosity flows. Namely, dilatation dynamically affects the magnitude of the vorticity and enstrophy, while also changing the form of the viscous stress tensor. Second, transport properties, particularly the viscosity, are strong functions of the local thermodynamic state. For example, Sutherland's law for the viscosity of an ideal gas yields $\mu(T) \propto T^{3/2}/(T + C) \lessapprox T^{1/2}$ for typical combustion temperatures (where C is a gas-dependent constant) [204]. Hence, the influence of viscous dissipation increases from the reactants to products. Finally, the combined action of density and pressure gradients influences the turbulence evolution, as expressed through the baroclinic torque terms. The baroclinic torque is generally thought to contribute to "flame-generated" turbulence and is only substantially non-zero where gradients of density and pressure are both large and misaligned.

In non-reacting, incompressible turbulent flows with constant transport properties, only the first (i.e., vortex stretching) and last (i.e., viscous transport) terms in the above transport equations are non-zero. The vortex stretching term, in particular, has received considerable attention due to its role in the production and destruction of vorticity. As with studies of scalar gradient dynamics, it has been common over the past three decades to examine this term via the alignments between the vorticity and the three eigenvectors of the strain rate tensor. In particular, it can be shown that the vortex stretching term appearing in Eq. (31)

can be written as

$$\omega_i S_{ij} \omega_j = S \left(\lambda_1 |\boldsymbol{e}_1 \cdot \boldsymbol{\omega}|^2 + \lambda_2 |\boldsymbol{e}_2 \cdot \boldsymbol{\omega}|^2 + \lambda_3 |\boldsymbol{e}_3 \cdot \boldsymbol{\omega}|^2 \right) . \tag{32}$$

In non-reacting homogeneous isotropic turbulence, the result of the vortex stretching process is to preferentially align vorticity with the eigenvector of the strain rate corresponding to the intermediate eigenvalue, or $\boldsymbol{e}_2$ [194]. There is preferential misalignment with the eigenvector corresponding to the most negative eigenvalue, $\boldsymbol{e}_3$, and relatively weak alignment with the most positive eigenvector, $\boldsymbol{e}_1$. The alignment with $\boldsymbol{e}_2$ has been shown to result from the nonlinear coupling between the vorticity and strain rate [205, 206], although preferential alignment with the most extensional eigenvector of the background or large-scale strain rate has also been identified [207, 208].

In a premixed jet flame, Coriton & Frank [203] found that the presence of combustion increased the magnitude of the vortex stretching term and the associated alignment of the vorticity with $\boldsymbol{e}_2$ due to the increased spatial correspondence between large magnitudes of vorticity and strain rate. Ultimately, this change was found to be due to the effects of the increased shear in the reacting jet flame, as compared to a corresponding non-reacting jet, and the consequent formation of overlapping "sheets" of large vorticity and strain rate magnitudes.

Using numerical simulations, Hamlington *et al.* [128] examined the properties and interactions of the vorticity, strain rate, and scalar gradient in statistically planar premixed flames for a range of turbulence intensities, including high intensities (spanning Karlovitz numbers between 3.9 and 174). It was found that dilatation and baroclinic torque were significant with respect to vortex stretching for low intensities, but that these two effects became less significant at higher intensities. Moreover, the flame generated anisotropy in the orientations of ω_i and the strain rate eigenvectors at low intensities, but this anisotropy was lost for higher intensities. The alignments between ω_i, χ_i, and the strain rate eigenvectors were similar to those found in non-reacting flows for high intensities (that is, ω_i was misaligned with χ_i and preferentially aligned with $\boldsymbol{e}_2$), but for low intensities there was increased alignment between ω_i and $\boldsymbol{e}_1$, as well as increased alignment between ω_i and χ_i

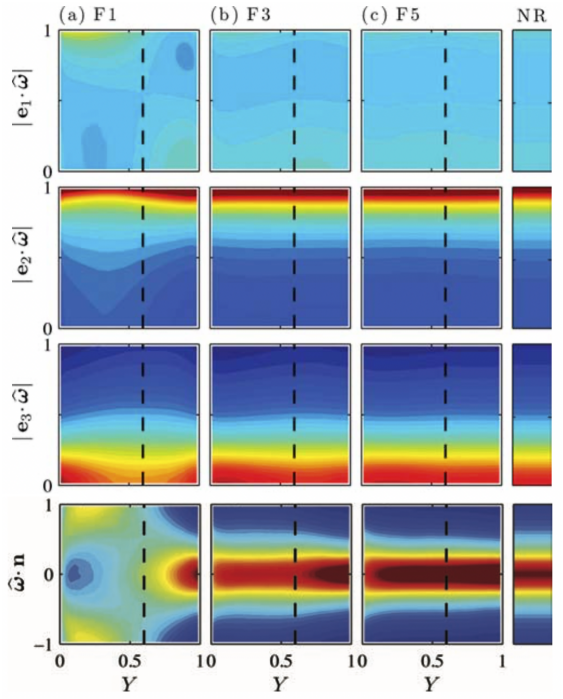

Figure 35: Alignments between the strain rate eigenvectors $\boldsymbol{e}_i$, the vorticity direction vector $\widehat{\omega}_i = \omega_i/\omega$, and the flame normal vector $n_i = \chi_i/\chi$ conditioned on the local instantaneous value of the reactant mass fraction Y for a statistically planar premixed flame at increasing turbulence intensity (left to right), with corresponding non-reacting results shown in the last column. The colorbar goes from 0 (blue) to 1 (red), with larger values indicating better alignment. Vertical dashed black lines indicate the approximate separation between preheat ($Y > 0.6$) and reaction ($Y < 0.6$) zones in the flame. Modified from Ref. [128] with permission from AIP Publishing.

(see Fig. 35).

Many of these results were attributed to the influence of dilatation due to fluid expansion by the flame on the coupled dynamics of ω_i, S_{ij}, and χ_i, although this study did not include explicit temperature-dependent viscous transport or dissipation terms in the governing equations solved by the simulations. However, the decreasing magnitude of the baroclinic torque and dilatation terms relative to the vortex stretching and viscous dissipation terms has been confirmed in a number of other studies of statistically planar premixed flames with homogeneous isotropic turbulence in the reactants, including those by Bobbitt *et al.* [209], Ranjan *et al.* [181], and Papapastolou *et al.* [210].

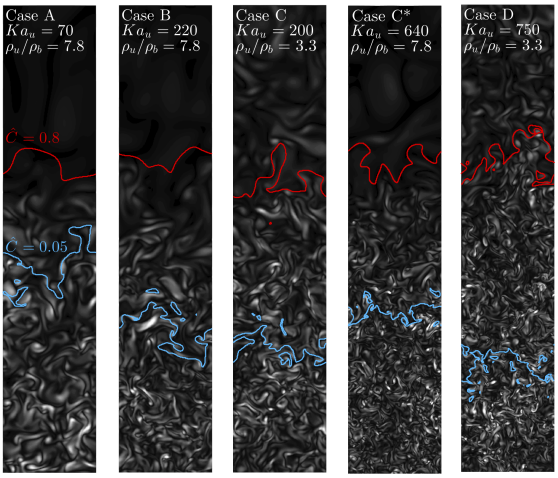

Figure 36: Fields of the vorticity magnitude $|\boldsymbol{\omega}|$ from DNS of a statistically planar n-heptane and air premixed flame. The unburnt Karlovitz number and density ratio for each case are labeled at the top of the panels. Reprinted from Ref. [209] with permission from AIP Publishing.

In particular, using DNS of statistically planar premixed flames, including temperature-dependent viscosity, Bobbitt *et al.* [209] showed that, at high $\mathrm{Ka}_{\delta,\mathrm{K}}$ (this study spanned Karlovitz numbers between 70 and 750), the primary balance in the vorticity transport equation was between viscous dissipation and the vortex stretching term. Contrary to low $\mathrm{Ka}_{\delta,\mathrm{K}}$ conditions where dilatation plays a significant role in the dynamics, generally resulting in vorticity suppression, at high $\mathrm{Ka}_{\delta,\mathrm{K}}$ the vorticity magnitude continues to decrease, but due almost exclusively to the increase in kinematic viscosity across the flame. Indeed, as $\mathrm{Ka}_{\delta,\mathrm{K}}$ increases, Bobbitt *et al.* [209] showed that the normalized change in vorticity magnitude became insignificant, when the normalization was performed using local values of the kinematic viscosity and dissipation to construct the Kolmogorov scales. Consequently, vorticity magnitude decreased across the flame, but the dependence on density ratio (connected to dilatation), became weaker as $\mathrm{Ka}_{\delta,\mathrm{K}}$ increased (see, for example, Fig. 36). As $\mathrm{Ka}_{\delta,\mathrm{K}}$ increases, baroclinic torque, vortex stretching, and viscous dissipation all increase in magnitude, but the scaling of the baroclinic torque with $\mathrm{Ka}_{\delta,\mathrm{K}}$ is weaker than for the other two effects, resulting in the dominance of the vortex stretching and dissipation terms at high $\mathrm{Ka}_{\delta,\mathrm{K}}$ (see Fig. 37).

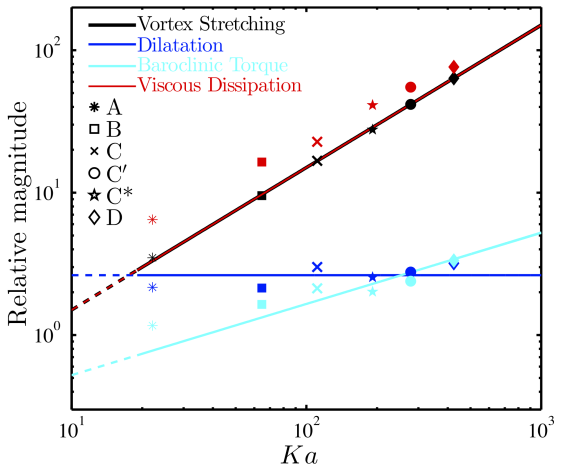

Figure 37: Scaling of the vortex stretching, dilatation, baroclinic torque, and viscous dissipation terms as a function of $\mathrm{Ka}_{\delta,\mathrm{K}}$ in the dynamics of the enstrophy. Data are obtained from DNS of statistically planar *n*-heptane and air premixed flames. Reprinted from Ref. [209] with permission from AIP Publishing.

Papapastolou *et al.* [210] examined the enstrophy transport equation in statistically planar hydrogen-air premixed flames spanning three different values of $\mathrm{Ka}_{\delta,\mathrm{K}}$ (i.e., 0.75, 14, and 126), finding that baroclinic torque has an increasingly minor contribution to the overall dynamics as $\mathrm{Ka}_{\delta,\mathrm{K}}$ increases. In this study, Papapastolou *et al.* [210] further conditioned the analysis on the local flow topology, based on the three invariants of the velocity gradient tensor $\partial u_i/\partial x_j$, showing that topologies corresponding to positive dilatation have an increasingly weak impact on the dynamics as $\mathrm{Ka}_{\delta,\mathrm{K}}$ increases. A related topologically conditioned analysis of a statistically planar premixed flame yielded similar results [211].

Through an analysis of vorticity alignment for the same statistically planar premixed flame configuration as that studied in Bobbitt *et al.* [209], Bobbitt & Blanquart [212] have further shown that turbulence anisotropy generated by the flame becomes less pronounced as $\mathrm{Ka}_{\delta,\mathrm{K}}$ increases. The alignments between ω_i and the eigenvectors of S_{ij} are similar to those found in non-reacting homogeneous isotropic turbulence at high $\mathrm{Ka}_{\delta,\mathrm{K}}$. For low $\mathrm{Ka}_{\delta,\mathrm{K}}$, the vorticity alignment and corresponding vortex stretching term are altered, and the effect of the flame on the vortex stretching term was identified as the primary source of the vorticity anisotropy. Wang *et al.* [112] similarly found using DNS of a highly turbulent methane-

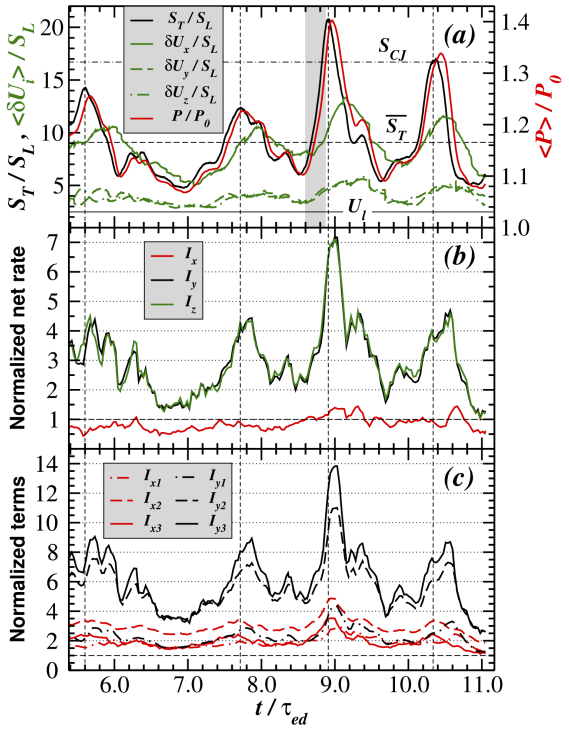

Figure 38: Flame speeds, turbulent velocity fluctuations, and average pressure (a), normalized total vorticity production rates, I_i, in different directions i (b), and normalized vortex stretching I_{i1}, dilatation I_{i2}, and baroclinic torque, I_{i3} terms in direction i (c) as functions of time for a highly turbulent statistically planar premixed flame [214].

air premixed jet flame that the alignments between ω_i and the eigenvectors of S_{ij} were similar to those found in non-reacting flows (i.e., preferential alignment between ω_i and $\boldsymbol{e}_2$). Moreover, ω_i was preferentially aligned with the most extensional strain rate of the mean flow, and was preferentially misaligned (or orthogonal) to the local flame normal n_i. The former result is similar to that obtained for sheared non-reacting flows, and the latter result is consistent with results for statistically planar flames [128]. Zhao *et al.* [213] also observed a misalignment between ω_i and n_i for a near-wall quenched premixed flame.

Despite the overall demonstration in these prior studies of the decreasing significance of baroclinic torque and flame generated anisotropy as the turbulence intensity increases, substantial generation of vorticity and anisotropy by baroclinic torque can occur locally and for short periods of time, even at high turbulence intensities. Significantly, Poludnenko

[214] showed that, even for highly turbulent conditions, statistically planar premixed flames can self-accelerate and undergo substantial vorticity generation by baroclinic torque during periods of high system pressures (see Fig. 38). Moreover, this turbulence generation was found to be strongly anisotropic, with the bulk of the baroclinic torque production occurring transverse to the direction of the mean flow.

Substantial changes to the dynamics of the vorticity and strain rate have also been observed for non-unity Lewis numbers, Le. Using DNS of statistically planar premixed flames spanning Karlovitz numbers from 0.54 to 19.5, Chakraborty *et al.* [215, 216] found that the vorticity magnitude decreases across statistically planar premixed flames and that the vorticity vector is predominantly aligned with $\boldsymbol{e}_2$ at higher $\mathrm{Ka}_{\delta,\mathrm{K}}$, in agreement with results from studies examining premixed flames for unity (or close to unity) Le. Interestingly, however, alignment with $\boldsymbol{e}_1$ increases in the region of peak heat release within the flame. In particular, for lower $\mathrm{Ka}_{\delta,\mathrm{K}}$ with unity Le and for all $\mathrm{Ka}_{\delta,\mathrm{K}}$ with $\mathrm{Le} < 1$, there is increased, although unstable, alignment with $\boldsymbol{e}_1$. For small $\mathrm{Ka}_{\delta,\mathrm{K}}$ and Le, increased alignment was observed with $\boldsymbol{e}_3$. These changes with Le and $\mathrm{Ka}_{\delta,\mathrm{K}}$ were found to be the result of changes in the influence of dilatation in the flame relative to the effects of vortex stretching. In two related studies, Chakraborty *et al.* [217] and Dopazo *et al.* [218] also showed that there is increased vorticity magnitude generated within the flame as Le decreases (see Fig. 39), and that this is accompanied by increased vorticity anisotropy. These changes were attributed to the increasing influence of dilatation and baroclinic torque as Le decreases for all $\mathrm{Ka}_{\delta,\mathrm{K}}$.

A number of other studies, spanning a range of conditions and configurations, have also contributed to, and largely confirmed, our understanding of vorticity-strain rate dynamics and properties during highly turbulent premixed combustion in statistically planar and jet flames. Nilsson *et al.* [201] examined statistically planar flames spanning a range of very high $\mathrm{Ka}_{\delta,\mathrm{K}}$ from 65 to 3,350, showing that the flow-induced strain rate becomes increasingly larger than the strain rate associated with fluid expansion (i.e., dilatation) by the flame as $\mathrm{Ka}_{\delta,\mathrm{K}}$ increases. The scalar gradient is correspondingly aligned with $\boldsymbol{e}_3$, as in passive scalar evolution in many non-reacting flows. It was also shown that, across the flame, the vorticity magnitude decreases and the characteristic size of intense vortical structures increases.

Ahmed *et al.* [219] have performed a multiscale analysis of wall bounded turbulent premixed flames, using a bandpass filtering approach to examine the contribution of variously sized eddies on the vorticity and strain rate fields. It was found, in particular, that flame-wall interactions alter vortex stretching by reducing the contribution of non-local strain rates and increasing the effect of small-scale turbulence. It remains unclear, however, to what extent these effects are also present in non-reacting flows, where substantial variations in the flow and vortex stretching process can also occur in the near-wall region.

It should be noted that much of the current understanding of vorticity dynamics and vorticity-strain properties in highly turbulent premixed combustion is based on studies of statistically planar and jet flames. However, recent studies of more realistic configurations have shown that in instances where there are mean pressure gradients imposed on the flow, such as those found in converging channels [220] and in high-swirl combustors [221, 222], the baroclinic torque term can become the dominant effect in the overall dynamics, resulting in substantial flame-generated vorticity. Geikie & Ahmed [220] have shown that the baroclinic torque is increasingly dominant in the dynamics as the magnitude of the pressure gradient increases. Kazbekov *et al.* [221, 222] observed a similar dominance of the barocinic torque term, even for high turbulence intensities, in a swirl combustor close to the burnt product gases (see the results for $\mathrm{Ka}_{\delta,\mathrm{K}} = 20$, 35, and 50 in Fig. 40). Lai *et al.* [223] also found an increase in the effect of the baroclinic torque in the near-wall region of a quenched high-

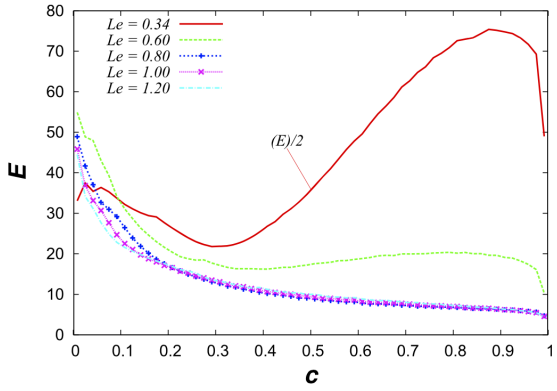

Figure 39: Mean enstrophy Ω (denoted 'E' here) conditioned on the local progress variable for different Lewis numbers, Le, from DNS of statistically planar premixed flames [218].

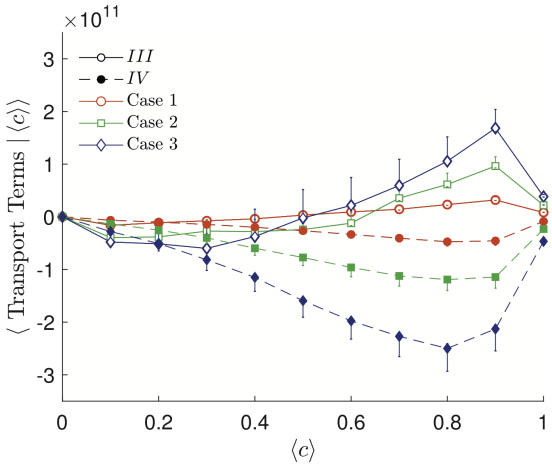

Figure 40: Mean baroclinic torque (III) and viscous transport (IV) condition on the mean progress variable in a turbulent premixed swirl flame, where Cases 1–3 correspond to Karlovitz numbers of 20, 35, and 50, respectively. Reprinted from Ref. [222] with permission from Elsevier.

intensity turbulent premixed flame.

Compared to studies of the vorticity, and vorticity-strain rate interactions in particular, studies of the strain rate field itself have been somewhat more limited. Coriton & Frank [224] examined the strain rate fields and intermittency in turbulent partially-premixed jet flames, and Hampp *et al.* [225] examined strain rate and vorticity conditioned to different isosurfaces in a lean premixed opposed jet configuration at low Da, showing that there is an increase in tangential strain rate due to dilatation. Steinberg *et al.* [202] examined the transport of the principal components of the strain rate in a premixed jet flame, including measurements of the strain-strain and vorticity interaction terms in the dynamics. These terms were found to be weaker in regions with significant heat release, due to the effects of pressure and density gradients.

To summarize our current understanding of vorticity and strain rate characteristics for highly turbulent premixed combustion, the properties and dynamics of the vorticity and strain rate at high $\mathrm{Ka}_{\delta,\mathrm{K}}$ generally correspond to non-reacting results, for Le close to unity, outside of periods of large system pressure increases, and for flows without a mean pressure gradient. Consequently, studies of statistically planar and jet flame configurations

with Lewis numbers close to unity have generally found that the effects of dilatation and baroclinic torque become less pronounced at higher $\mathrm{Ka}_{\delta,\mathrm{K}}$, and that the orientation of the vorticity and strain rate eigenvectors (including their relative alignments and anisotropy) are also less affected by the flame. However, recent studies of statistically planar flames with large pressure oscillations [214], non-unity Lewis numbers [215, 216], as well as studies of more realistic geometries with non-zero mean pressure gradients [220–222], indicate that the correspondence between turbulence in non-reacting flows and high-$\mathrm{Ka}_{\delta,\mathrm{K}}$ premixed combustion requires continued study.

It is also important to note that many of the statistically planar cases discussed here involve some type of forcing to sustain turbulence in the region of the flame, resulting in a statistically stationary DNS that is amenable to longer term statistical analysis. As in DNS studies of non-reacting turbulence that date back over three decades [226], this forcing is typically implemented as a body force in the Navier-Stokes equations and is designed to introduce energy primarily at the largest scales of the flow, even when the forcing is also applied within the region of the flame. Both broadband [127, 209, 212] and spectrally truncated [227] linear forcing schemes, as well as stochastic methods [69, 110, 128, 214] that introduce velocity perturbations at large scales, have been used to study turbulent premixed combustion at higher Karlovitz numbers than are typically achievable experimentally. In each of these cases, the forcing is applied both before, within, and downstream of the flame, mimicking energy input by larger-scale flow phenomena that are independent of the flame itself. To avoid interactions between the forcing and the flame, others have pre-computed 3D volumes of homogeneous isotropic turbulence which are then fed into the domain [210], or have forced only the region immediately upstream of the flame [201]. In each case, however, the intent is to create a statistically stationary turbulent flame that allows for more straightforward statistical analyses than the temporally decaying cases studied by, for example, Nishiki *et al.* [228] and Chakraborty *et al.* [168, 215, 216].

Despite the variety of forcing methods for statistically planar cases, however, observations regarding the vorticity, strain rate, and scalar gradient dynamics are consistent amongst all studies, even those where the forcing is sustained in the flame region and those where the

turbulence is allowed to decay. Although some quantitative differences do exist, particularly when discussing the specific Karlovitz numbers at which different phenomena are observed, the general trends for low and high Karlovitz behaviors are consistent across different studies. This conclusion is also supported by Klein *et al.* [229], who compared premixed flame results from DNS using decaying turbulence, boundary forcing, and linear forcing, finding no notable advantages or disadvantages of any particular approach. It is nevertheless still important to specify when and how forcing is implemented in numerical simulations, since turbulence properties within and downstream of the flame do depend, at least in part, on the details of the forcing scheme.

4.2.3. Coherent structures

Up to this point, the discussion of vorticity and strain rate has focused on field quantities, rather than on coherent or isolated structures. In the past, a number of studies have explored the interactions between isolated, often 2D, vortices and flame sheets (see, e.g., Mueller *et al.* [230]). However, the dynamical significance of such structures has been called into question, even in non-reacting flows, given their apparent lack of impact on nonlinearity and inertial range dynamics [231].

Nevertheless, many illustrations of turbulence in both non-reacting and reacting flows continue to show isosurfaces of the vorticity magnitude to reveal characteristic tube-like structures, for example those shown in Fig. 41 for a statistically planar premixed flame spanning a range of turbulence intensities [128]. Steinberg *et al.* [232–234] examined the coupled dynamics of the vorticity and strain rate, including the evolution of intense vorticity and strain rate structures, in a premixed Bunsen flame. Wang *et al.* [235] examined the structure of turbulent premixed methane-air jet flames over a wide range of turbulence intensities, including very large $\mathrm{Ka}_{\delta,\mathrm{K}}$, with a particular focus on the effects of turbulent eddies on preheat and reaction zone widths. Skiba *et al.* [113] have similarly examined the influence of large eddies on the wrinkling and broadening of flame fronts in highly turbulent premixed jet flames, finding that large eddies can in fact broaden the flame.

Beginning with the work of Tanahashi *et al.* [236], it has been known that intense turbu-

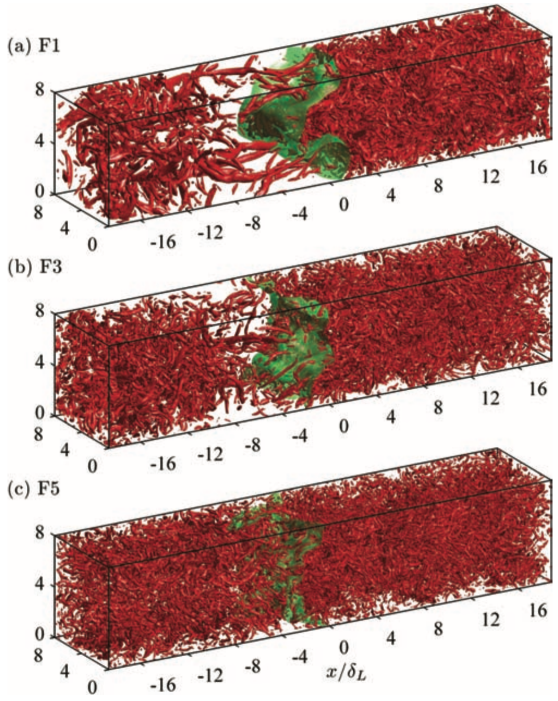

Figure 41: Isosurfaces of large vorticity magnitude in simulations of statistically planar premixed flames with increasing turbulence intensity (corresponding to Karlovitz numbers of 3.9, 32, and 174 from top to bottom) [128]. Semi-transparent green isosurfaces correspond to the flame surface.

lent vortical structures become less prevalent in premixed flames. Moreover, the orientation of intense vortices becomes increasingly anisotropic. However, this anisotropy is again lost as the turbulence intensity increases. Hamlington *et al.* [128] studied the alignment of intense vorticity within a statistically planar premixed flame and just downstream of the flame brush, showing that such intense vorticity is strongly aligned with the mean flame normal direction for low intensities. This alignment is much more pronounced than for the vorticity field as a whole (i.e., including less intense vorticity). Within the reaction zone of the flame, intense vorticity is preferentially aligned with the flame normal direction; this alignment is again more pronounced than for the vorticity field as a whole (i.e., not just intense vorticity).

There are additional questions about the representativeness of isolated 2D or quasi-2D structures in highly turbulent flows with substantial 3D complexity and nonlinear interactions between vortical structures spanning a wide range of scales. In particular, using the

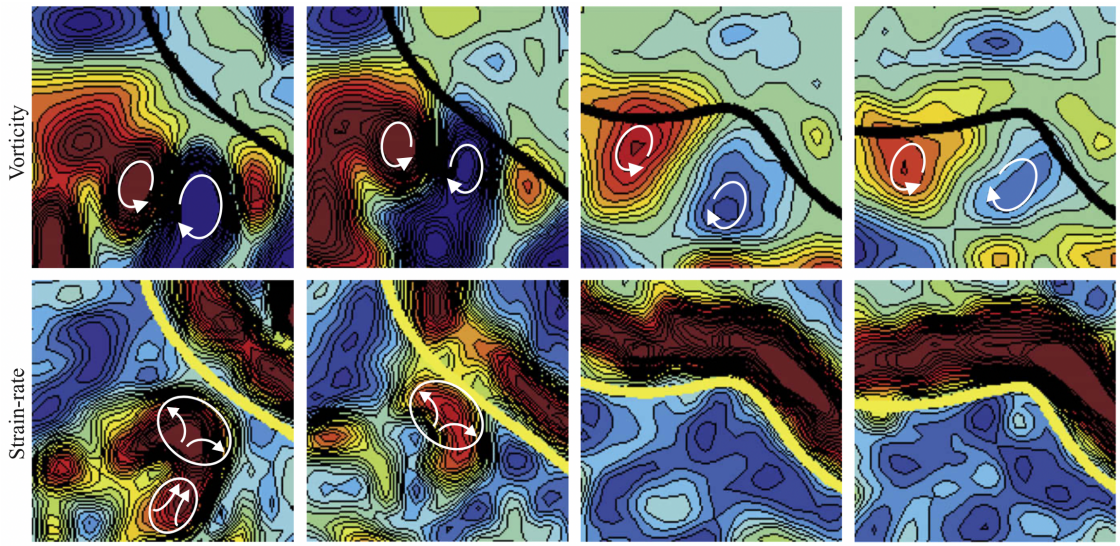

(a) Measured vortical and strain-rate structures in the canonical configuration at $t = 0$ ms.

(b) At $t = 0.9$ ms, the leading strain-rate structure interacted with the flame. The vortical structures had not yet interacted and the trailing strain-rate structure had been attenuated.

(c) At $t = 5.4$ ms, the vortical structures had interacted, wrinkling the flame. There was no longer any strain-rate exerted.

(d) At $t = 7.2$ ms, the flame wrinkle formed a cusp due to propagation.

Figure 42: Intense vorticity (top row) and strain-rate (bottom row) structures interacting with a premixed flame. The flame is represented by the thick lines and the reactants are towards the bottom left of each panel. Reprinted from Ref. [233] with permission from Elsevier.

cinema stereoscopic particle image velocimetry (PIV) techniques described in Steinberg *et al.* [232, 234], Steinberg & Driscoll [233] examined the effects of isolated vortices and vortex pairs on flame curvature and wrinkling, but found that such canonical configurations were present less than 10% of the time in the experimental data record. More often, much more complex 3D vortical structures interacted with the flame front. It was further found in this study that straining of the flame surface was caused by coherent strain rate structures, while vortical structures were primarily responsible for flame wrinkling. This result is consistent with the formulation of the governing equations for χ_i and χ in Eqs. (25) and (26), respectively, where the strain rate has impacts on both quantities, while the vorticity only has an explicit impact on χ_i and, hence, the local flame orientation n_i. Similar strain rate structures were also shown by Steinberg *et al.* [177] to be important for turbulence-flame interactions in premixed Bunsen flames (see Fig. 42).

Connected to the appearance of small-scale coherent structures is the highly intermittent

spatial distribution of intense velocity gradients in high Reynolds number turbulent flows [237, 238]. In particular, the dissipation rate field is comprised of many fine-scale features and is concentrated at small scales, resulting in much of the energy in a flow being dissipated within a very small fraction of the total flow volume [239, 240]. As the Reynolds number increases, the fraction of the total volume in which most of the dissipation occurs decreases, corresponding to an increasingly wide distribution of dissipation rates relative to the mean dissipation rate.

This intermittency was also noted in Section 3.1 in the context of scalar gradients and is evident in comparisons of vorticity and strain rate magnitude PDFs. Generally, the vorticity displays a wider range of values than the dissipation rate, but both are characterized by local instantaneous values that can be orders of magnitude larger than the mean values. These distributions reflect the spatial structure of the vorticity and dissipation rate values, which are small nearly everywhere in high Reynolds number flows, but are punctuated by extremely large values at widely spaced locations. It has been shown [192] that these behaviors remain generally valid in highly turbulent premixed flames, but there are variations in the degree of intermittency through the flame. Further study across a broader range of flame configurations is, however, still required.

4.3. Spectral and multi-scale characteristics

High Reynolds number turbulent flows are characterized by wide spatial and temporal scale ranges [231], and a number of approaches have been used to characterize the multi-scale structure and dynamics of turbulence. These approaches include spatial and temporal correlation functions, structure functions, and spectra (computed using either Fourier or other basis functions). In the following, we will primarily focus on velocity correlation and structure functions spanning different scale separations, denoted $\boldsymbol{r}$, and on Fourier spectra of the kinetic energy spanning different wavevectors $\boldsymbol{k}$.

Using these analyses, substantial research has been devoted over the last decade to addressing the following questions in premixed reacting flows spanning a range of turbulence intensities:

1. How is the multi-scale structure of turbulence affected by chemical heat release from premixed flames for different conditions (e.g., $\mathrm{Ka}_{\delta,\mathrm{K}}$) and at different locations (e.g., in the unburnt reactants or burnt products)?
2. Is there flame-generated turbulence and transfer of kinetic energy from small to large scales due to chemical heat release?
3. Are there universal aspects of multi-scale turbulence structure and dynamics that span different flame configurations and conditions?
4. Can classical theories of multi-scale turbulence structure and dynamics developed for non-reacting flows be applied to highly turbulent premixed flames?

The first question is motivated by the need to quantify the multi-scale structure of turbulence in a variety of contexts, and has spawned a number of studies of premixed flames using different multi-scale analysis approaches, as described in the next section. The second question is primarily motivated by the need to understand whether the flame disrupts the predominantly net forward (or down-scale) cascade of kinetic energy found in most non-reacting turbulent flows, or whether there is net up-scale transfer of energy. This information, in turn, dictates the dynamical effects that must be captured by SFS models for LES of highly turbulent premixed reacting flows. The third question is motivated by the observation that kinetic energy spectra in a variety of non-reacting flows (see, e.g., Refs. [82, 241]) collapse to a single universal form. It is thus of interest to determine whether there are similar universal aspects of multi-scale turbulence structure and dynamics, either across different premixed reacting flows or across both non-reacting and reacting flows.

The final question is motivated by the success of the Richardson energy cascade concept and the Kolmogorov hypotheses [242] in describing multi-scale turbulence structure and dynamics in non-reacting flows. Briefly, the three Kolmogorov hypotheses are the following [82]: (*i*) Turbulence at sufficiently small scales is homogeneous, isotropic, and stationary, (*ii*) Turbulence statistics at sufficiently small scales are universal and depend only on the kinematic viscosity ν, the mean dissipation rate ε, and the scale (i.e., r in physical space or the wavenumber k in Fourier space), and (*iii*) Turbulence statistics in an intermediate

range of scales smaller than the energy input scale and larger than the dissipation scale are universal and depend only on ε and the scale. These hypotheses are fundamentally based on the Richardson cascade model of energy transfer in turbulent flows [240], whereby energy input at large scales is assumed to be transferred non-dissipatively from larger to smaller scales until viscous dissipation becomes sufficiently strong to dissipate energy at small scales. The third hypothesis, in particular, establishes the existence of an 'inertial' range of scales where energy cascades non-dissipatively between scales.

Although the Kolmogorov hypotheses and Richardson cascade concept are substantial simplifications of the true physics governing real-world flows, both have proven remarkably successful at providing physical space and spectral scaling laws that are in close agreement with experimental and DNS data across a wide range of flows [82, 241]. These scaling laws include the prediction of a $k^{-5/3}$ inertial range scaling of the kinetic energy spectrum, where $k = |\boldsymbol{k}|$ is the wavevector magnitude, and of an $r^{N/3}$ scaling of the Nth-order velocity structure function, where $r = |\boldsymbol{r}|$ is the magnitude of the spatial separation vector. These scaling laws, which are fundamentally based on the Kolmogorov hypotheses and Richardson cascade concept, are generally successful for small N in non-reacting (i.e., constant density and viscosity) turbulence [231], but are known to become inaccurate for larger N due to intermittency effects [240]. Departures from these classical scaling relations in highly turbulent reacting flows will be discussed in more detail in the context of spectral and multi-scale structure in Section 4.3.1.

In the following, we review recent research on spectral and multi-scale analyses of turbulence during highly turbulent premixed combustion. Early efforts to understand spectra and multi-scale structure in turbulent combustion were made by examining reactants and products separately (i.e., outside the flame) [243, 244], and also by examining non-premixed flames [245]. Here we review more recent attempts to understand the spectral and multi-scale characteristics of turbulence across a range of conditions and flame locations during highly turbulent premixed combustion, with a particular focus on attempts to address the questions outlined above.

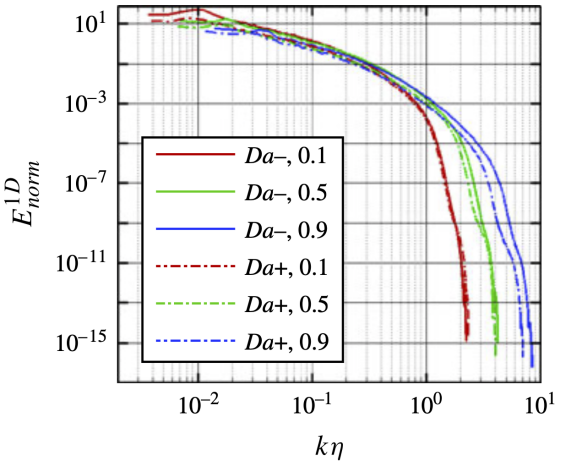

Figure 43: Normalized one-dimensional kinetic energy spectra for high (Da−) and low (Da+) intensity temporally evolving premixed slot jet flame DNS. Results are shown for three locations in the flame, corresponding to Favre-averaged progress variables of $\widetilde{c}$ = 0.1, 0.5, and 0.9. Reprinted from Ref. [84] with permission from Cambridge University Press.

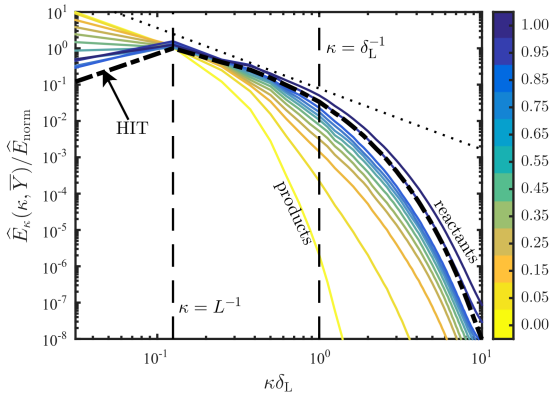

Figure 44: Normalized 2D kinetic energy spectra conditioned on the planar averaged reactant mass fraction for a statistically planar premixed flame with a turbulence intensity of $u_\ell/S_{\rm L}$ = 2.5. A corresponding spectrum for homogeneous isotropic turbulence (HIT; heavy black dash-dot line) and a $k^{-5/3}$ slope (dotted line) are also shown, where $k = |\boldsymbol{k}|$ is the wavevector magnitude. Reprinted from Ref. [88] with permission from the American Physical Society.

4.3.1. Spectral and multi-scale structure

A number of approaches have recently been used to understand spectral properties of turbulence in premixed flames, including both physical and Fourier space analyses. The governing equation for the two-point velocity correlation was examined in detail by Kolla

et al. [84, 85] for a temporally developing premixed shear layer at a range of turbulence intensities. In these studies, it was found that there is a spectral bump in the kinetic energy spectrum near the scale of the flame, and that this feature is due specifically to dilatation associated with the flame (see Fig. 43). Using conditional density-weighted kinetic energy and scalar spectra, Kolla *et al.* [84] further showed that turbulence spectra collapse to classical Kolmogorov predictions (i.e., the $k^{-5/3}$ inertial range scaling) only at intermediate scales far from the flame scale.

Using 2D kinetic energy spectra conditioned on the planar-averaged reactant mass fraction, Towery *et al.* [88] examined DNS of a lower intensity statistically planar premixed flame (with $\mathrm{Ka}_{\delta,\mathrm{K}} = 20$, but a turbulence intensity of only $u_\ell/S_\mathrm{L} = 2.5$) to show that turbulent small-scale motions are suppressed in the burnt combustion products (see Fig. 44). This result persists even for higher turbulence intensities, as was shown for a similar statistically planar premixed flame configuration using a conditional wavelet analysis by Kim *et al.* [246]. Due to the use of non-density weighted statistics, however, neither of these studies revealed a spectral bump near the scale of the flame, as was found in the studies by Kolla *et al.* [84, 85].

It should be noted that each of these prior analyses were based on planar-averaged combustion progress variables, complicating the interpretation of the results in physical space. As a result of this difficulty, conditionally averaged structure functions have recently been used to study the multiscale structure of turbulence in highly turbulent premixed combustion. Velocity structure functions correspond to moments of velocity difference distributions for different separation distances; that is $\langle |u_i(\boldsymbol{x}+\boldsymbol{r}) - u_i(\boldsymbol{x})|^N \rangle$, where the average $\langle \cdot \rangle$ denotes either a conditional or unconditional, ensemble or Favre, average and N is the structure function order. Structure functions are closely related to the correlation functions studied by Kolla *et al.* [84, 85], and research on non-reacting turbulence has shown that these structure functions have power-law r dependencies as predicted using scale similarity and dimensional arguments, but their exponent values indicate increasing non-Gaussianity and intermittency as the order increases [231].

Using DNS of statistically planar premixed flames, Whitman *et al.* [247] examined conditional velocity structure functions over turbulence intensities $u_\ell/S_\mathrm{L} \approx 2$–$10$ (corresponding

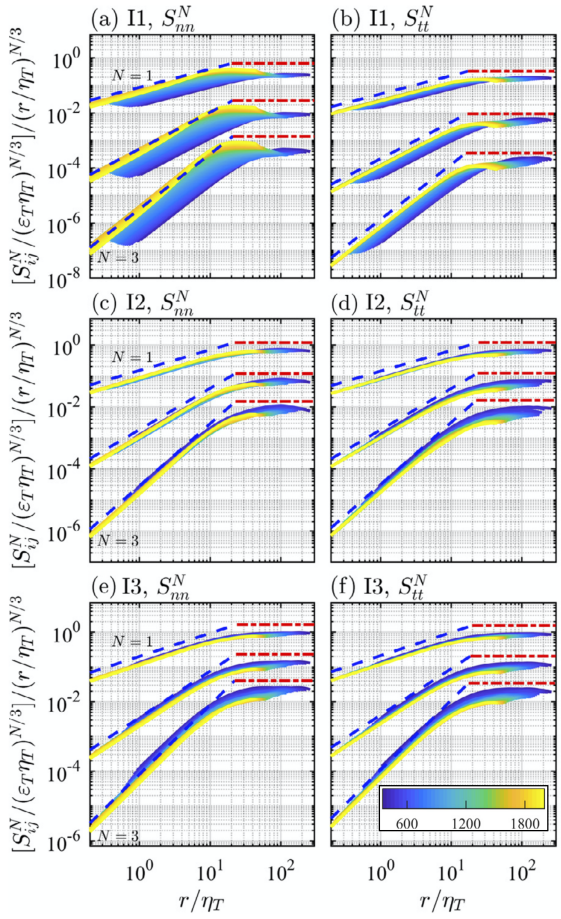

Figure 45: Compensated conditional structure functions from order $N = 1$ to 3 normalized by the conditional dissipation rate and Kolmogorov length scale for statistically planar flames at three intensities: (a,b) $u_\ell/S_\mathrm{L} = 2.5$, (c,d) $u_\ell/S_\mathrm{L} = 7.3$, and (e,f) $u_\ell/S_\mathrm{L} = 9.9$. Results are shown for longitudinal structure functions both (a,c,e) normal and (b,d,f) tangential to the flame. Blue curves correspond to conditioning on lower temperatures, and yellow curves correspond to higher temperatures. The analytic scaling r^N is shown by blue dashed lines and the Kolmogorov scaling $r^{N/3}$ is shown by red dash-dot lines. Reprinted from Ref. [247] with permission from Elsevier.

to $\mathrm{Ka}_{\delta,\mathrm{K}} \approx 20$–$170$). The conditioning was based on the local flame temperature at the first of the two points used to compute each velocity difference, and both separation directions and velocity components were aligned either parallel or tangentially to the local flame normal. It was found that, for high $\mathrm{Ka}_{\delta,\mathrm{K}}$ conditions, the structure functions approached the $r^{N/3}$ scaling predicted using the Kolmogorov hypotheses for sufficiently large r, and that

the curves at different locations in the flame could be collapsed using conditionally averaged values of the Kolomogorov scale and dissipation rate (see Fig. 45). At low $\mathrm{Ka}_{\delta,\mathrm{K}}$, the importance of heat release, most likely due to the increasing importance of dilatation and baroclinic torque in the dynamics, was found to prevent the collapse of the different curves. Interestingly, the collapse at higher $\mathrm{Ka}_{\delta,\mathrm{K}}$ observed by Whitman *et al.* [247] mirrors the earlier results from Bobbitt *et al.* [209], who showed that, when normalizing by local values of the kinematic viscosity and dissipation rate (i.e., using local Kolmogorov scales), the normalized vorticity magnitude was similaron either side of a highly turbulent premixed flame. The collapse in both cases reflects the purely kinematic effect of the flame on turbulence at highly turbulent conditions in statistically planar configurations; that is, heat release by the flame increases the fluid viscosity which, in turn, increases viscous dissipation and reduces the local Reynolds number.

Sabelnikov *et al.* [248, 249] also performed conditional structure analyses of statistically planar premixed flames, although for lower turbulence intensities and using conditioning based on whether the two velocity locations were in the reactants, flame region, or products. Due to the low intensity of the cases examined, substantial differences in the structure function statistics were observed compared to non-reacting flows, with a substantial impact from dilatation by the flame. This dilatation also generated increased anisotropy in the flame. A related analysis by Brearley *et al.* [250] examined the same conditional structure functions for a more turbulent premixed flame, again finding substantial effects due to dilatation and the creation of anisotropy by the flame. Interestingly, this study showed that even structure functions computed purely in the reactants just upstream of the flame differ from non-reacting results.

Ultimately, the multi-scale characterization of turbulence structure in premixed flames remains a subject of substantial ongoing research. It is unclear, in particular, to what extent the spatial variability associated with premixed flames has affected all results obtained to date. Each of the studies described here have sought to examine multi-scale structure at different locations within, or near, premixed flames, and various Fourier and spatial domain approaches have been used. However, as noted by Kim *et al.* [246], questions requiring both

spatial and spectral localization are ill-posed due to the uncertainty principle applied to such analyses. That is, the degree of spatial localization decreases as the spectral localization increases, and vice versa. In this respect, the wavelet analysis used by Kim *et al.* [246] offers the best control over the respective spatial and spectral localizations, at the expense of substantially increased complexity compared to other approaches. Even using this and related approaches, however, the limitations of the uncertainty principle are fundamental and cannot be overcome.

Connected to the study of multi-scale structure, a renewed focus must be placed on understanding the effects of internal intermittency and on developing new phenomenological theories of turbulence at highly turbulent conditions. Even in non-reacting flows, the Kolmogorov hypotheses become increasingly inaccurate for higher-order quantities, such as velocity structure functions of order four or higher [240]. These deviations from Kolmogorov scaling laws are often called "anomalous" scaling, and are the result of internal intermittency at the intermediate range of scales. Such intermittency causes a break-down in the assumption of scale similarity within the inertial range, and corrections to the Kolmogorov scaling laws have been proposed by Kolmogorov and many others (see Ref. [231] for a review). Given these observations in non-reacting flows, it is difficult to disentangle the underlying reasons for the departures from classical scaling laws, for example for structure functions of order $N = 3$ and 4 in Fig. 45. These departures could be due simply to the increasing importance of intermittency effects as N increases, but during premixed combustion, particularly in the presence of non-unity Lewis numbers and mean pressure gradients, modifications of the Kolmogorov scaling laws may be necessary.

4.3.2. Spectral and multi-scale dynamics

Even after the spectral and multi-scale structure of turbulence has been quantified through the flame, there is the remaining matter of exactly which direction (i.e., up or down scale) combustion processes cause energy to move in a turbulent reacting flow. In the classical picture of turbulence developed by Richardson and Kolmogorov [242, 252], energy input on large scales cascades non-dissipatively through the inertial range until it is even-

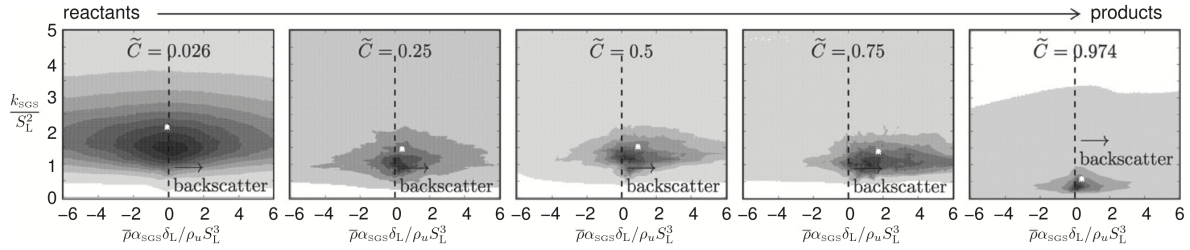

Figure 46: Normalized joint probability density functions conditioned on the local Favre-filtered progress variable (left to right) for SFS kinetic energy k_{SFS} versus SFS production rate α_{SFS} in a statistically planar premixed flame at $u_\ell/S_{\mathrm{L}} = 2.5$. Larger positive values of α_{SFS} are indicative of energy transfer from small to large scales (i.e., energy backscatter). Reprinted from Ref. [251] with permission from Elsevier.

tually dissipated as heat by viscous processes at small scales. Despite this classical picture, however, it is still possible for energy to be transferred from small to large scales; that is, it is possible for there to be "backscatter" of energy. There are at least three possible sources of backscatter in turbulent combustion, as described in the following.

1. From the dynamics of the energy cascade in spectral-space, it can be shown that even though the *net* cascade is typically down-scale in 3D turbulent flows, nonlinear inertial processes are responsible for a measurable amount of up-scale energy transfer [253]. This up-scale transfer occurs even in non-reacting homogeneous isotropic turbulence and is typically examined through calculation and partitioning of triadic interactions [254–259] into positive (i.e., down-scale) and negative (i.e., up-scale) contributions. The existence of this up-scale energy transfer is well-known [82] and many efforts have been made to capture this physical backscatter in SFS models for LES [253, 260–266]. In most cases, however, such SFS models have proven to be insufficiently dissipative due to inaccurate predictions of local, instantaneous backscatter, resulting in unstable simulations for most practical problems [266].
2. Heat release by combustion causes fluid expansion, which results in a suppression of small-scale turbulence [128]. Moreover, recent results indicate that while small scales are suppressed, there is a corresponding increase in the kinetic energy of large scales (or the mean flow). There are indications that much of this change occurs due

to pressure-dilatation effects [251], although turbulent advective processes associated with the cascade process have also been shown to create net energy backscatter near the scale of the flame [88]. Another manifestation of combustion-related backscatter is a large-scale change in the flow due to a small-scale event. This can occur, for example, when there is a locally extreme temperature or pressure that causes, for example, auto-ignition [267] or deflagration to detonation transition (DDT) [268]. A recent study by Poludnenko [214] has also shown that certain flames exhibit a "pulsating behavior", resulting in pressure pulses emitted from the flame that affect distant locations. These events are typically initiated at very small scales but can have enormous consequences for the larger-scale behavior of the system.

3. In strictly 2D turbulent flows, which occur most frequently in geophysical contexts at very large scales (e.g., hurricanes and mesoscale eddies in the ocean), the nonlinear vortex stretching process that leads to the transfer of energy from large to small scales in most 3D flows is no longer active. As a result, it has been observed that in 2D turbulence, there is an inverse cascade of kinetic energy and a forward cascade of enstrophy, or vorticity magnitude [269]. From a physical standpoint, this means that small eddies in 2D turbulence coalesce to form larger eddies, by contrast to the break-up of large eddies into smaller eddies found in classical non-reacting 3D turbulence. This is a very particular type of energy backscatter that is likely to only be present in 2D simulations of turbulent combustion, or in certain special circumstances where anisotropy generated by the flame results in quasi-2D flow.

It should additionally be noted that both computations [270–272] and experiments [273, 274] have revealed a "bump" in the kinetic energy spectrum near the transition between the inertial and dissipation ranges. Although not an example of backscatter in the traditional sense, this bump is associated with the build-up of kinetic energy at the bottom of the inertial range and results in a modest and localized increase in spectral kinetic energy at large wavenumbers, by contrast to the monotonically decreasing spectral kinetic energy associated with the classical cascade process. The resulting effect is termed the "bottleneck" and has

been explained [275] as resulting from the relatively rapid decrease of spectral kinetic energy at small scales (i.e., in the dissipation range). In the Richardson-Kolmogorov cascade, it is assumed that much of the energy is transferred by inertial processes from large to small scales, but at sufficiently small scales there are insufficient smaller scales to accept the energy. As a result, the energy collects at the bottom of the inertial range and creates a bump in the energy spectrum. When there is insufficient dissipation of energy in an LES or DNS of a turbulent flow, energy can also "pile-up" at small-scales and begin to pollute larger scale motions. This effect is, however, non-physical and could be termed the "numerical bottleneck."

The relative importance of each source of backscatter in the list above is still being understood in premixed combustion. Using differential filtering in physical space, O'Brien *et al.* [251, 276] examined energy transfer between subfilter and resolved scales in the compressible, Favre-filtered Navier-Stokes equations using DNS of both diffusion [276] and premixed [251] flames. An analysis of DNS data for a statistically planar premixed flame at a turbulence intensity of $u_\ell/S_\mathrm{L} = 2.5$ ($\mathrm{Ka}_{\delta,\mathrm{K}} = 20$) showed that SFS backscatter occurs primarily in regions undergoing dilatation due to heat release (see Fig. 46). This net backscatter was found to be predominantly due to the correlation between the velocity and pressure-gradient in the region of highest heat release. Backscatter was also found to occur due to nonlinear advective effects, although this effect was generally weaker than that due to the velocity pressure-gradient dilatation. This result is largely consistent with the purely spatial domain analyses of the kinetic energy dynamics described in Section 4.1, and both Wang & Abraham [167] and MacArt *et al.* [166] have shown that, at low $\mathrm{Ka}_{\delta,\mathrm{K}}$, the velocity pressure-gradient correlation term is dominant in the kinetic energy dynamics.

With respect to the inter-scale transfer of energy by nonlinear advective effects, Towery *et al.* [88] used a conditional Fourier spectral analysis to examine the exchange of energy between scales and the net direction of the cascade process in a statistically planar premixed flame at $\mathrm{Ka}_{\delta,\mathrm{K}} = 20$. This analysis showed that, within the flame brush close to the burnt products, nonlinear advective processes preferentially transfer energy from small to large scales. This net backscatter of energy is contrary to the net forward cascade of energy found

in non-reacting turbulence. In this study, the inverse energy cascade was found to extend from slightly smaller than the scale of the flame up to the turbulence integral scale. However, determining whether this inverse cascade remains scale-local to the flame, or always extends to the integral scale, was made difficult by the relatively small separation between ℓ and δ_{L}^{0} in this study.

Finally, the conditional wavelet analysis of a higher intensity (where $\mathrm{Ka}_{\delta,\mathrm{K}} = 72$) statistically planar premixed flame by Kim *et al.* [246] showed that, in the flow as a whole, the spectral dynamics were largely similar to that found in non-reacting incompressible turbulent flows, with net down-scale transfers of energy due to advective and pressure gradient effects. Once again, however, within the flame brush near the region of greatest heat release, both of these effects reverse direction, resulting in up-scale transfer of kinetic energy. The resulting net effect is relatively weak up-scale energy transfer (or at least substantially weakened down-scale transfer) for intermediate values of the progress variable.

Returning to the questions posed at the beginning of this section, tentative and preliminary answers are now available. Turbulent small scale motions are generally suppressed through premixed flames at high turbulence intensities, due primarily to the effects of increased viscous dissipation associated with chemical heat release. At lower turbulence intensities, there is evidence of flame-generated turbulence, up-scale net energy transfer, and backscatter, none of which are explicitly addressed by purely (or mostly) dissipative SFS models developed for LES of non-reacting turbulence. At highly turbulent conditions, it appears that the Kolmogorov hypotheses remain relevant, at least for statistically planar premixed flames, and that results for different flame locations, conditions, and configurations can be collapsed using locally defined Kolmogorov scales. Tentatively, there are thus indications that there *may* be universal aspects of spectral and multi-scale turbulence characteristics during highly turbulent premixed combustion.

It should be cautioned, however, that although these studies provide a consistent view of up-scale kinetic energy transfer by nonlinear advective and pressure-gradient effects in premixed flames at moderate values of $\mathrm{Ka}_{\delta,\mathrm{K}}$, each study was focused on DNS data of statistically planar premixed flames stochastically forced at large scales. Moreover, two

of these studies (i.e., Refs. [88, 251]) examined the same DNS data set. It is thus now important to perform similar analyses of spectral kinetic energy dynamics in a broader range of flows, particularly those involving mean shear, geometric complexity, and persistent pressure gradients. The effects of different forcing mechanisms—including the absence of forcing, as in DNS of premixed flames interacting with decaying turbulence—must also be examined in more detail to quantify the dependence of these results on the energy injection method. Stronger claims of universality, in particular, cannot be made until these studies have been undertaken. Kazbekov & Steinberg [277] have begun taking initial steps in this direction using experimental measurements of premixed swirl flames and physical space filtering, revealing that energy mean up-scale energy transfer within the flame structure across scales in the range of the laminar flame thickness for moderate Karlovitz numbers.

4.4. Summary

Our understanding of the properties — both kinematic and dynamic — of turbulence during highly turbulent premixed combustion has advanced considerably over the past decade. From the studies and prior research summarized in this section, we now know, in particular, that:

1. *Turbulence characteristics are similar to those found in corresponding non-reacting flows for highly turbulent statistically planar and jet premixed flames.* This includes the dynamics of the turbulence kinetic energy and stresses, the coupled dynamics and properties of the vorticity and strain rate, and the applicability of the Kolmogorov hypotheses and Richardson cascade concept. The creation of anisotropy by the flame also weakens as the turbulence intensity increases for these flows.
2. *The primary effect of the flame on turbulence for highly turbulent statistically planar and jet premixed flames is kinematic in nature and results from the increase in temperature dependent viscosity due to chemical heat release.* This accounts for the collapse of vorticity and structure function results when normalizing statistics either side of a premixed flame using local (or conditioned) values of the kinematic viscosity and viscous dissipation rate.

3. *Turbulence characteristics can be substantially affected by the flame, beyond simply the kinematic viscous effect, even at highly turbulent conditions due to non-unity Lewis numbers, mean pressure-gradients, and pressure pulsations.* These conditions result in the continued importance, and even dominance, of dilatation, baroclinic torque, and velocity-pressure gradient effects as the turbulence intensity increases, weakening the similarity to corresponding non-reacting flows during highly turbulent premixed combustion.
4. *The gradient transport (or Boussinesq) hypothesis is as applicable for highly turbulent premixed statistically planar and jet flames as for corresponding non-reacting flows, but this hypothesis is unlikely to remain valid in more practically relevant flows.* In particular, non-unity Lewis numbers and mean pressure gradients are likely to create counter-gradient transport even at highly turbulent conditions, similar to results for lower turbulence intensities.
5. *There is a weakening of the forward kinetic energy cascade even in highly turbulent statistically planar premixed flames, and there is a net backscatter of energy for lower turbulence intensities.* As a result, even in reacting flows where there is no net backscatter of energy, the assumption of a filter cutoff for LES in the inertial range, as well as the assumption of uniform equilibrium down-scale transfer of energy, may become inaccurate.

It should be noted that the last two summary points relate to the manner in which turbulence is modeled, in either RANS or LES approaches, for highly turbulent conditions. Although no model has yet been developed to explicitly account for these insights, recent studies of highly turbulent statistically planar and jet flames have shown that many of the assumptions central to models for non-reacting flows (e.g., the gradient transport hypothesis and net down-scale energy transfer) are still relevant at highly turbulent conditions. However, the same may not be true for more complicated and physically realistic flows, such as swirl [221, 222] and bluff body [220] configurations where there is known to be substantial turbulence production at small scales by baroclinic torque. Before non-reacting models

can be confidently applied at highly turbulent conditions, additional work must be done to understand kinetic energy dynamics in these and other more realistic configurations.

5. Outlook

Through this paper, we hope to have provided a succinct summary of the current state-of-knowledge regarding the structure and dynamics of highly turbulent premixed flames. Summary points are included at the ends of Sections 2–4 and are not repeated here. Instead, we present a brief outlook; although we have substantially increased our knowledge of highly turbulent premixed combustion in a relatively short period of time, our current understanding does motivate several new areas of inquiry and study.

Fundamentally, the community needs to critically assess the validity and utility of defining combustion regimes in real configurations at highly turbulent conditions. At a minimum, consensus must be reached on a standardized method of characterizing flames in systems with widely varying turbulence properties, many of which simultaneously generate and attenuate turbulence over the flame brush. Furthermore, additional care must be taken in the design of experimental configurations to ensure that the rapid mixing between the targeted experiment and the surroundings—induced by intense turbulence—does not alter the thermochemistry in the flame brush. While both experiments and DNS have progressed considerably, there remain leading order discrepancies (e.g., between measured and simulated turbulent flame speed enhancement) that require reconciliation through improved understanding of both the combustion thermochemistry and turbulence dynamics.

From the perspective of advancing understanding of thermochemistry in highly turbulent flames, one approach is to quantify the multi-dimensional thermochemical space; e.g., its dimensionality, dynamic evolution, and impact on local and global flame characteristics, etc. The underlying physico-chemical conditions that create this high-dimensional space should also be understood and quantified. In particular, connecting the dynamics of turbulent flames to fundamental flame properties—such as laminar flame speed, extinction and ignition residence times in perfectly stirred reactors, and homogeneous auto-ignition—can be attempted. Experimentally, simultaneous multi-scalar and/or scalar-velocity measurements

can facilitate such understanding, in particular under conditions that are computationally challenging for DNS. Theoretically, scaling analysis of the turbulent flame speed should be expanded to consider contributions from the local conditions, instead of relying on a single laminar flame speed to scale the entire thermochemistry.

With established physical understanding and quantitative description of thermochemistry, improvements in modeling can be attempted. One particular challenge in modeling highly turbulent premixed flames is that the rich small-scale flame structures and dynamics can potentially occur entirely at sub-filter scales. As most existing turbulent combustion models have certain intrinsic assumptions regarding the dimensionality of the thermochemical space, it is important to incorporate the latest understanding into modeling studies.

Two approaches have emerged going forward: one is to continue improving existing turbulent combustion models, leveraging new physical understanding, DNS data, and computational and experimental diagnostics. This approach has been constantly pursued and progressively perfected. The second approach is to develop adaptive modeling [278]. The adaptivity can manifest in terms of adaptive mesh resolutions around different flame features. For example, recent developments on combining adaptive mesh refinement [279] with local flame feature detection resolve premixed flame fronts such that local flame speed can be adequately captured. Embedding DNS into LES is another idea to ensure that multi-modal flame features can be captured without prohibitive computational cost. The adaptivity can also manifest as model adaptivity, such as in [106, 279] where different turbulent combustion models are selected for different regions of a turbulent flame. For either approach, robust coupling and transition among different combustion models or different mesh resolutions remain outstanding challenges.

Chemical kinetic modelling is closely connected to turbulent combustion closure models. The recent development of lumped chemical kinetic models, such as HyChem [20, 21], has set a good example in reducing the complexities of chemistry for real fuels. Further model reduction to 10–30 species is often required to enable DNS or LES. It is important to recognize the impact from abundant, and sometimes extreme, thermochemical states in highly turbulent flames when constructing reduced kinetic models; their verification and

validation should be expanded to account for possible thermochemical states that are created in turbulent flames. Construction and reduction of chemical kinetic models is another area that benefits from a physical and quantitative understanding of the high-dimensional thermochemical state space.

In order to understand this state space under more practical conditions, characterization of large hydrocarbon fuels under pressurized conditions is necessary to reach conditions close to those in Table 1. Moreover, most existing studies focus on gaseous flames; interactions between highly turbulent reacting flows and sprays are comparatively less studied. Droplet motion, evaporation, and heat transfer introduce additional sinks/sources to alter local compositional space (i.e., temperature and species), and introduce additional time and length scales to the dynamics of combustion. An experimental framework targeting at model validation, such as those reported in [280] for dilute acetone/ethanol sprays, should be initiated for a larger variety of fuels under highly turbulent conditions. Development of DNS in simulating spray flames should also receive more attention.

From the perspective of understanding turbulence structure and dynamics, the analyses of turbulence kinetic energy, stresses, and fluxes described in Section 4.1, as well as the spectral and multi-scale analyses described in Section 4.3, must now be extended to more realistic flows and conditions that include non-unity Lewis numbers, mean pressure gradients, solid boundaries, and other practically relevant flow effects. Recent research has shown that our understanding of turbulence properties based on the study of only statistically planar and jet configurations is incomplete and not necessarily representative of more realistic configurations. However, progress has already been made towards understanding vorticity dynamics in such configurations [220–222], and similar studies must now be undertaken to more fully understand impacts on turbulence statistics and spectra.

The further study of these statistics and spectra will also provide insights into new model forms for numerical simulations of practical highly turbulent premixed combustion using RANS and LES approaches. Current studies have demonstrated the inadequacy of the gradient transport hypothesis and purely and uniformly dissipative SFS models, particularly for moderate and low turbulence intensities, and now further work must be carried out to

formulate new models that are sensitive to local flow conditions (e.g., the local Karlovitz and Damköhler numbers) across a broader range of practical configurations.

The renewed study of internal intermittency as a function of configuration and local turbulence-flame conditions is also an important area of further research. From an operational standpoint, turbulence can lead to unexpectedly high probabilities of extreme events, such as local increases in pressure, temperature, and scalar gradients. Each of these events can lead to undesirable transient phenomena such as extinction, ignition, or deflagration to detonation transition of reactive mixtures at difficult-to-predict locations and times. The onset of these extreme events—which arise locally, often at small scales, with significant global consequences—is intrinsically connected to the intermittent character of turbulence.

In general, internal intermittency becomes more pronounced as the turbulence intensity increases, and increased probabilities of extreme gradients (e.g., in temperature or pressure) associated with highly turbulent conditions may result in global changes to system properties. Recent research, for example, has indicated that turbulence-induced fluctuations in thermodynamic quantities can lead to detonation formation in highly turbulent auto-igniting reactant mixtures [227], as well as in highly turbulent deflagrating systems [214, 281]. The understanding of how such transitions can be predicted, particularly at highly turbulent conditions, remains an important direction for future study. Further study is also required to determine whether the fundamental assumptions encompassed by the Kolmogorov hypotheses, including the presence of a universal equilibrium range, remain valid in premixed reacting flows over a variety of conditions.

Finally, complexity and turbulent mixing have also been characterized in non-reacting flows through the dispersion of fluid parcels or tracer quantities. This dispersion can be quantified in an Eulerian sense using fluxes, but can also be characterized through a Lagrangian approach that tracks the separation of two initially close fluid parcels in time [282]. In turbulent flows, these parcels move apart at a rate specified by the Lyapunov exponents, where positive exponents indicate a nonlinear unstable dynamical system characterized by an extreme sensitivity to initial conditions. The separation of these tracer parcels has been connected to turbulent diffusion, with studies showing more rapid separation of tracers in

turbulent, as compared to laminar, flows (see Refs. [283, 284] for reviews). Similar to the new insights obtained from Lagrangian analyses of thermochemical trajectories, Lagrangian analyses of turbulence properties and fluid particle dispersion may result in new models of turbulent transport during highly turbulent premixed combustion.

6. Acknowledgements

The authors acknowledge the support of AFOSR grants FA9550-17-0011, FA9550-17-1-0144, FA9550-18-1-0173, and Project Monitor Dr. Chiping Li. P. E. Hamlington acknowledges support from NSF award 1847111, as well as helpful discussions with Dr. Ryan Darragh, Dr. Colin Towery, Mr. Michael Meehan, and Mr. Samuel Whitman. X. Zhao acknowledges Mr. Ji-Woong Park and Mr. Peiyu Zhang for their helpful contribution in generating laminar flame databases.

References

[1] S. Pope, Turbulent premixed flames, Annu. Rev. Fluid Mech. 19 (1987) 237–270.

[2] N. Peters, Laminar flamelet concepts in turbulent combustion, Proc. Combust. Inst. 21 (1) (1988) 1231 – 1250.

[3] D. Bradley, How fast can we burn?, Proc. Combust. Inst. 24 (1992) 247–262.

[4] K. Bray, The challenge of turbulent combustion, Proc. Combust. Inst. 26 (1) (1996) 1–26. doi:10.1016/S0082-0784(96)80195-0.

[5] C. Law, C. Sung, Structure, aerodynamics, and geometry of premixed flamelets, Prog. Energy Combust. Sci. 26 (4) (2000) 459 – 505.

[6] A. Lipatnikov, J. Chomiak, Turbulent flame speed and thickness: phenomenology, evaluation, and application in multi-dimensional simulations, Prog. Energy Combust. Sci. 28 (2002) 1–74.

[7] R. Bilger, S. Pope, K. Bray, J. Driscoll, Paradigms in turbulent combustion research, Proc. Combust. Inst. 30 (1) (2005) 21 – 42. doi:https://doi.org/10.1016/j.proci.2004.08.273.

[8] J. F. Driscoll, Turbulent premixed combustion: Flamelet structure and its effect on turbulent burning velocities, Prog. Energy Combust. Sci. 34 (1) (2008) 91–134.

[9] A. Lipatnikov, J. Chomiak, Effects of premixed flames on turbulence and turbulent scalar transport, Prog. Energy Combust. Sci. 36 (1) (2010) 1–102. doi:10.1016/j.pecs.2009.07.001.

[10] A. Lipatnikov, Fundamentals of Premixed Turbulent Combustion, CRC Press, 2012.

[11] J. F. Driscoll, J. H. Chen, A. W. Skiba, C. D. Carter, E. R. Hawkes, H. Wang, Premixed flames subjected to extreme turbulence: Some questions and recent answers, Prog. Energy Combust. Sci. 76 (2020) 100802. doi:10.1016/j.pecs.2019.100802.

[12] C. Xu, J.-W. Park, C. S. Yoo, J. H. Chen, T. Lu, Identification of premixed flame propagation modes using chemical explosive mode analysis, Proc. Combust. Inst.doi:https://doi.org/10.1016/j.proci.2018.07.069.

[13] J. H. Chen, E. R. Hawkes, R. Sankaran, S. D. Mason, H. G. Im, Direct numerical simulation of ignition front propagation in a constant volume with temperature inhomogeneities: I. fundamental analysis and diagnostics, Combust. Flame 145 (1) (2006) 128 – 144.

[14] P. Pal, M. Valorani, P. G. Arias, H. G. Im, M. S. Wooldridge, P. P. Ciottoli, R. M. Galassi, Computational characterization of ignition regimes in a syngas/air mixture with temperature fluctuations, Proc. Combust. Inst. 36 (3) (2017) 3705 – 3716.

[15] C. S. Yoo, T. Lu, J. H. Chen, C. K. Law, Direct numerical simulations of ignition of a lean n-heptane/air mixture with temperature inhomogeneities at constant volume: Parametric study, Combust. Flame 158 (9) (2011) 1727 – 1741.

[16] J. B. Martz, G. A. Lavoie, H. G. Im, R. J. Middleton, A. Babajimopoulos, D. N. Assanis, The propagation of a laminar reaction front during end-gas auto-ignition, Combust. Flame 159 (6) (2012) 2077 – 2086.

[17] O. Schulz, N. Noiray, Autoignition flame dynamics in sequential combustors, Combust. Flame 192 (2018) 86 – 100.

[18] D. M. Smooke, J. A. Miller, R. J. Kee, Determination of adiabatic flame speeds by boundary value methods, Combust. Sci. Technol. 34 (1-6) (1983) 79–90.

[19] R. J. Kee, J. F. Grcar, M. D. Smooke, J. Miller, E. Meeks, Premix: a fortran program for modeling steady laminar one-dimensional premixed flames, Sandia National Labs., Livermore, CA (USA) Report No. SAND85-8249.

[20] H. Wang, R. Xu, K. Wang, C. Bowman, D. Davidson, R. Hanson, K. Brezinsky, F. Egolfopoulos, A physics-based approach to modeling real-fuel combustion chemistry - i. evidence from experiments, and thermodynamic, chemical kinetic and statistical considerations, Combust. Flame 193 (2018) 502–519.

[21] R. Xu, K. Wang, S. Banerjee, J. Shao, T. Parise, Y. Zhu, S. Wang, A. Movaghar, D. Lee, R. Zhao, X. Han, Y. Gao, T. Lu, K. Brezinsky, F. Egolfopoulos, D. Davidson, R. Hanson, C. Bowman, H. Wang, A physics-based approach to modeling real-fuel combustion chemistry – II. Reaction kinetic models of jet and rocket fuels, Combust. Flame 193 (2018) 520–537.

[22] H. Wang, X. You, A. Joshi, S. Davis, F. A. Laskin, High-temperature combustion reaction model of H_2/CO/C_1-C_4 compounds, `http://ignis.usc.edu/usc_mech_ii.htm`, uSC Mech Version II (2007).

[23] M. Ihme, L. Shunn, J. Zhang, Regularization of reaction progress variable for application to flamelet-based combustion models, J. Comput. Phys. 231 (2012) 7715–7721.

[24] R. S. Barlow, G. Magnotti, H. C. Cutcher, A. R. Masri, On defining progress variable for Raman/Rayleigh experiments in partially-premixed methane flames, Combust. Flame 179 (9) (2017) 117–129.

[25] E. Ranzi, M. Dente, A. Goldaniga, G. Bozzano, T. Faravelli, Lumping procedures in detailed kinetic modeling of gasification, pyrolysis, partial oxidation and combustion of hydrocarbon mixtures, Prog. Energy Combust. Sci. 27 (2001) 99 – 139.

[26] T. Poinsot, D. Veynante, Theoretical and Numerical Combustion, 3rd Edition, R.T. Edwards, 2012.

[27] S. R. Turns, An Introduction to Combustion: Concepts and Applications, third edition Edition, McGraw-Hill, 2012.

[28] F. Williams, Combustion theory. Second edition, CRC Press, 1985.

[29] O. Gicquel, N. Darabiha, D. Thvenin, Laminar premixed hydrogen/air counterflow flame simulations using flame prolongation of ildm with differential diffusion, Proc. Combust. Inst. 28 (2) (2000) 1901 – 1908. doi:https://doi.org/10.1016/S0082-0784(00)80594-9.

[30] J. van Oijen, L. de Goey, Modelling of premixed laminar flames using flamelet-generated manifolds, Combust. Sci. Technol. 161 (1) (2000) 113–137.

[31] E. Hawkes, R. Cant, A flame surface density approach to large-eddy simulation of premixed turbulent combustion, Proc. Combust. Inst. 28 (1) (2000) 51 – 58. doi:https://doi.org/10.1016/S0082-0784(00)80194-0.

[32] H. Pitsch, A consistent level set formulation for large-eddy simulation of premixed turbulent combustion, Combust. Flame 143 (4) (2005) 587 – 598, special Issue to Honor Professor Robert W. Bilger on the Occasion of His Seventieth Birthday. doi:https://doi.org/10.1016/j.combustflame.2005.08.031.

[33] S. J. Shanbhogue, S. Husain, T. Lieuwen, Lean blowoff of bluff body stabilized flames: scaling and dynamics, Prog. Energy Combust. Sci. 35 (1) (2009) 98 – 120. doi:https://doi.org/10.1016/j.pecs.2008.07.003.

[34] Y. Huang, V. Yang, Dynamics and stability of lean-premixed swirl-stabilized combustion, Prog. Energy Combust. Sci. 35 (4) (2009) 293 – 364. doi:https://doi.org/10.1016/j.pecs.2009.01.002.

[35] J. O'Connor, V. Acharya, T. Lieuwen, Transverse combustion instabilities: Acoustic, fluid mechanic, and flame processes, Prog. Energy Combust. Sci. 49 (2015) 1 – 39. doi:https://doi.org/10.1016/j.pecs.2015.01.001.

[36] J. Kariuki, A. Dowlut, R. Yuan, R. Balachandran, E. Mastorakos, Heat release imaging in turbulent premixed methane-air flames close to blow-off, Proc. Combust. Inst. 35 (2) (2015) 1443–1450. doi:10.1016/j.proci.2014.05.144.

[37] J. Kariuki, A. Dowlut, R. Balachandran, E. Mastorakos, Heat release imaging in turbulent premixed ethylene-air flames near blow-off, Flow. Turb. Combust. 96 (4) (2016) 1039–1051. doi:10.1007/s10494-016-9720-y.

[38] B. Roy Chowdhury, B. M. Cetegen, Experimental study of the effects of free stream turbulence on characteristics and flame structure of bluff-body stabilized conical lean premixed flames, Combust. Flame 178 (2017) 311–328. doi:10.1016/j.combustflame.2016.12.019.

[39] B. R. Chowdhury, J. A. Wagner, B. M. Cetegen, Experimental study of the effect of turbulence on the structure and dynamics of a bluff-body stabilized lean premixed flame, Proc. Combust. Inst. 36 (2) (2017) 1853 – 1859.

[40] M. Gregor, F. Seffrin, F. Fuest, D. Geyer, A. Dreizler, Multi-scalar measurements in a premixed swirl burner using ID Raman/Rayleigh scattering, Proc. Combust. Inst. 32 (2) (2009) 1739–1746. doi:10.1016/j.proci.2008.06.133.

[41] R. Cheng, D. Littlejohn, P. Strakey, T. Sidwell, Laboratory investigations of a low-swirl injector with H_2 and CH_4 at gas turbine conditions, Proc. Combust. Inst. 32 II (2) (2009) 3001–3009. doi:10.1016/j.proci.2008.06.141.

[42] K.-J. Nogenmyr, C. Fureby, X. Bai, P. Petersson, R. Collin, M. Linne, Large eddy simulation and laser diagnostic studies on a low swirl stratified premixed flame, Combust. Flame 156 (1) (2009) 25–36. doi:10.1016/j.combustflame.2008.06.014.

[43] K.-J. Nogenmyr, P. Petersson, X. Bai, C. Fureby, R. Collin, A. Lantz, M. Linne, M. Aldén, Structure and stabilization mechanism of a stratified premixed low swirl flame, Proc. Combust. Inst. 33 (1) (2011) 1567–1574. doi:10.1016/j.proci.2010.06.011.

[44] M. J. Dunn, A. R. Masri, R. W. Bilger, A new piloted premixed jet burner to study strong finite-rate chemistry effects, Combust. Flame 151 (1-2) (2007) 46–60. doi:10.1016/j.combustflame.2007.05.010.

[45] M. J. Dunn, A. R. Masri, R. W. Bilger, R. S. Barlow, G.-H. Wang, The compositional structure of highly turbulent piloted premixed flames issuing into a hot coflow, Proc. Combust. Inst. 32 (2009) 1779–1786. doi:10.1007/s10494-010-9280-5.

[46] M. J. Dunn, A. R. Masri, R. W. Bilger, R. S. Barlow, Finite rate chemistry effects in highly sheared turbulent premixed flames, Flow. Turb. Combust. 85 (3-4) (2010) 621–648. doi:10.1007/s10494-010-9280-5.

[47] B. Zhou, C. Brackmann, Q. Li, Z. Wang, P. Petersson, Z. Li, M. Aldén, X. song Bai, Distributed reactions in highly turbulent premixed methane/air flames. Part I. Flame structure characterization, Combust. Flame 162 (7) (2015) 2937–2953. doi:10.1016/j.combustflame.2014.12.021.

[48] B. Zhou, C. Brackmann, Z. Li, M. Aldén, X. S. Bai, Simultaneous multi-species and temperature visualization of premixed flames in the distributed reaction zone regime, Proc. Combust. Inst. 35 (2)

(2015) 1409–1416. doi:10.1016/j.proci.2014.06.107.

[49] J. Rosell, X.-S. Bai, J. Sjoholm, B. Zhou, Z. Li, Z. Wang, P. Pettersson, Z. Li, M. Richter, M. Alden, , Combust. Flame 182 (2017) 324–338. doi:10.1016/j.combustflame.2017.04.003.

[50] X. Wang, T. Jin, K. H. Luo, Response of heat release to equivalence ratio variations in high Karlovitz premixed H_2/air flames at 20 atm, Int. J. Hydrog. 44 (5) (2019) 3195–3207. doi:10.1016/j.ijhydene.2018.12.027.

[51] F. T. Yuen, Ö. L. Gülder, Premixed turbulent flame front structure investigation by Rayleigh scattering in the thin reaction zone regime, Proc. Combust. Inst. 32 (2009) 1747–1754. doi:10.1016/j.proci.2008.08.005.

[52] F. T. C. Yuen, Ö. L. Gülder, Dynamics of Lean-Premixed Turbulent Combustion at High Turbulence Intensities, Combust. Sci. Technol. 182 (4-6) (2010) 544–558. doi:10.1080/00102200903463274.

[53] F. Yuen, O. Gülder, Turbulent premixed flame front dynamics and implications for limits of flamelet hypothesis, Proc. Combust. Inst. 34 (2013) 1393–1400.

[54] P. Tamadonfar, Ö. L. Gülder, Experimental investigation of the inner structure of premixed turbulent methane/air flames in the thin reaction zones regime, Combust. Flame 162 (1) (2015) 115–128. doi:10.1016/j.combustflame.2014.07.001.

[55] J. R. Osborne, S. A. Ramji, C. D. Carter, A. M. Steinberg, Relationship between local reaction rate and flame structure in turbulent premixed flames from simultaneous 10 kHz TPIV, OH PLIF, and CH_2O PLIF, Proc. Combust. Inst. 36 (2) (2017) 1835–1841. doi:10.1016/j.proci.2016.07.124.

[56] T. M. Wabel, A. W. Skiba, J. F. Driscoll, Turbulent burning velocity measurements: Extended to extreme levels of turbulence, Proc. Combust. Inst. 36 (2) (2017) 1801–1808. doi:10.1016/j.proci.2016.08.013.

[57] T. M. Wabel, A. W. Skiba, J. E. Temme, J. F. Driscoll, Measurements to determine the regimes of premixed flames in extreme turbulence, Proc. Combust. Inst. 36 (2) (2017) 1809–1816. doi:10.1016/j.proci.2016.08.065.

[58] A. W. Skiba, T. M. Wabel, C. D. Carter, S. D. Hammack, J. E. Temme, J. F. Driscoll, Premixed flames subjected to extreme levels of turbulence part I: Flame structure and a new measured regime diagram, Combust. Flame 189 (2018) 407 – 432.

[59] T. M. Wabel, R. S. Barlow, A. M. Steinberg, Reaction zone stratification in piloted highly-turbulent fuel-lean premixed jets, Combust. Flame 208 (2019) 327 – 329.

[60] D. Fries, B. A. Ochs, A. Saha, D. Ranjan, S. Menon, Flame speed characteristics of turbulent expanding flames in a rectangular channel, Combust. Flame 199 (2019) 1 – 13.

[61] B. A. Ochs, D. Fries, D. Ranjan, S. Menon, Turbulent flame speeds of premixed supersonic flame kernels, Flow. Turb. Combust. 101 (3) (2018) 927–951.

[62] S. Yang, A. Saha, W. Liang, F. Wu, C. K. Law, Extreme role of preferential diffusion in turbulent flame propagation, Combust. Flame 188 (2018) 498 – 504.

[63] S. Yang, A. Saha, Z. Liu, C. K. Law, Role of darrieus-landau instability in propagation of expanding turbulent flames, J. Fluid Mech. 850 (2018) 784–802. doi:10.1017/jfm.2018.426.

[64] J. Sosa, J. Chambers, K. A. Ahmed, A. Poludnenko, V. N. Gamezo, Compressible turbulent flame speeds of highly turbulent standing flames, Proc. Combust. Inst. 37 (3) (2019) 3495 – 3502. doi:https://doi.org/10.1016/j.proci.2018.07.039.

[65] H. Wang, E. R. Hawkes, B. Savard, J. H. Chen, Direct numerical simulation of a high Ka CH4/air stratified premixed jet flame, Combust. Flame 193 (2018) 229–245. doi:10.1016/j.combustflame.2018.03.025.

[66] C. Xu, A. Y. Poludnenko, X. Zhao, H. Wang, T. Lu, Structure of strongly turbulent premixed n-dodecane–air flames: Direct numerical simulations and chemical explosive mode analysis, Combust. Flame 209 (2019) 27–40. doi:10.1016/j.combustflame.2019.07.027.

[67] S. Lapointe, B. Savard, G. Blanquart, Differential diffusion effects, distributed burning, and local extinctions in high Karlovitz premixed flames, Combust. Flame 162 (9) (2015) 3341–3355. doi:10.1016/j.combustflame.2015.06.001.

[68] H. G. Im, Direct Numerical Simulations for Combustion Science: Past, Present, and Future, in: S. De, A. K. Agarwal, S. Chaudhuri, S. Sen (Eds.), Modeling and Simulation of Turbulent Combustion, Springer Singapore, Singapore, 2018, pp. 99–132. doi:10.1007/978-981-10-7410-3_4.

[69] A. J. Aspden, M. S. Day, J. B. Bell, Turbulence-flame interactions in lean premixed hydrogen: Transition to the distributed burning regime, J. Fluid Mech. 680 (2011) 287–320. doi:10.1017/jfm.2011.164.

[70] P. E. Hamlington, R. Darragh, C. A. Briner, C. A. Towery, B. D. Taylor, A. Y. Poludnenko, Lagrangian analysis of high-speed turbulent premixed reacting flows: thermochemical trajectories in hydrogen–air flames, Combust. Flame 186 (2017) 193–207. doi:10.1016/j.combustflame.2017.08.001.

[71] G. V. Nivarti, R. S. Cant, Scalar transport and the validity of damköhler's hypotheses for flame propagation in intense turbulence, Phys. Fluids 29 (8) (2017) 085107.

[72] M. Klein, N. Chakraborty, K. W. Jenkins, R. S. Cant, Effects of initial radius on the propagation of premixed flame kernels in a turbulent environment, Phys. Fluids 18 (5).

[73] H. Shalaby, D. Thévenin, Statistically significant results for the propagation of a turbulent flame kernel using direct numerical simulation, Flow Turb. Combust. 84 (3) (2010) 357–367.

[74] H. A. Uranakara, S. Chaudhuri, H. L. Dave, P. G. Arias, H. G. Im, A flame particle tracking analysis of turbulence-chemistry interaction in hydrogen-air premixed flames, Combust. Flame 163 (2016) 220–240. doi:10.1016/j.combustflame.2015.09.033.

[75] T. Falkenstein, S. Kang, L. Cai, M. Bode, H. Pitsch, DNS study of the global heat release rate during

early flame kernel development under engine conditions, Combust. Flame 213 (2020) 455–466, arXiv: 1908.07556. doi:10.1016/j.combustflame.2019.11.031.

[76] A. Krisman, P. Meagher, X. Zhao, J.-W. Park, T. Lu, J. H. Chen, A direct numerical simulation of jet A flame kernel quenching, Combust. FlameIn production.

[77] L. Wang, Y. Jiang, L. Pan, Y. Xia, R. Qiu, Lagrangian investigation and chemical explosive mode analysis of extinction and re-ignition in H2/CO/N2 syngas non-premixed flame, Int. J. Hydrog. 41 (8) (2016) 4820–4830. doi:10.1016/j.ijhydene.2016.01.043.

[78] H. Wang, E. R. Hawkes, J. H. Chen, B. Zhou, Z. Li, M. Aldén, Direct numerical simulations of a high Karlovitz number laboratory premixed jet flame – an analysis of flame stretch and flame thickening, J. Fluid Mech. 815 (2017) 511–536. doi:10.1017/jfm.2017.53.

[79] H. Wang, E. R. Hawkes, J. H. Chen, A direct numerical simulation study of flame structure and stabilization of an experimental high Ka CH_4/air premixed jet flame, Combust. Flame 180 (2017) 110–123. doi:10.1016/j.combustflame.2017.02.022.

[80] R. Sankaran, E. R. Hawkes, J. H. Chen, T. Lu, C. K. Law, Structure of a spatially developing turbulent lean methane–air Bunsen flame, Proc. Combust. Inst. 31 (1) (2007) 1291–1298. doi:10.1016/j.proci.2006.08.025.

[81] H. Wang, E. R. Hawkes, B. Zhou, J. H. Chen, Z. Li, M. Aldén, A comparison between direct numerical simulation and experiment of the turbulent burning velocity-related statistics in a turbulent methane-air premixed jet flame at high Karlovitz number, Proc. Combust. Inst. 36 (2) (2017) 2045–2053. doi:10.1016/j.proci.2016.07.104.

[82] S. B. Pope, Turbulent flows, Cambridge University Press, 2000.

[83] S. Lapointe, G. Blanquart, Fuel and chemistry effects in high Karlovitz premixed turbulent flames, Combust. Flame 167 (2016) 294–307. doi:10.1016/j.combustflame.2016.01.035.

[84] H. Kolla, E. R. Hawkes, A. R. Kerstein, N. Swaminathan, J. H. Chen, On velocity and reactive scalar spectra in turbulent premixed flames, J. Fluid Mech. 754 (2014) 456–487. doi:10.1017/jfm.2014.392.

[85] H. Kolla, X.-Y. Zhao, J. H. Chen, N. Swaminathan, Velocity and Reactive Scalar Dissipation Spectra in Turbulent Premixed Flames, Combust. Sci. Technol. 188 (9) (2016) 1424–1439. doi:10.1080/00102202.2016.1197211.

[86] A. J. Aspden, M. S. Day, J. B. Bell, Turbulence-chemistry interaction in lean premixed hydrogen combustion, Proc. Combust. Inst. 35 (2) (2015) 1321–1329. doi:10.1016/j.proci.2014.08.012.

[87] X. Zhao, Y. Tao, H. Wang, T. Lu, Sensitivities of direct numerical simulations to chemical kinetic uncertainties: spherical flame kernel evolution of a real jet fuel, Combust. Flame 209 (2019) 117 – 132.

[88] C. A. Z. Towery, A. Y. Poludnenko, J. Urzay, J. O'Brien, M. Ihme, P. E. Hamlington, Spectral kinetic energy transfer in turbulent premixed reacting flows, Phys. Rev. E 93 (5) (2016) 053115.

doi:10.1103/PhysRevE.93.053115.

[89] N. Peters, Length scales in laminar and turbulent flames, in: E. Oran, J. Boris (Eds.), Numerical Approaches to Combustion Modeling, Vol. 135, AIAA, 1991, pp. 155–182.

[90] J. Jiménez, A. A. Wray, P. G. Saffman, R. S. Rogallo, The structure of intense vorticity in isotropic turbulence, J. Fluid Mech. 265 (1993) 65–90.

[91] K. A. Buch, W. J. A. Dahm, Experimental study of the fine-scale structure of conserved scalar mixing in turbulent shear flows. Part 1. Sc≫1, J. Fluid Mech. 317 (1996) 21–71. doi:10.1017/S0022112096000651.

[92] K. A. BUCH, W. J. A. DAHM, Experimental study of the fine-scale structure of conserved scalar mixing in turbulent shear flows. part 2. sc*approx*1, J. Fluid Mech. 364 (1998) 1–29. doi:10.1017/S0022112098008726.

[93] B. Ganapathisubramani, K. Lakshminarasimhan, N. T. Clemens, Investigation of three-dimensional structure of fine scales in a turbulent jet by using cinematographic stereoscopic particle image velocimetry, J. Fluid Mech. 598 (2008) 141–175. doi:10.1017/S0022112007009706.

[94] W. Han, H. Wang, G. Kuenne, E. R. Hawkes, J. H. Chen, J. Janicka, C. Hasse, Large eddy simulation/dynamic thickened flame modeling of a high Karlovitz number turbulent premixed jet flame, Proc. Combust. Inst. 37 (2) (2019) 2555–2563. doi:10.1016/j.proci.2018.06.228.

[95] F. Williams, Criteria for existence of wrinkled laminar flame structure of premixed turbulent flames, Combust. Flame 26 (1976) 269.

[96] R. Borghi, Turbulent combustion modelling, Prog. Energy Combust. Sci. 14 (4) (1988) 245 – 292.

[97] A. M. Klimov, Laminar flame in a turbulent flow, Prikladnoy Mekhaniki i Tekhnicheskoy Fiziki Zhurnal 3 (1963) 49–58.

[98] I. Gökalp, An evaluation of the Klimov-Williams criterion, Combust. Flame 67 (1987) 111–119.

[99] G. Damköhler, Der Einfluss der Turbulenz auf die Flammengeschwindigkeit in Gasgemischen, Z. Elektrochem. 11 (1940) 601–652.

[100] S. R. Turns, An Introduction to Combustion: Concepts and Applications, 1st Edition, McGraw-Hill, 1995.

[101] F. Williams, Progress in knowledge of flamelet structure and extinction, Prog. Energy Combust. Sci. 26 (4) (2000) 657 – 682.

[102] H. B. Ebrahimi, Overview of gas turbine augmentor design, operation, and combustion oscillation, in: 42nd AIAA/ASME/SAE/ASEE Joint Propulsion Conference & Exhibit, American Institute of Aeronautics and Astronautics, Sacramento, California, 2006.

[103] A. Cavaliere, M. de Joannon, MILD combustion, Prog. Energy Combust. Sci. 30 (4) (2004) 329 – 366. doi:https://doi.org/10.1016/j.pecs.2004.02.003.

[104] A. A. Perpignan, A. G. Rao, D. J. Roekaerts, Flameless combustion and its potential towards gas turbines, Prog. Energy Combust. Sci. 69 (2018) 28 – 62. doi:https://doi.org/10.1016/j.pecs.2018.06.002.

[105] A. J. Aspden, M. S. Day, J. B. Bell, Towards the distributed burning regime in turbulent premixed flames, J. Fluid Mech. 871 (2019) 1–21.

[106] H. Wu, Y. C. See, Q. Wang, M. Ihme, A pareto-efficient combustion framework with submodel assignment for predicting complex flame configurations, Combust. Flame 162 (11) (2015) 4208 – 4230.

[107] S. A. Filatyev, J. F. Driscoll, C. D. Carter, J. M. Donbar, Measured properties of turbulent premixed flames for model assessment, including burning velocities, stretch rates, and surface densities, Combust. Flame 141 (1) (2005) 1 – 21. doi:https://doi.org/10.1016/j.combustflame.2004.07.010.

[108] Z. Chen, On the extraction of laminar flame speed and markstein length from outwardly propagating spherical flames, Combust. Flame 158 (2) (2011) 291 – 300.

[109] A. Poludnenko, T. A. Gradiner, E. S. Oran, Spontaneous transition of turbulent flames to detonations in unconfined media, Phys. Rev. Lett. 107 (5) (2011) 054501.

[110] A. Poludnenko, E. Oran, The interaction of high-speed turbulence with flames: Turbulent flame speed, Combust. Flame 158 (2) (2011) 301 – 326.

[111] T. M. Wabel, P. Zhang, X. Zhao, H. Wang, E. Hawkes, A. M. Steinberg, Assessment of chemical scalars for heat release rate measurement in highly turbulent premixed combustion including experimental factors, Combust. Flame 194 (2018) 485–506. doi:10.1016/j.combustflame.2018.04.016.

[112] H. Wang, E. R. Hawkes, J. H. Chen, Turbulence-flame interactions in DNS of a laboratory high Karlovitz premixed turbulent jet flame, Phys. Fluids 28 (9) (2016) 095107. doi:10.1063/1.4962501.

[113] A. W. Skiba, C. D. Carter, S. D. Hammack, J. D. Miller, J. R. Gord, J. F. Driscoll, The influence of large eddies on the structure of turbulent premixed flames characterized with stereo-PIV and multi-species PLIF at 20 kHz, Proc. Combust. Inst. 37 (2) (2019) 2477–2484. doi:10.1016/j.proci.2018.07.122.

[114] M. Klein, A. Herbert, H. Kosaka, B. Böhm, A. Dreizler, N. Chakraborty, V. Papapostolou, H. G. Im, J. Hasslberger, Evaluation of flame area based on detailed chemistry DNS of premixed turbulent hydrogen-air flames in different regimes of combustion, Flow. Turb. Combust. 104 (2020) 403 – 419.

[115] C. Chen, S. Sohrab, Upstream interactions between planar symmetric laminar methane premixed flames, Combust. Flame 101 (3) (1995) 360 – 370.

[116] J. H. Chen, T. Echekki, W. Kollmann, The mechanism of two-dimensional pocket formation in lean premixed methane-air flames with implications to turbulent combustion, Combust. Flame 116 (1) (1999) 15 – 48.

[117] B. Ranganath, T. Echekki, Effects of preferential and differential diffusion on the mutual annihilation of two premixed hydrogenair flames, Combust. Theory Model. 9 (4) (2005) 659–672.

[118] J. R. Osborne, S. A. Ramji, C. D. Carter, S. Peltier, S. Hammack, T. Lee, A. M. Steinberg, Simul-

taneous 10 khz tpiv, oh plif, and ch2o plif measurements of turbulent flame structure and dynamics, Exp. Fluids 57 (2016) 65.

[119] G. V. Nivarti, R. S. Cant, S. Hochgreb, Reconciling turbulent burning velocity with flame surface area in small-scale turbulence, J. Fluid Mech. 858 (2019) R1. doi:10.1017/jfm.2018.841.

[120] A. Bouaniche, N. Jaouen, P. Domingo, L. Vervisch, Vitiated high karlovitz n-decane/air turbulent flames: scaling laws and micro-mixing modeling analysis, Flow. Turb. Combust. 102 (1) (2019) 235–252. doi:10.1007/s10494-018-9946-y.

[121] A. J. Aspden, M. S. Day, J. B. Bell, Three-dimensional direct numerical simulation of turbulent lean premixed methane combustion with detailed kinetics, Combust. Flame 166 (2016) 266–283. doi:10.1016/j.combustflame.2016.01.027.

[122] B. Savard, G. Blanquart, Effects of dissipation rate and diffusion rate of the progress variable on local fuel burning rate in premixed turbulent flames, Combust. Flame 180 (2017) 77–87. doi:10.1016/j.combustflame.2017.02.025.

[123] A. J. Aspden, J. B. Bell, M. S. Day, F. N. Egolfopoulos, Turbulence-flame interactions in lean premixed dodecane flames, Proc. Combust. Inst. 36 (2) (2017) 2005–2016. doi:10.1016/j.proci.2016.07.068.

[124] B. Zhou, C. Brackmann, Z. Wang, Z. Li, M. Richter, M. Aldén, X. S. Bai, Thin reaction zone and distributed reaction zone regimes in turbulent premixed methane/air flames: Scalar distributions and correlations, Combust. Flame 175 (2017) 220–236. doi:10.1016/j.combustflame.2016.06.016.

[125] B. Zhou, M. Costa, Z. Li, M. Aldén, X. S. Bai, Characterization of the reaction zone structures in a laboratory combustor using optical diagnostics: From flame to flameless combustion, Proc. Combust. Inst. 36 (3) (2017) 4305–4312. doi:10.1016/j.proci.2016.06.182.

[126] B. Savard, S. Lapointe, A. Teodorczyk, Numerical investigation of the effect of pressure on heat release rate in iso-octane premixed turbulent flames under conditions relevant to SI engines, Proc. Combust. Inst. 36 (3) (2017) 3543–3549. doi:10.1016/j.proci.2016.07.056.

[127] B. Savard, B. Bobbitt, G. Blanquart, Structure of a high Karlovitz n-C7H16 premixed turbulent flame, Proc. Combust. Inst. 35 (2) (2015) 1377–1384. doi:10.1016/j.proci.2014.06.133.

[128] P. E. Hamlington, A. Y. Poludnenko, E. S. Oran, Interactions between turbulence and flames in premixed reacting flows, Phys. Fluids 23 (12) (2011) 125111. doi:10.1063/1.3671736.

[129] S. Chaudhuri, H. Kolla, H. L. Dave, E. R. Hawkes, J. H. Chen, C. K. Law, Flame thickness and conditional scalar dissipation rate in a premixed temporal turbulent reacting jet, Combust. Flame 184 (2017) 273–285. doi:10.1016/j.combustflame.2017.02.027.

[130] A. W. Skiba, C. D. Carter, S. D. Hammack, T. Lee, A simplified approach to simultaneous multi-scalar imaging in turbulent flames, Combust. Flame 189 (2018) 207 – 211. doi:https://doi.org/10.1016/j.combustflame.2017.10.035.

[131] A. J. Aspden, A numerical study of diffusive effects in turbulent lean premixed hydrogen flames, Proc. Combust. Inst. 36 (2) (2017) 1997–2004. doi:10.1016/j.proci.2016.07.053.

[132] B. Savard, H. Wang, A. Wehrfritz, E. R. Hawkes, Direct numerical simulations of rich premixed turbulent n-dodecane/air flames at diesel engine conditions, Proc. Combust. Inst. 37 (4) (2019) 4655–4662. doi:10.1016/j.proci.2018.08.022.

[133] A. Masri, Partial premixing and stratification in turbulent flames, Proc. Combust. Inst. 35 (2) (2015) 1115 – 1136.

[134] C. S. Yoo, R. Sankaran, J. H. Chen, Three-dimensional direct numerical simulation of a turbulent lifted hydrogen jet flame in heated coflow: flame stabilization and structure, J. Fluid Mech. 640 (2009) 453–481.

[135] R. S. Barlow, M. J. Dunn, M. S. Sweeney, S. Hochgreb, Effects of preferential transport in turbulent bluff-body-stabilized lean premixed CH_4/air flames, Combust. Flame 159 (8) (2012) 2563 – 2575.

[136] H. Turkeri, X. Zhao, S. B. Pope, M. Muradoglu, Large eddy simulation/probability density function simulations of the cambridge turbulent stratified flame series, Combust. Flame 199 (2019) 24 – 45.

[137] F. C. C. Galeazzo, B. Savard, H. Wang, E. R. Hawkes, J. H. Chen, G. C. Krieger Filho, Performance assessment of flamelet models in flame-resolved LES of a high Karlovitz methane/air stratified premixed jet flame, Proc. Combust. Inst. 37 (2) (2019) 2545 – 2553.

[138] W. Han, H. Wang, G. Kuenne, E. R. Hawkes, J. H. Chen, J. Janicka, C. Hasse, Large eddy simulation/dynamic thickened flame modeling of a high karlovitz number turbulent premixed jet flame, Proc. Combust. Inst. 37 (2) (2019) 2555 – 2563.

[139] P. Zhang, T. Xie, H. Kolla, H. Wang, E. R. Hawkes, J. H. Chen, H. Wang, A priori analysis of a power-law mixing model for transported pdf model based on high karlovitz turbulent premixed dns flames, Proc. Combust. Inst.

[140] D. Dasgupta, W. Sun, M. Day, T. Lieuwen, Effect of turbulence–chemistry interactions on chemical pathways for turbulent hydrogen–air premixed flames, Combust. Flame 176 (2017) 191 – 201.

[141] S. Yang, R. Ranjan, V. Yang, W. Sun, S. Menon, Sensitivity of predictions to chemical kinetics models in a temporally evolving turbulent non-premixed flame, Combust. Flame 183 (2017) 224–241.

[142] D. Dasgupta, W. Sun, M. S. Day, T. C. Lieuwen, Turbulence effects on the chemical pathways for premixed methane/air flames, in: 55th AIAA Aerospace Sciences Meeting, American Institute of Aeronautics and Astronautics, Grapevine, Texas, 2017, pp. 1–15. arXiv:https://arc.aiaa.org/doi/pdf/10.2514/6.2017-1782, doi:10.2514/6.2017-1782.

[143] D. Dasgupta, W. Sun, M. Day, A. J. Aspden, T. Lieuwen, Analysis of chemical pathways and flame structure for n-dodecane/air turbulent premixed flames, Combust. Flame 207 (2019) 36 – 50.

[144] S. Karimkashi, M. Bolla, H. Wang, E. R. Hawkes, A direct numerical simulation study of turbulence

intensity effects on NOx formation in freely propagating premixed flames, 20th Australasian Fluid Mechanics Conference December (2016) 8–11.

[145] M. Frenklach, H. Wang, M. J. Rabinowitz, Optimization and analysis of large chemical kinetic mechanisms using the solution mapping method—combustion of methane, Prog. Energy Combust. Sci. 18 (1) (1992) 47 – 73.

[146] H. Wang, Chapter 14 - uncertainty quantification and minimization, in: T. Faravelli, F. Manenti, E. Ranzi (Eds.), Mathematical Modelling of Gas-Phase Complex Reaction Systems: Pyrolysis and Combustion, Vol. 45 of Computer Aided Chemical Engineering, Elsevier, 2019, pp. 723 – 762.

[147] A. Aspden, M. Day, J. Bell, Characterization of low lewis number flames, Proc. Combust. Inst. 33 (1) (2011) 1463 – 1471. doi:https://doi.org/10.1016/j.proci.2010.05.090.

[148] J. Smolke, F. Carbone, F. N. Egolfopoulos, H. Wang, Effect of n-dodecane decomposition on its fundamental flame properties, Combust. Flame 190 (2018) 65–73.

[149] A. Krisman, E. R. Hawkes, M. Talei, A. Bhagatwala, J. H. Chen, Characterisation of two-stage ignition in diesel engine-relevant thermochemical conditions using direct numerical simulation, Combust. Flame 172 (2016) 326 – 341.

[150] K. Aditya, A. Gruber, C. Xu, T. Lu, A. Krisman, M. R. Bothien, J. H. Chen, Direct numerical simulation of flame stabilization assisted by autoignition in a reheat gas turbine combustor, Proc. Combust. Inst. 37 (2) (2019) 2635 – 2642.

[151] R. L. Gordon, A. R. Masri, S. B. Pope, G. M. Goldin, A numerical study of auto-ignition in turbulent lifted flames issuing into a vitiated co-flow, Combust. Theory Model. 11 (3) (2007) 351–376.

[152] A. Krisman, E. R. Hawkes, J. H. Chen, The structure and propagation of laminar flames under autoignitive conditions, Combust. Flame 188 (2018) 399 – 411.

[153] S. Lam, Using CSP to understand complex chemical kinetics, Combust. Sci. Technol. 89 (5-6) (1993) 375–404.

[154] S. Lam, D. GOUSSIS, The csp method for simplifying kinetics, Int. J. Chem. Kinet. 26 (1994) 461486.

[155] M. Valorani, H. N. Najm, D. A. Goussis, CSP analysis of a transient flame-vortex interaction, Combust. Flame 134 (1-2) (2003) 35–53.

[156] M. Valorani, P. P. Ciottoli, R. M. Galassi, Tangential stretching rate (TSR) analysis of non premixed reactive flows, Proc. Combust. Inst. 36 (1) (2017) 1357 – 1367.

[157] T. Lu, C. K. Law, C. S. Yoo, J. H. Chen, Dynamic stiffness removal for direct numerical simulations, Combust. Flame 156 (8) (2009) 1542 – 1551.

[158] Z. Luo, C. S. Yoo, E. S. Richardson, J. H. Chen, C. K. Law, T. Lu, Chemical explosive mode analysis for a turbulent lifted ethylene jet flame in highly-heated coflow, Combustion and Flame 159 (1) (2012) 265 – 274.

[159] S. H.LAM, Reduced chemistry-diffusion coupling, Combust. Sci. Technol. 179 (4) (2007) 767–786.

[160] P. Boivin, A. Dauptain, C. Jimnez, B. Cuenot, Simulation of a supersonic hydrogenair autoignition-stabilized flame using reduced chemistry, Combust. Flame 159 (4) (2012) 1779 – 1790.

[161] C. Fureby, K. Nordin-Bates, K. Petterson, A. Bresson, V. Sabelnikov, A computational study of supersonic combustion in strut injector and hypermixer flow fields, Proc. Combust. Inst. 35 (2) (2015) 2127 – 2135.

[162] B. Savard, E. R. Hawkes, K. Aditya, H. Wang, J. H. Chen, Regimes of premixed turbulent spontaneous ignition and deflagration under gas-turbine reheat combustion conditions, Combust. Flame 208 (2019) 402 – 419.

[163] Q. Mal, O. Vermorel, F. Ravet, T. Poinsot, Direct numerical simulations and models for hot burnt gases jet ignition, Combust. Flame 223 (2021) 407 – 422.

[164] S. Hartl, D. Geyer, A. Dreizler, G. Magnotti, R. S. Barlow, C. Hasse, Regime identification from raman/rayleigh line measurements in partially premixed flames, Combust. Flame 189 (2018) 126 – 141.

[165] S. Hartl, D. Geyer, C. Hasse, X. Zhao, H. Wang, R. S. Barlow, Assessing an experimental approach for chemical explosive mode and heat release rate using dns data, Combust. Flame 209 (2019) 214 – 224.

[166] J. F. MacArt, T. Grenga, M. E. Mueller, Effects of combustion heat release on velocity and scalar statistics in turbulent premixed jet flames at low and high Karlovitz numbers, Combust. Flame 191 (2018) 468–485. doi:10.1016/j.combustflame.2018.01.022.

[167] Z. Wang, J. Abraham, Effects of Karlovitz number on turbulent kinetic energy transport in turbulent lean premixed methane/air flames, Phys. Fluids 29 (8) (2017) 085102. doi:10.1063/1.4995303.

[168] N. Chakraborty, M. Katragadda, R. S. Cant, Statistics and Modelling of Turbulent Kinetic Energy Transport in Different Regimes of Premixed Combustion, Flow. Turb. Combust. 87 (2-3) (2011) 205–235. doi:10.1007/s10494-010-9312-1.

[169] J. F. MacArt, T. Grenga, M. E. Mueller, Evolution of flame-conditioned velocity statistics in turbulent premixed jet flames at low and high Karlovitz numbers, Proc. Combust. Inst. 37 (2) (2019) 2503–2510. doi:10.1016/j.proci.2018.08.030.

[170] J. Lee, J. F. MacArt, M. E. Mueller, Heat release effects on the Reynolds stress budgets in turbulent premixed jet flames at low and high Karlovitz numbers, Combust. Flame 216 (2020) 1–8. doi:10.1016/j.combustflame.2020.02.014.

[171] F. C. C. Galeazzo, B. Savard, H. Wang, E. R. Hawkes, J. H. Chen, G. C. Krieger Filho, Performance assessment of flamelet models in flame-resolved LES of a high Karlovitz methane/air stratified premixed jet flame, Proc. Combust. Inst. 37 (2) (2019) 2545–2553. doi:10.1016/j.proci.2018.09.025.

[172] B. Coriton, S.-K. Im, M. Gamba, J. H. Frank, Flow field and scalar measurements in a series of turbulent partially-premixed dimethyl ether/air jet flames, Combust. Flame 180 (2017) 40–52. doi:10.1016/j.combustflame.2017.02.014.

[173] A. Gruber, E. S. Richardson, K. Aditya, J. H. Chen, Direct numerical simulations of premixed and stratified flame propagation in turbulent channel flow, Phys. Rev. Fluids 3 (11) (2018) 110507. doi:10.1103/PhysRevFluids.3.110507.

[174] U. Ahmed, A. L. Pillai, N. Chakraborty, R. Kurose, Statistical behavior of turbulent kinetic energy transport in boundary layer flashback of hydrogen-rich premixed combustion, Phys. Rev. Fluids 4 (10) (2019) 103201. doi:10.1103/PhysRevFluids.4.103201.

[175] T. M. Wabel, A. W. Skiba, J. F. Driscoll, Evolution of turbulence through a broadened preheat zone in a premixed piloted Bunsen flame from conditionally-averaged velocity measurements, Combust. Flame 188 (2018) 13–27. doi:10.1016/j.combustflame.2017.09.013.

[176] L. Paxton, J. Smolke, F. N. Egolfopoulos, Effects of heat release and fuel type on highly turbulent premixed jet flames, Proc. Combust. Inst. 37 (2) (2019) 2565–2572. doi:10.1016/j.proci.2018.08.041.

[177] A. M. Steinberg, J. F. Driscoll, N. Swaminathan, Statistics and dynamics of turbulence–flame alignment in premixed combustion, Combust. Flame 159 (8) (2012) 2576–2588. doi:10.1016/j.combustflame.2011.12.001.

[178] M. Klein, C. Kasten, N. Chakraborty, N. Mukhadiyev, H. G. Im, Turbulent scalar fluxes in H_2-air premixed flames at low and high Karlovitz numbers, Combust. Theory Model. 22 (6) (2018) 1033–1048. doi:10.1080/13647830.2018.1468034.

[179] P. E. Hamlington, W. J. A. Dahm, Reynolds stress closure for nonequilibrium effects in turbulent flows, Phys. Fluids 20 (11) (2008) 115101. doi:10.1063/1.3006023.

[180] A. Lipatnikov, S. Nishiki, T. Hasegawa, Closure relations for fluxes of flame surface density and scalar dissipation rate in turbulent premixed flames, Fluids 4 (1) (2019) 43. doi:10.3390/fluids4010043.

[181] R. Ranjan, B. Muralidharan, Y. Nagaoka, S. Menon, Subgrid-scale modeling of reaction-diffusion and scalar transport in turbulent premixed flames, Combust. Sci. Technol. 188 (9) (2016) 1496–1537. doi:10.1080/00102202.2016.1198336.

[182] S. H. Kim, H. Pitsch, Scalar gradient and small-scale structure in turbulent premixed combustion, Phys. Fluids 19 (11) (2007) 115104. doi:10.1063/1.2784943.

[183] N. Chakraborty, N. Swaminathan, Influence of the Damköhler number on turbulence-scalar interaction in premixed flames. I. Physical insight, Phys. Fluids 19 (4). doi:10.1063/1.2714070.

[184] N. Chakraborty, M. Klein, N. Swaminathan, Effects of Lewis number on the reactive scalar gradient alignment with local strain rate in turbulent premixed flames, Proc. Combust. Inst. 32 I (1) (2009) 1409–1417. doi:10.1016/j.proci.2008.06.021.

[185] N. Chakraborty, J. W. Rogerson, N. Swaminathan, The scalar gradient alignment statistics of flame kernels and its modelling implications for turbulent premixed combustion, Flow. Turb. Combust. 85 (1) (2010) 25–55. doi:10.1007/s10494-010-9250-y.

[186] G. Hartung, J. Hult, C. F. Kaminski, J. W. Rogerson, N. Swaminathan, Effect of heat release on turbulence and scalar-turbulence interaction in premixed combustion, Phys. Fluids 20 (3) (2008) 1–16. doi:10.1063/1.2896285.

[187] M. Mustafa Kamal, B. Coriton, R. Zhou, J. H. Frank, S. Hochgreb, Scalar dissipation rate and scales in swirling turbulent premixed flames, Proc. Combust. Inst. 36 (2) (2017) 1957–1965. doi:10.1016/j.proci.2016.08.067.

[188] M. M. Kamal, R. S. Barlow, S. Hochgreb, Conditional analysis of turbulent premixed and stratified flames on local equivalence ratio and progress of reaction, Combust. Flame 162 (10) (2015) 3896–3913. doi:10.1016/j.combustflame.2015.07.026.

[189] G. Magnotti, R. S. Barlow, Effects of high shear on the structure and thickness of turbulent premixed methane/air flames stabilized on a bluff-body burner, Combust. Flame 162 (1) (2015) 100–114. doi:10.1016/j.combustflame.2014.06.015.

[190] R. Sankaran, E. R. Hawkes, C. S. Yoo, J. H. Chen, Response of flame thickness and propagation speed under intense turbulence in spatially developing lean premixed methane–air jet flames, Combust. Flame 162 (9) (2015) 3294–3306. doi:10.1016/j.combustflame.2015.05.019.

[191] N. Chakraborty, R. S. Cant, Effects of Lewis number on scalar transport in turbulent premixed flames, Phys. Fluids 21 (3) (2009) 1–11. doi:10.1063/1.3097007.

[192] P. E. Hamlington, A. Y. Poludnenko, E. S. Oran, Intermittency in premixed turbulent reacting flows, Phys. Fluids 24 (7) (2012) 075111. doi:10.1063/1.4729615.

[193] R. M. Kerr, Higher-order derivative correlations and the alignment of small-scale structures in isotropic numerical turbulence, J. Fluid Mech. 153 (1985) 31–58. doi:10.1017/S0022112085001136.

[194] W. T. Ashurst, A. R. Kerstein, R. M. Kerr, C. H. Gibson, Alignment of vorticity and scalar gradient with strain rate in simulated Navier-Stokes turbulence., Phys. Fluids 30 (1987) 2343.

[195] K. K. Nomura, S. E. Elghobashi, The structure of inhomogeneous turbulence in variable density nonpremixed flames, Theor. Comp. Fluid Dyn. 5-5 (4-5) (1993) 153–175. doi:10.1007/BF00271656.

[196] O. N. Boratav, S. E. Elghobashi, R. Zhong, On the alignment of strain, vorticity and scalar gradient in turbulent, buoyant, nonpremixed flames, Phys. Fluids 10 (9) (1998) 2260–2267. doi:10.1063/1.869747.

[197] N. Swaminathan, R. W. Grout, Interaction of turbulence and scalar fields in premixed flames, Phys. Fluids 18 (4). doi:10.1063/1.2186590.

[198] B. Coriton, J. H. Frank, Impact of heat release on strain rate field in turbulent premixed Bunsen flames, Proc. Combust. Inst. 36 (2) (2017) 1885–1892. doi:10.1016/j.proci.2016.07.006.

[199] F. Hampp, R. Lindstedt, Strain distribution on material surfaces during combustion regime transitions, Proc. Combust. Inst. 36 (2) (2017) 1911–1918. doi:10.1016/j.proci.2016.07.018.

[200] B. Zhou, J. H. Frank, Effects of heat release and imposed bulk strain on alignment of strain rate eigenvectors in turbulent premixed flames, Combust. Flame 201 (2019) 290–300. doi:10.1016/j.combustflame.2018.12.016.

[201] T. Nilsson, H. Carlsson, R. Yu, X.-S. Bai, Structures of turbulent premixed flames in the high Karlovitz number regime – DNS analysis, Fuel 216 (2018) 627–638. doi:10.1016/j.fuel.2017.12.046.

[202] A. Steinberg, B. Coriton, J. Frank, Influence of combustion on principal strain-rate transport in turbulent premixed flames, Proc. Combust. Inst. 35 (2) (2015) 1287–1294. doi:10.1016/j.proci.2014.06.089.

[203] B. Coriton, J. H. Frank, Experimental study of vorticity-strain rate interaction in turbulent partially premixed jet flames using tomographic particle image velocimetry, Phys. Fluids 28 (2) (2016) 025109. doi:10.1063/1.4941528.

[204] W. Sutherland, Lii. the viscosity of gases and molecular force, The London, Edinburgh, and Dublin Philosophical Magazine and Journal of Science 36 (223) (1893) 507–531. arXiv:https://doi.org/10.1080/14786449308620508, doi:10.1080/14786449308620508.

[205] J. Jimenez, Kinematic alignment effects in turbulent flows., Phys. Fluids A 4 (4) (1992) 652.

[206] K. K. Nomura, G. K. Post, The structure and dynamics of vorticity and rate of strain in incompressible homogeneous turbulence, J. Fluid Mech. 377 (1998) 65–97. doi:10.1017/S0022112098003024.

[207] P. E. Hamlington, J. Schumacher, W. J. A. Dahm, Local and nonlocal strain rate fields and vorticity alignment in turbulent flows, Phys. Rev. E 77 (2) (2008) 026303. doi:10.1103/PhysRevE.77.026303.

[208] P. E. Hamlington, J. Schumacher, W. J. A. Dahm, Direct assessment of vorticity alignment with local and nonlocal strain rates in turbulent flows, Phys. Fluids 20 (11) (2008) 111703. doi:10.1063/1.3021055.

[209] B. Bobbitt, S. Lapointe, G. Blanquart, Vorticity transformation in high Karlovitz number premixed flames, Phys. Fluids 28 (1) (2016) 015101. doi:10.1063/1.4937947.

[210] V. Papapostolou, D. H. Wacks, N. Chakraborty, M. Klein, H. G. Im, Enstrophy transport conditional on local flow topologies in different regimes of premixed turbulent combustion, Sci. Rep. 7 (1) (2017) 11545. doi:10.1038/s41598-017-11650-x.

[211] D. Wacks, N. Chakraborty, Flow topology and alignments of scalar gradients and vorticity in turbulent spray flames: A Direct Numerical Simulation analysis, Fuel 184 (2016) 922–947. doi:10.1016/j.fuel.2016.04.061.

[212] B. Bobbitt, G. Blanquart, Vorticity isotropy in high Karlovitz number premixed flames, Phys. Fluids 28 (10) (2016) 105101. doi:10.1063/1.4962305.

[213] P. Zhao, L. Wang, N. Chakraborty, Vectorial structure of the near-wall premixed flame, Phys. Rev. Fluids 4 (6) (2019) 063203. doi:10.1103/PhysRevFluids.4.063203.

[214] A. Y. Poludnenko, Pulsating instability and self-acceleration of fast turbulent flames, Phys. Fluids 27 (1) (2015) 014106. doi:10.1063/1.4905298.

[215] N. Chakraborty, Statistics of vorticity alignment with local strain rates in turbulent premixed flames, Eur. J. Mech. B-Fluids 46 (2014) 201–220. doi:10.1016/j.euromechflu.2014.01.002.

[216] N. Chakraborty, L. Wang, I. Konstantinou, M. Klein, Vorticity statistics based on velocity and density-weighted velocity in premixed reactive turbulence, J. Turbul. 18 (9) (2017) 825–853. doi:10.1080/14685248.2017.1334905.

[217] N. Chakraborty, I. Konstantinou, A. Lipatnikov, Effects of Lewis number on vorticity and enstrophy transport in turbulent premixed flames, Phys. Fluids 28 (1) (2016) 015109. doi:10.1063/1.4939795.

[218] C. Dopazo, L. Cifuentes, N. Chakraborty, Vorticity budgets in premixed combusting turbulent flows at different Lewis numbers, Phys. Fluids 29 (4) (2017) 045106. doi:10.1063/1.4981219.

[219] U. Ahmed, N. A. K. Doan, J. Lai, M. Klein, N. Chakraborty, N. Swaminathan, Multiscale analysis of head-on quenching premixed turbulent flames, Phys. Fluids 30 (10) (2018) 105102. doi:10.1063/1.5047061.

[220] M. K. Geikie, K. A. Ahmed, Pressure-gradient tailoring effects on the turbulent flame-vortex dynamics of bluff-body premixed flames, Combust. Flame 197 (2018) 227–242. doi:10.1016/j.combustflame.2018.08.001.

[221] A. Kazbekov, K. Kumashiro, A. M. Steinberg, Enstrophy transport in swirl combustion, J. Fluid Mech. 876 (2019) 715–732. doi:10.1017/jfm.2019.551.

[222] A. Kazbekov, A. M. Steinberg, Flame- and flow-conditioned vorticity transport in premixed swirl combustion, Proceedings of the Combustion Institutedoi:https://doi.org/10.1016/j.proci.2020.06.211.

[223] J. Lai, N. Chakraborty, A. Lipatnikov, Statistical behaviour of vorticity and enstrophy transport in head-on quenching of turbulent premixed flames, Eur. J. Mech. B/Fluids 65 (2017) 384–397. doi:10.1016/j.euromechflu.2016.10.013.

[224] B. Coriton, J. H. Frank, High-speed tomographic PIV measurements of strain rate intermittency and clustering in turbulent partially-premixed jet flames, Proc. Combust. Inst. 35 (2) (2015) 1243–1250. doi:10.1016/j.proci.2014.06.045.

[225] F. Hampp, S. Shariatmadar, R. Lindstedt, Quantification of low Damkhler number turbulent premixed flames, Proc. Combust. Inst. 37 (2) (2019) 2373–2381. doi:10.1016/j.proci.2018.06.079.

[226] V. Eswaran, S. Pope, An examination of forcing in direct numerical simulations of turbulence, Computers & Fluids 16 (3) (1988) 257–278.

[227] C. A. Towery, A. Y. Poludnenko, P. E. Hamlington, Detonation initiation by compressible turbulence thermodynamic fluctuations, Combust. Flame 213 (2020) 172–183. doi:10.1016/j.combustflame.2019.11.025.

[228] S. Nishiki, T. Hasegawa, R. Borghi, R. Himeno, Modeling of flame-generated turbulence based on direct numerical simulation databases, Proceedings of the Combustion Institute 29 (2) (2002) 2017–2022. doi:10.1016/S1540-7489(02)80246-2.

[229] M. Klein, N. Chakraborty, S. Ketterl, A comparison of strategies for direct numerical simulation of turbulence chemistry interaction in generic planar turbulent premixed flames, Flow. Turb. Combust. 99 (3-4). doi:10.1007/s10494-017-9843-9.

[230] C. Mueller, Vorticity generation and attenuation as vortices convect through a premixed flame, Combust. Flame 112 (3) (1998) 342–346. doi:10.1016/S0010-2180(97)00122-3.

[231] K. R. Sreenivasan, R. A. Antonia, The phenomenology of small-scale turbulence, Ann. Rev. Fluid Mech. 29 (1) (1997) 435–472. doi:10.1146/annurev.fluid.29.1.435.

[232] A. M. Steinberg, J. F. Driscoll, S. L. Ceccio, Three-dimensional temporally resolved measurements of turbulence–flame interactions using orthogonal-plane cinema-stereoscopic PIV, Exp. Fluids 47 (3) (2009) 527–547. doi:10.1007/s00348-009-0677-7.

[233] A. M. Steinberg, J. F. Driscoll, Straining and wrinkling processes during turbulence–premixed flame interaction measured using temporally-resolved diagnostics, Combust. Flame 156 (12) (2009) 2285–2306. doi:10.1016/j.combustflame.2009.06.024.

[234] A. M. Steinberg, J. F. Driscoll, S. L. Ceccio, Measurements of turbulent premixed flame dynamics using cinema stereoscopic PIV, Exp. Fluids 44 (6) (2008) 985–999. doi:10.1007/s00348-007-0458-0.

[235] Z. Wang, B. Zhou, S. Yu, C. Brackmann, Z. Li, M. Richter, M. Aldn, X.-S. Bai, Structure and burning velocity of turbulent premixed methane/air jet flames in thin-reaction zone and distributed reaction zone regimes, Proc. Combust. Inst. 37 (2) (2019) 2537–2544. doi:10.1016/j.proci.2018.09.023.

[236] M. Tanahashi, M. Fujimura, T. Miyauchi, Coherent fine-scale eddies in turbulent premixed flames, Proc. Combust. Inst. 28 (1) (2000) 529–535. doi:10.1016/S0082-0784(00)80252-0.

[237] C. Meneveau, K. R. Sreenivasan, Simple multifractal cascade model for fully developed turbulence, Phys. Rev. Lett. 59 (13) (1987) 1424–1427. doi:10.1103/PhysRevLett.59.1424.

[238] K. R. Sreenivasan, Fluid turbulence, Rev. Mod. Phys. 71 (2) (1999) S383–S395. doi:10.1103/revmodphys.71.s383.

[239] C. Meneveau, Dual spectra and mixed energy cascade of turbulence in the wavelet representation, Phys. Rev. Lett. 66 (11) (1991) 1450.

[240] U. Frisch, Turbulence: The Legacy of A.N. Kolmogorov, Cambridge University Press, 1995.

[241] P. E. Dimotakis, The mixing transition in turbulent flows, J. Fluid Mech. 409 (2000) 69–98.

[242] A. N. Kolmogorov, The local structure of turbulence in incompressible viscous fluid for very large Reynolds numbers., Dokl. Akad. Nauk SSSR 30 (1941) 299–303.

[243] J. Furukawa, E. Harada, T. Hirano, Local reaction zone thickness of a high intensity turbulent pre-

mixed flame., Proc. Combust. Inst. 23 (1) (1990) 789–794.

[244] J. Furukawa, Y. Noguchi, T. Hirano, F. A. Williams, Anisotropic enhancement of turbulence in large-scale, low-intensity turbulent premixed propane–air flames, J. Fluid Mech. 462 (2002) 209–243. doi:10.1017/S0022112002008650.

[245] R. Knaus, C. Pantano, On the effect of heat release in turbulence spectra of non-premixed reacting shear layers, J. Fluid Mech. 626 (2009) 67–109.

[246] J. Kim, M. Bassenne, C. A. Z. Towery, P. E. Hamlington, A. Y. Poludnenko, J. Urzay, Spatially localized multi-scale energy transfer in turbulent premixed combustion, J. Fluid Mech. 848 (2018) 78–116. doi:10.1017/jfm.2018.371.

[247] S. H. Whitman, C. A. Towery, A. Y. Poludnenko, P. E. Hamlington, Scaling and collapse of conditional velocity structure functions in turbulent premixed flames, Proc. Combust. Inst. 37 (2) (2019) 2527–2535. doi:10.1016/j.proci.2018.07.010.

[248] V. A. Sabelnikov, A. N. Lipatnikov, S. Nishiki, T. Hasegawa, Application of conditioned structure functions to exploring influence of premixed combustion on two-point turbulence statistics, Proc. Combust. Inst. 37 (2) (2019) 2433–2441. doi:10.1016/j.proci.2018.08.029.

[249] V. A. Sabelnikov, A. N. Lipatnikov, S. Nishiki, T. Hasegawa, Investigation of the influence of combustion-induced thermal expansion on two-point turbulence statistics using conditioned structure functions, J. Fluid Mech. 867 (2019) 45–76. doi:10.1017/jfm.2019.128.

[250] P. Brearley, U. Ahmed, N. Chakraborty, A. Lipatnikov, Statistical behaviors of conditioned two-point second-order structure functions in turbulent premixed flames in different combustion regimes, Phys. Fluids 31 (11) (2019) 115109. doi:10.1063/1.5124143.

[251] J. O'Brien, C. A. Towery, P. E. Hamlington, M. Ihme, A. Y. Poludnenko, J. Urzay, The cross-scale physical-space transfer of kinetic energy in turbulent premixed flames, Proc. Combust. Inst. 36 (2) (2017) 1967–1975. doi:10.1016/j.proci.2016.05.005.

[252] P. A. Davidson, Turbulence: An Introduction for Scientists and Engineers, Oxford University Press, 2004.

[253] U. Piomelli, W. H. Cabot, P. Moin, S. Lee, Subgridscale backscatter in turbulent and transitional flows, Phys. Fluids A 3 (1991) 1766–1771.

[254] J. A. Domaradzki, R. S. Rogallo, Local energy transfer and nonlocal interactions in homogeneous, isotropic turbulence, Phys. Fluids A 2 (1990) 413.

[255] F. Waleffe, The nature of triad interactions in homogeneous turbulence, Phys. Fluids A 4 (1992) 350–363.

[256] Y. Zhou, Degrees of locality of energy transfer in the inertial range, Phys. Fluids A 5 (1993) 1092–1094.

[257] J. A. Domaradzki, W. Liu, C. Hartel, L. Kleiser, Energy transfer in numerically simulated wall-

bounded turbulent flows, Phys. Fluids 6 (1994) 1583.

[258] J. G. Brasseur, C. Wei, Interscale dynamics and local isotropy in high Reynolds number turbulence within triadic interactions, Phys. Fluids 6 (2) (1994) 842–870. doi:10.1063/1.868322.

[259] J. A. Domaradzki, D. Carati, An analysis of the energy transfer and the locality of nonlinear interactions in turbulence, Phys. Fluids 19: 085112.

[260] U. Piomelli, High Reynolds number calculations using the dynamic subgridscale stress model, Phys. Fluids A 5 (1993) 1484–1490.

[261] M. Germano, U. Piomelli, P. Moin, W. H. Cabot, A dynamic subgridscale eddy viscosity model, Phys. Fluids A 3 (1991) 1760–1765.

[262] P. Moin, K. Squires, W. Cabot, S. Lee, A dynamic subgrid-scale model for compressible turbulence and scalar transport, Phys. Fluids A 3 (1991) 2746–2757.

[263] D. Carati, S. Ghosal, P. Moin, On the representation of backscatter in dynamic localization models, Phys. Fluids 7 (1995) 606–616.

[264] U. Schumann, Stochastic backscatter of turbulence energy and scalar variance by random subgrid-scale fluxes, Proc. R. Soc. Lond. A 451 (1995) 293–318.

[265] J. A. Domaradzki, E. M. Saiki, Backscatter models for Large-Eddy simulations, Theor. Comp. Fluid Dyn. 9 (1997) 75–83.

[266] C. Meneveau, J. Katz, Scale-Invariance and Turbulence Models for Large-Eddy Simulation, Ann. Rev. Fluid Mech. 32 (1) (2000) 1–32. doi:10.1146/annurev.fluid.32.1.1.

[267] N. Peters, Multiscale combustion and turbulence, Proc. Comb. Inst. 32 (2009) 1–25.

[268] E. S. Oran, V. N. Gamezo, Origins of the deflagration-to-detonation transition in gas-phase combustion, Comb. Flame 148 (2007) 4–47.

[269] G. Boffetta, R. E. Ecke, Two-Dimensional Turbulence, Annu. Rev. Fluid Mech. 44 (2012) 427–451.

[270] P. K. Yeung, Y. Zhou, Universality of the Kolmogorov constant in numerical simulations of turbulence, Phys. Rev. E 56 (2) (1997) 1746–1752. doi:10.1103/PhysRevE.56.1746.

[271] T. Gotoh, D. Fukayama, T. Nakano, Velocity field statistics in homogeneous steady turbulence obtained using a high-resolution direct numerical simulation, Phys. Fluids 14 (3) (2002) 1065–1081. doi:10.1063/1.1448296.

[272] Y. Kaneda, T. Ishihara, M. Yokokawa, K. Itakura, A. Uno, Energy dissipation rate and energy spectrum in high resolution direct numerical simulations of turbulence in a periodic box, Phys. Fluids 15 (2) (2003) L21–L24. doi:10.1063/1.1539855.

[273] S. G. Saddoughi, S. V. Veeravalli, Local isotropy in turbulent boundary layers at high reynolds number., J. Fluid Mech. 268 (1994) 333–372.

[274] Z. She, E. Jackson, On the universal form of energy spectra in fully developed turbulence, Phys. Fluids

A 5 (7) (1993) 1526–1528. doi:10.1063/1.858591.

[275] M. K. Verma, D. Donzis, Energy transfer and bottleneck effect in turbulence, J. Phys. A: Math. Theor. 40 (2007) 4401–4412.

[276] J. O'Brien, J. Urzay, M. Ihme, P. Moin, A. Saghafian, Subgrid-scale backscatter in reacting and inert supersonic hydrogen-air turbulent mixing layers., J. Fluid Mech. 743 (2014) 554–584.

[277] A. Kazbekov, A. M. Steinberg, Experimental measurement of filtered kinetic energy dynamics in premixed swirl flames, in: AIAA Scitech 2020 Forum, American Institute of Aeronautics and Astronautics, Orlando, FL, 2020. doi:10.2514/6.2020-0914.

[278] S. Pope, Small scales, many species and the manifold challenges of turbulent combustion, Proc. Combust. Inst. 34 (1) (2013) 1 – 31.

[279] C. Xu, M. M. Ameen, S. Som, J. H. Chen, Z. Ren, T. Lu, Dynamic adaptive combustion modeling of spray flames based on chemical explosive mode analysis, Combust. Flame 195 (2018) 30 – 39, special Commemorative Issue: Professor Chung King (Ed) Law 70th Birthday.

[280] J. D. Gounder, A. Kourmatzis, A. R. Masri, Turbulent piloted dilute spray flames: flow fields and droplet dynamics, Combust. Flame 159 (11) (2012) 3372 – 3397. doi:https://doi.org/10.1016/j.combustflame.2012.07.014.

[281] A. Y. Poludnenko, J. Chambers, K. Ahmed, V. N. Gamezo, B. D. Taylor, A unified mechanism for unconfined deflagration-to-detonation transition in terrestrial chemical systems and type Ia supernovae, Science 366 (6465) (2019) eaau7365. doi:10.1126/science.aau7365.

[282] R. Darragh, C. A. Towery, A. Y. Poludnenko, P. E. Hamlington, Particle pair dispersion and eddy diffusivity in a high-speed premixed flame, Proceedings of the Combustion Institute- doi:https://doi.org/10.1016/j.proci.2020.06.056.

[283] B. Sawford, Turbulent Relative Dispersion, Ann. Rev. Fluid Mech. 33 (2001) 289–317.

[284] J. P. Salazar, L. R. Collins, Two-particle dispersion in isotropic turbulent flows, Ann. Rev. Fluid Mech. 41 (1) (2009) 405–432. doi:10.1146/annurev.fluid.40.111406.102224.